Regulation of mitochondrial quality control by membrane fission

A thesis submitted in partial fulfilment of the requirements of the degree of Doctor of Philosophy

विद्या वाचस्पति की

उपाधि की अपेक्षाओं की आंशिक पूर्ति में प्रस्तुत शोध प्रबंध

By / द्वारा

Krishnendu Roy

Registration No./ पंजीकरण सं.: 20162005

Thesis Supervisor / शोध प्रबंध पर्यवेक्षक: Prof. Thomas Pucadyil

INDIAN INSTITUTE OF SCIENCE EDUCATION AND RESEARCH PUNE

भारतीय विज्ञान शिक्षा एवं अनुसंधान संस्थान पुणे

2023

Certificate

Certified that the work incorporated in the thesis entitled '**Regulation of mitochondrial quality control by membrane fission'** submitted by **Krishnendu Roy** was carried out by the candidate, under my supervision. The work presented here or any part of it has not been included in any other thesis submitted previously for the award of any degree or diploma from any other University or institution.

Date: 15.12.2023

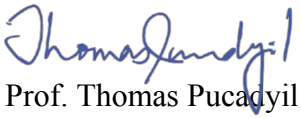

Prof. Thomas Pucadyil

(Supervisor)

Declaration

I declare that this written submission represents my ideas in my own words and wherever others' ideas have been included, I have adequately cited and referenced the original sources. I also declare that I have adhered to all principles of academic honesty and integrity and have not misrepresented or fabricated or falsified any idea/data/fact/source in my submission. I understand that violation of the above will be cause for disciplinary action by the Institute and can also evoke penal action from the sources which have thus not been properly cited or from whom proper permission has not been taken when needed.

Date: 15.12.2023

Krishnendu Roy

Roll no.: 20162005

Acknowledgements

First, I would like to thank my thesis supervisor Prof. Thomas Pucadyil for his constant support and encouragement. Whatever I have learnt about doing science from thinking about scientific problems, making testable hypotheses to actually doing experiments, analyzing data and writing manuscripts, I have learnt from him. I have always admired his vast knowledge about existing literature and his way of thinking which I have tried to imbibe over these years. During my entire tenure in Pucadyil lab, whenever I have asked for help, scientific or non-scientific, he was there to help me out. In a world where people constantly crib about their thesis supervisors, I was lucky to have him as my mentor and guide. I can't but be eternally grateful for what he has done for me during these years in the lab.

I would like to thank Maa and Baba for all the hardships that they had to endure over the years to give me a proper education so that I could achieve what I wanted to. I would like thank Didi, my first teacher, who sacrificed so much so that her younger brother could be successful. Special thanks to Joyeeta, Prakash Da and Pavo for lighting up our lives and making it even more beautiful.

I would like to express my sincere gratitude to my RAC members, Prof. Jayant Udgaonkar, Dr. Siddhesh Kamat and Dr. Durba Sengupta. They provided constructive criticism throughout my tenure in yearly meetings and whenever I have asked them which has helped streamline the work immensely.

I would like to acknowledge the support of all the past and present members of Pucadyil lab for their constant support, criticism and encouragement. Special thanks to Soumya, Sannnidhya and Gurmail for all those discussions that has helped me immensely to think critically about my project.

I would like to thank my childhood friends Basu and Rounak for being unwavering constants in my life. I would like to thank Saptashwa, Arunabha, Sukanya, Aslam for giving me memories of a lifetime. Thanks to Arkajit, Yogesh and all my teammates from the cricket community in IISER for all the memories that we made together during our tours for IISM or during IPL.

Finally, I would like to thank IISER Pune, Bio-office and all the facility staffs for making this journey easier and CSIR for providing me a graduate student fellowship during my PhD tenure.

Table of contents

List of Figures and Tables

Figures:

Tables:

Abbreviations

Abbreviation	Definition
BAR domain	Bin-Amphiphysin-Rvs domain
*Bc*PI-PLC	Bacillus cereus PI-specific phospholipase C
BNIP3	BCL2/adenovirus E1B 19 kDa protein-interacting protein 3
CCCP	Cyanide 3-chlorophenylhydrazone
CL	Cardiolipin
CME	Clathrin-mediated endocytosis
DAG	Diacylglycerol
Dnm1/2	Dynamin 1/2
Drp1	Dynamin-related protein 1
DTT	Dithiothreitol
ECAR	Extracellular acidification rate
EndoB1/2	Endophilin B1/2
FRAP	Fluorescence Recovery After Photobleaching
FRET	Fluorescence Resonance Energy Transfer
FUNDC1	FUN14 domain-containing protein 1
GABARAP	Gamma amino butyric acid type A receptor-associated protein
GDP	Guanosine diphosphate
GTP	Guanosine triphosphate
IMM	Inner mitochondrial membrane
LC3	Microtubule-associated protein 1A/1B-light chain 3
MAPL	Mitochondria-associated protein ligase
MDV	Mitochondria-derived vesicle
MFF	Mitochondrial fission factor
Mfn 1/2	Mitofusin 1/2
*Mm*PKD	Mus musculus Protein Kinase D
MPP	Mitochondrial processing peptidase
NDP52	Nuclear dot protein 52 kDa
NIX	NIP3-like protein X
OCR	Oxygen consumption rate
OMM	Outer mitochondrial membrane
OPTN	Optineurin
OSC	Oxygen scavenging cocktail
PA	Phosphatidic acid
PC	Phosphatidyl choline
PD	Parkinson's Disease
PG	Phosphatidyl glycerol
PI	Phosphatidyl inositol
PINK1	PTEN-induced kinase 1
PLIMAP	Proximity-based Labelling of Membrane-Associated Proteins
ROS	Reactive oxygen species
SD	Standard Deviation
SH3 domain	Src homology 3 domain
SMrT	Supported membrane templates
TEAB	Triethylammonium bicarbonate

UVRAG	UV radiation Resistance-associated gene
VSVG	Vesicular Somatitis Virus G
α-Syn	α-synuclein

Synopsis

Membrane fission is a central theme in cellular physiology which involves the formation of two membrane-bound compartments from one. Membrane fission is critical for organelle division, transport vesicle biogenesis, *de-novo* organelle formation, endocytosis and cell division. Membrane fission involves bending a tube-like membrane intermediate with circumferential forces to thin it down to an extent that the lipids in the membrane end up taking non-bilayer conformations spontaneously leading to fission. Although membrane fission is critical for multiple cellular processes, relatively less is known about the proteins which drive membrane fission at different locations in the cell. The most well-known family of proteins implicated in membrane fission are the soluble members of the Dynamin superfamily of proteins. Endocytic dynamins have been shown to be critical for endocytosis at the plasma membrane. Mitochondrial dynamin, Dynamin-related protein 1 (Drp1) has been shown to be necessary and sufficient for mitochondrial fission.

Mitochondria are double-membrane bound compartments which are involved in ATP generation, beta-oxidation of fatty acids, maintenance of redox equilibrium, Ca^{2+} homeostasis and apoptosis. Mitochondria exist as a dynamic network in eukaryotic cells undergoing constant cycles of fission and fusion. Since mitochondria are involved in a variety of biochemical processes, they are also prone to insults and subsequent damage. Cells have devised ways to selectively rid the network of the damaged or dysfunctional components. The most well-known form of mitochondrial quality control is through mitophagy. Mitophagy involves taking parts of the mitochondria which are non-functional and targeting it to lysosomes for degradation. Since, mitochondria exists as a network, a critical step for mitophagy is the separation of the damaged part form the rest of the network. Previous studies have shown that Drp1 is necessary for mitochondrial fission preceding mitophagy. However, what regulates Drp1's recruitment to the mitochondria to specifically separate out the damaged parts remains elusive.

Chapter 1 of this thesis will discuss about the different quality-control pathways that exists for the mitochondria, the importance of lipids in the processes and the requirement of fission for each of these pathways.

Chapter 2 describes the reconfiguration of supported membrane template (SMrT) assay system to monitor diacylglycerol (DAG)-dependent membrane remodeling reactions. DAG has been shown to be important for mitochondrial clearance through mitophagy but the

molecular mechanism of action remains elusive. Our results indicate that DAG can be incorporated in SMrTs such that it is accessible for proteins to monitor DAG-dependent membrane remodeling reactions. Moreover, we find that *de novo* DAG synthesis on the membrane template leads to changes in the membrane architecture.

Chapter 3 discusses the importance of DAG in Drp1-mediated membrane fission reactions on cardiolipin (CL)-containing templates. Our results indicate DAG facilitates not only recruitment of Drp1 on to the membrane surface but also aids in subsequent mechanochemical steps post membrane binding leading to fission. Moreover, this facilitatory role of DAG is also apparent on templates mimicking the mitochondria containing adapter proteins for Drp1.

The BAR domain-containing protein Endophilin B1 has been shown to be important for DAG-dependent mitophagy in mammalian cells. Endophilin B1 is an adaptor protein which has been shown to recruit the generic autophagic machinery to different organellar surface including mitochondria. However, the exact mechanism by which Endophilins get recruited to the mitochondria during mitophagy is not known. **Chapter 4** discusses how DAG helps recruit Endophilins on to CL-containing membranes. Additionally, Endophilin B1 and its related homologue Endophilin B2 shows DAG-dependent membrane tubulation reactions. Together these results help us understand the molecular basis for the importance of DAG during mitophagy.

Another form of mitochondrial quality control is through the formation of mitochondria-derived vesicles (MDVs). MDVs are 75-200nm vesicles that are formed from the mitochondria containing either one or both membranes of the mitochondria. MDV-generation usually happens in a short time span (1-2 hours) whereas mitophagy usually happens over days. MDVs have been shown to be involved not only in quality control and organelle maintenance but also other pathways like mitochondrial antigen presentation and peroxisome biogenesis. Although MDV formation seems to be a central pathway for multiple cellular processes, the membrane fission catalyst that helps in the formation of MDVs remained elusive.

Chapter 5 describes a biochemical screen that aims to find out fission catalysts that are involved in the formation of MDVs from the mitochondria. Our results show that brain lysate has a nucleotide-independent, CL-specific membrane fission catalyst. Biochemical separation followed by proteomic analyses showed that the Parkinson's Disease (PD)-related protein alpha-synuclein (α-Syn) is necessary for the fission activity in brain cytosol. Moreover, mammalian cell lines expressing the protein also shows a similar CL- and α-Syn-dependent

membrane fission reaction indicating a general ability of the protein to cause membrane fission irrespective of the source.

Chapter 6 aims to understand the biochemical properties of α-Syn that help it to engage with the membrane. Our results indicate that recombinantly purified α-Syn binds best to membranes containing the mitochondria-specific lipid CL. Moreover, it engages with the membrane in a curvature-dependent manner. Unsurprisingly, purified α-Syn is able to cause membrane fission of CL-containing membrane tubes suggesting that the protein is sufficient for this activity. Collectively, these results indicate a possible native function of the protein which for a long time has remained elusive.

α-Syn has mostly been studied in the context of PD. Mutations in the α-Syn gene leads to early-onset familial PD. **Chapter 7** aims to understand the effect of having familial mutations in membrane binding and remodelling activities of the protein. Our results show that PD-associated mutants of α-Syn have varied membrane-binding abilities. Interestingly, however, Parkinsonian mutants of α-Syn are defective in catalysing membrane fission linking neurodegeneration in patients containing such mutations to lack of membrane remodelling functions of α-Syn.

Chapter 8 attempts to understand the functions of α-Syn in a cellular context. For this we generated a α-Syn knock-out (KO) cell line using CRISPR-Cas9. Our results indicate that absence of α-Syn causes respiratory dysfunctions of the mitochondria. Specifically, mitochondria in α-Syn KO cells shows lesser oxygen consumption rate under basal and stress conditions. The KO cells also show an over-dependence on glycolysis for their energy requirements indicating sub-optimally functioning mitochondria. Quantitative proteomic analysis of wild-type and α-Syn KO cells showed that in the absence of the protein, the mitochondria shows an altered proteome indicating possible reasons for sub-optimal activity of these mitochondria.

Chapter 1:

Introduction

1.1 Mitochondrial stress and quality control mechanisms:

Mitochondria are double membrane-bound organelles which are involved in a plethora of cellular reactions. Mitochondria produce ATP through oxidative phosphorylation making it the primary energy generator of the cell. Apart from this, mitochondria are involved in maintaining redox equilibria, phospholipid biosynthesis, Ca2+ homeostasis, innate immune signaling and apoptosis (Spinelli and Haigis, 2018). All these reactions are central to cellular physiology and survival making it one of the most utilized organelles in the cell. As such, mitochondria become prone to different kinds of stress resulting in dysfunction or damage of the organelle.

The most common form of mitochondrial stress is a loss of H^+ potential across the inner mitochondrial membrane (IMM). Small molecules like Rotenone or Antimycin A which targets specific complexes of oxidative phosphorylation ends up disrupting the proton gradient in the mitochondria. Protonophores like carbonyl cyanide 3-chlorophenylhydrazone (CCCP) can totally abolish the proton gradient directly leading to mitochondrial stress. Disruption of proton gradient leads to sub-optimal functioning of the mitochondria which leads to the activation of mitochondrial quality control pathways.

Apart from the loss of proton gradient, hypoxia is a physiologically relevant mitochondrial stress trigger (Solaini et al, 2010). Hypoxia, which is caused by unavailability of oxygen leads to the disruption of normal mitochondrial functions and a global change in gene expression leading to the dependence on glycolysis for energy production. Mitochondria also performs a lot of redox reactions which leads to the stabilization of multiple reactive oxygen species (ROS). Mitochondria have ways to get rid of ROS since they are very detrimental to cell physiology as they can lead to oxidation of several classes of biomolecules like protein, lipids and nucleotides. These lead to dysfunction of the mitochondria and require the activation of quality control pathways to get rid of them.

Mitochondria imports nascent polypeptide chains inside it through multiple protein complexes situated in both the membranes of the organelle (Samluk et al, 2018). These nascent polypeptide chains are folded inside the mitochondria with the help of mitochondrial chaperones and any form of dysregulation in mitochondrial protein folding can cause the accumulation of these misfolded proteins leading to the activation of different mitochondrial quality control pathways to mitigate the stress.

Since mitochondria are prone to encountering different kinds of insults, cells have devised diverse but overlapping processes to relieve mitochondrial stress through different quality control mechanisms (Fig. 1.1). There are multiple protein quality control checkpoints that act prior to and after the import of nascent polypeptide chains in the mitochondria (Ruan et al, 2020). These include processes like mitochondria-associated degradation (MAD) and the utilization of the ubiquitin-proteasome (UPS) system for degradation of misfolded or stalled polypeptide chains within the mitochondrial import complexes. For the purpose of this thesis, I will restrict myself to discussing in detail the organellar quality control mechanisms. This includes mitophagy and the formation of mitochondria-derived vesicles (MDVs).

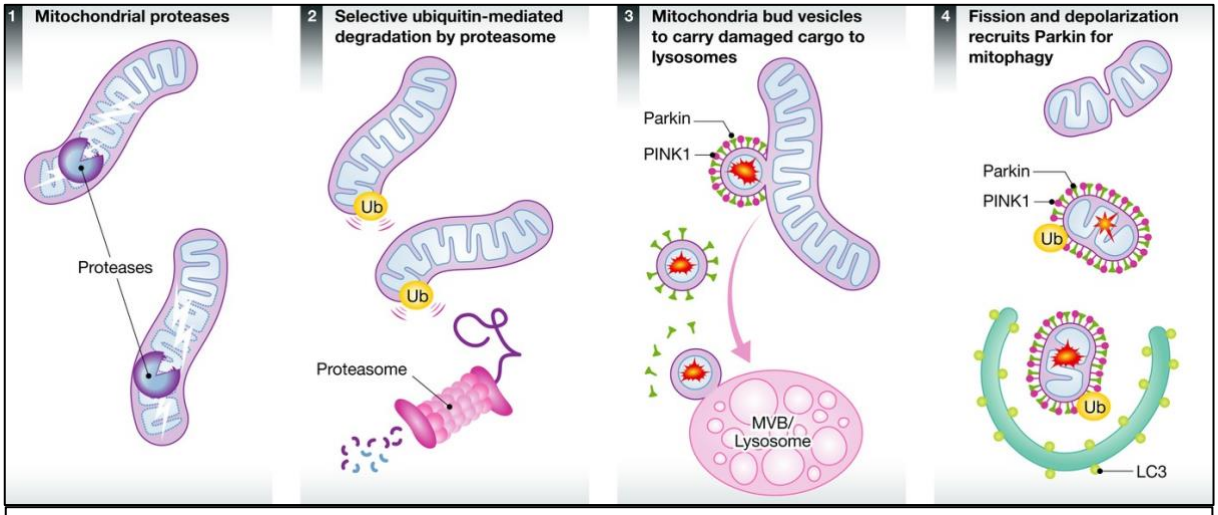

Figure 1.1- General pathways of mitochondrial quality control. (1) Mitochondrial proteases take care of misfolded or aggregated proteins within the mitochondria. (2) Ubiquitin-proteasome system selectively degrades proteins from the OMM. (3) Mitochondria-derived vesicle formation that targets damaged components of the mitochondria to the lysosomes for degradation. (4) PINK1-Parkin mediated mitophagy that degrades parts of the network upon loss of membrane potential. Reproduced from Sugiura et al, 2014.

1.2 Mitophagy:

Autophagy is the general process of nutrient recycling by which cells degrade macromolecules and organelles under different physiological conditions for their reutilization. This usually involves encapsulation of macromolecules or organelles within a membrane-bound compartment (called autophagosome) which is targeted eventually to the lysosomes for degradation. Quality control of the mitochondria is done similarly by selectively degrading the damaged portions of organelle which is referred to as mitophagy.

Mitophagy is absolutely essential for the maintenance of a healthy and functional mitochondrial network. Proteins involved in mitophagy have often been associated with

multiple neurodegenerative diseases like Alzheimer's disease (AD), Huntington disease (HD) and Parkinson's disease (PD) (Kitada et al., 1998; Valente et al., 2004, Ye at al., 2015, Khalil et al., 2015) thus, directly linking mitochondrial quality control to neurodegeneration, however, exact mechanisms linking both still remain elusive.

Cells usually carry out mitophagy at a basal rate which is often upregulated in response to environmental cues (Lee et al, JCB, 2018). These environmental cues can be differentiation or stem-cell pluripotency (Takano-Ohmuro et al., 2000; Diwan et al., 2007), hypoxia (Tracy et al 2007) or oocyte fertilization (Shitara et al, 2000). All these processes involve degradation of the entire organelle or selective parts of the organelle by recruiting a series of mitophagy adaptors to the surface of the organelle. These adaptors, in turn, recruit the autophagosome machinery on the mitochondrial surface leading to the engulfment of the organelle within the autophagosome.

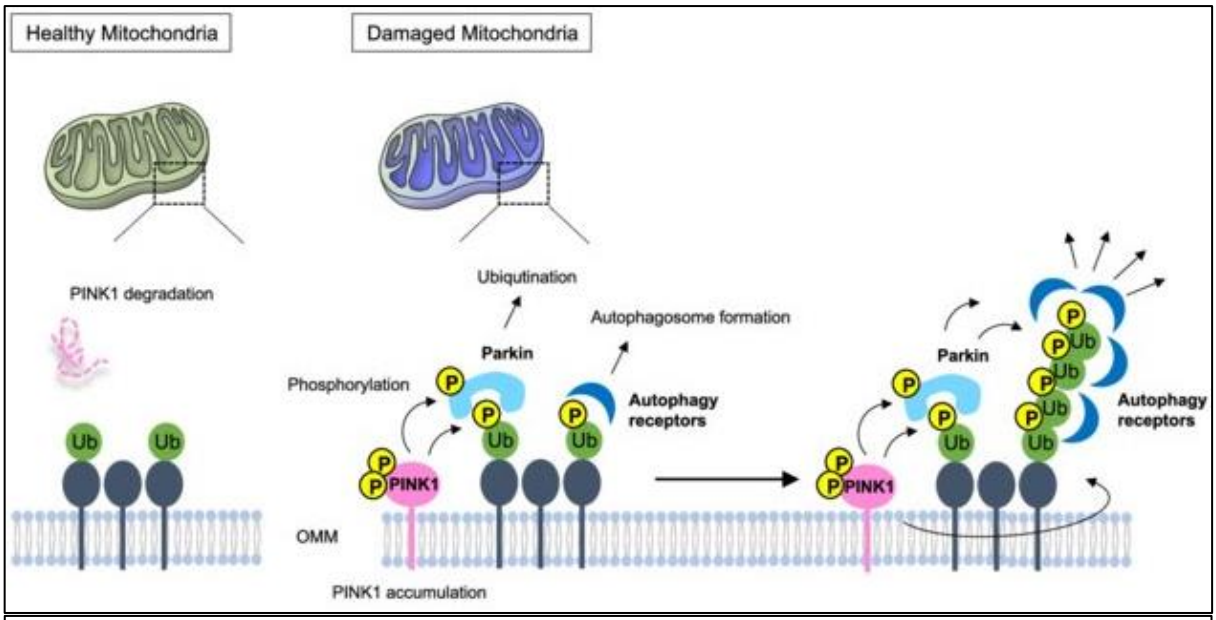

Figure 1.2- PINK1-Parkin dependent mitophagy. In a healthy mitochondria PINK1 is actively degraded which does not allow it stably associate with the mitochondria. However, in a damaged mitochondria which has lost its potential, PINK1 accumulates leading to the recruitment and phosphorylation of Parkin. Parkin ubiquitinylates OMM proteins leading to the recruitment of autophagy receptors on the mitochondria and subsequent sequestration within autophagosome. Adapted from from Sekine and Youle, 2018.

In mammalian cells, the molecular mechanism of mitophagy is usually divided into two pathways based on the recruitment of the kinase PINK1 and the associated E3 ubiquitin ligase Parkin: PINK1/Parkin-dependent and PINK1/Parkin-independent mitophagy. The PINK1-Parkin dependent mitophagy is the most extensively studied (Figure 1.2). PINK1 is a kinase

which is recruited to the mitochondria under basal conditions whereby it gets processed by mitochondrial proteases MPP and PARL upon which it is retro-translocated to the cytosol for degradation (Sekine and Youle, 2018). However, upon potential loss, PINK1 gets stabilized on the OMM surface, undergoes autophosphorylation and subsequently recruits and phosphorylates Parkin on the mitochondria. Phosphorylation of Parkin makes it active whereby it can ubiquitinylate proteins on the OMM. Ubiquitinylated OMM proteins recruits mitophagy adapters like OPTN and NDP52 which on the other hand binds to LC3 and GABARAP subfamilies of proteins on the autophagosomal membrane. This ends up recruiting the autophagosomal membrane to the mitochondria surface.

In PINK1/Parkin-independent mitophagy, OMM tethered proteins like BNIP3, BNIP3L and FUNDC1 are activated by phosphorylation, in turn, increasing their affinity for LC3/GABARAP like proteins (Yoo and Jung, 2018). In germline cells paternal mitochondria is exclusively degraded which happens in a NIP3-like protein X (NIX)-dependent manner (Ney et al, 2015). NIX has a cytosol-facing WXXL-like motif which is essential for it to bind LC3 and GABARAP. These mitophagy adapters thus end up recruiting the LC3-positive autophagosomal membrane to the mitochondrial surface promoting clearance of the organelle.

1.2.1 Mitochondrial fission and mitophagy:

Mitochondria in cells exist in an equilibrium between long reticular tubules and short fragmented units. Depending upon nutrient availability or environmental cues, mitochondria can exist as a completely fused reticular network or entirely fragmented into micron-sized entities in the cell (Youle and van der Bliek, 2012). The interplay between fused and fragmented states is brought about by a repertoire of proteins involved in mitochondrial fission and fusion. Fusion of the mitochondria is brought about by transmembrane proteins belonging to the dynamin superfamily like mitofusins (Mfn1/2) on the OMM and Optic atrophy 1 (Opa1) in the IMM. Mitochondrial fission, on the other hand, is dependent on yet another dynamin superfamily protein Dynamin related protein 1 (Drp1) along with its adapters on the OMM surface like mitochondria fission factor (MFF), Mid51 and Mid49 (Krauss et al, 2021).

Since mitochondria can exist as long tubular networks within cells, it poses an obvious problem for organellar quality control. How do cells specifically get rid of damaged parts of an organelle which exists as a reticular network? Hence, fission seems to an essential pre-requisite for efficient organelle clearance. In fact, Dnm1, the yeast orthologue of Drp1 has been shown to be absolutely necessary for mitophagy in yeast (Kanki et al, 2009). Dnm1 has been shown to interact with Atg11, a scaffolding protein that helps recruit other members of the Atg

family to the mitochondrial surface suggesting autophagic proteins work in concert with the fission apparatus to bring about efficient organelle clearance. In mammalian cell lines, downregulation of Drp1 activity has been shown to inhibit Parkin-dependent mitophagy (Tanaka et al, 2010). Consistent with this, in B-cells, mitophagy is severely downregulated in the presence of a dominant-negative Drp1 suggesting Drp1 functions are essential for mitophagy (Twig et al, 2008). Drp1 has also been shown to be involved in hypoxia-induced mitophagy by interacting with FUNDC1, a LC3-binding protein (Wu et al, 2016). Together, these reports suggest a necessary role for Drp1-mediated mitochondrial fission in regulating mitophagy.

Although, Drp1 is crucial for mitochondrial fragmentation during mitophagy, the exact cue for Drp1 to engage with the mitochondria to cause fission during mitophagy is not known. Drp1 has been shown to engage with the mitochondria at pre-defined sites marked by contact sites with organelles like the ER and lysosomes (Krauss et al, 2021). However, not every ER or lysosome contact site with the mitochondria undergoes division indicating that contact sites are necessary but, likely, not sufficient for mitochondrial fission. Moreover, if fission during mitophagy affects the entire network or is a localized event only at sites which have damaged mitochondria is not known as well. In the first part of this thesis, I have tried to address the role of a particular lipid, diacylglycerol (DAG), in regulating Drp1 functions during mitophagy. DAG has been known to get generated in the mitochondria in response to mitophagic cues, however, the exact molecular mechanism by which DAG promotes mitophagy was not known (Lin et al, 2022). The thesis tries to address the molecular mechanisms by which DAG promotes mitochondria division during mitophagy.

1.3 Mitochondria-derived vesicles (MDVs):

As the name suggests, mitochondria-derived vesicles (MDVs) are vesicular structures which are about 50-200nm in diameter emanating from the mitochondria (Sugiura et al, 2014). While mitophagy is a way to get rid of large portions of mitochondria which happens in the time scale of multiple hours to days, MDVs are considered a much quicker response which sort and release cargo from the mitochondria within a couple of hours under both basal conditions and in response to a stress (Soubannier et al, 2012). Moreover, MDVs can be single or double-membrane bound compartments and are thought to be cargo-selective (Fig 1.3).

MDVs were initially discovered as membrane-bound transport carriers that ferries the OMM protein mitochondria-anchored protein ligase (MAPL) to the peroxisome (Neuspiel et al, 2008). These vesicles are cargo-selective and excluded another outer membrane protein

Tom20. The vesicles were generated in a Drp1-independent manner and finally fused to SKL-positive peroxisomes. Subsequently, multiple reports have established different destinations for MDV-mediated delivery of mitochondrial cargos *viz*. to the lysosomes and the plasma membrane. MDVs are generated from the mitochondria during mitochondrial antigen presentation at the plasma membrane, an essential step in distinguishing normal and diseased cells. The initial mitophagy machinery like PINK1 and Parkin inhibits the formation of these carriers, whereas, Rab9 and Sorting nexin 9 are known to promote the formation of these MDVs (Matheoud et al, 2016).

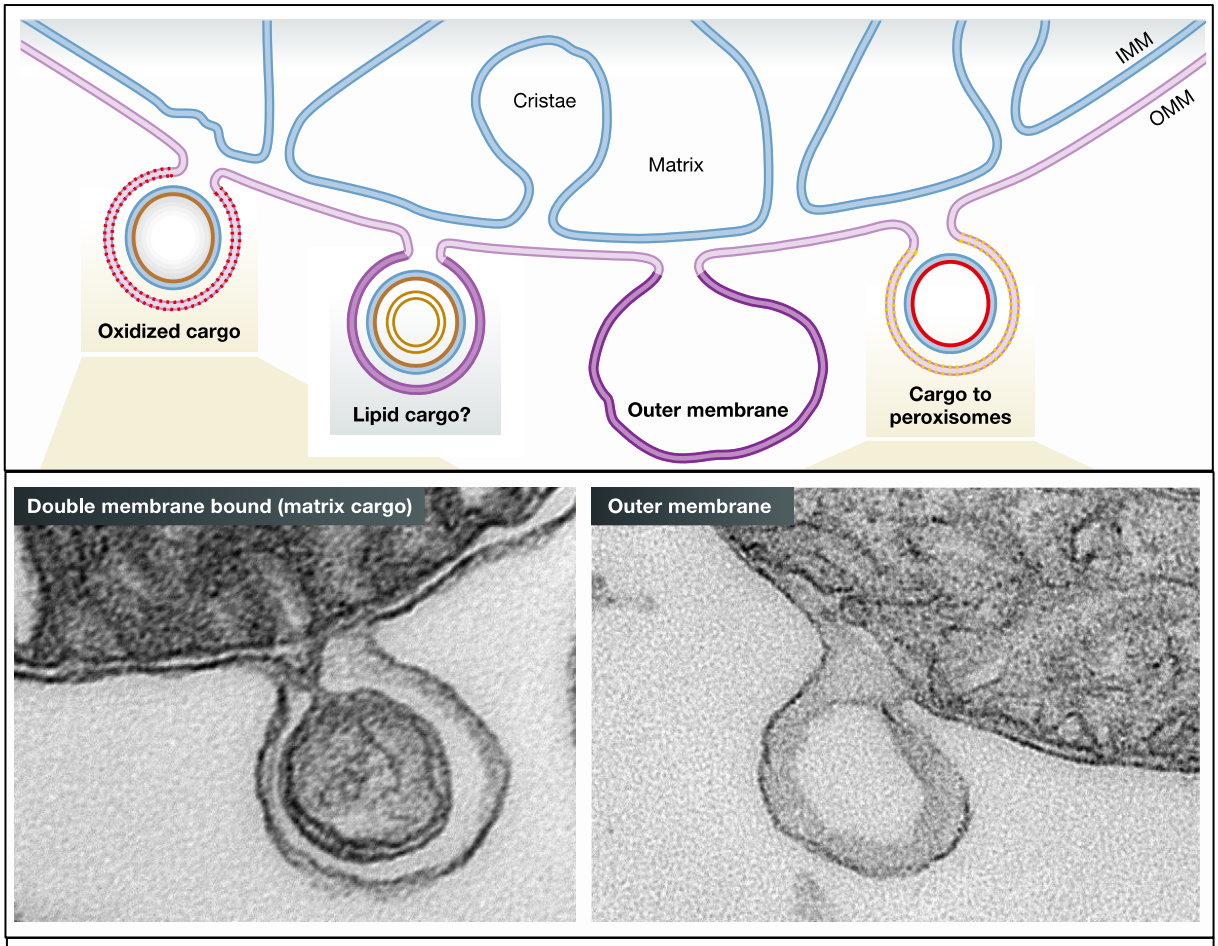

Figure 1.2- Mitochondria-derived vesicles (MDVs). MDVs contain different cargos that are destined for different regions in the cell. Moreover, they can also contain one or both mitochondrial membranes and is implicated in the release of oxidized/dysfunctional products of the mitochondria that are targeted to lysosomes for degradation. Adapted from Suguira et al, 2014.

The transport of cargo to the lysosomes is especially intriguing in the context of quality control of the organelle. Mitochondria carry out multiple redox reactions across the IMM during oxidative phosphorylation. This results in the generation of reactive oxygen species

(ROS). Mitochondria have enzymes like superoxide dismutase and catalase that specifically neutralize ROS. However, ROS is extremely detrimental to cells because it can irreversibly modify biomolecules leading to their loss of function. Oxidative stress is one of the leading ROS generators in a cell. Induced oxidative stress generated through change in carbon source from glucose to galactose or by enzymatic action leads to the production of cargo-selective MDVs in Cos7 cells (Soubannier et al, 2012). These vesicles ultimately fused with lysosomes in a ATG5 and LC3-independent manner suggesting the pathway to be distinct from canonical mitophagy. Reconstitution experiments showed that vesicles can be generated from isolated bovine heart mitochondria in response to oxidative stresses like Antimycin A or Xanthine oxidase (Soubannier et al., 2012). Ultrastructure analysis confirmed the presence of both single and double-membrane bound vesicles generated upon oxidative stress likely indicating different ways of MDV formation and cargo incorporation. These vesicles carry oxidised cargo and are cargo-selective depending on the kind of oxidative stressor used. Proteomic analysis of MDVs generated in vitro showed various subunit of complexes associated with oxidative phosphorylation are selectively enriched in the MDVs (Vasam et al, 2021). Furthermore, MDVs also contained different metabolic enzymes associated with the TCA cycle and fatty acid metabolism, Fe-S cluster containing proteins, redox enzymes and autophagy related proteins. Together, these reports indicate that induction of oxidative stress leads to the formation of transport carriers from the mitochondria selectively carrying oxidised cargo which are destined to the lysosome for degradation.

1.3.1 Membrane fission during MDV biogenesis:

MDVs are generated from the mitochondria under basal condition and during stress responses. However, the membrane fission catalyst that helps release these vesicles from the mitochondria remains unknown. Drp1, the canonical mitochondrial membrane fission catalyst has been shown to be not involved in the formation of these transport carriers from the mitochondria (Soubannier et al, 2012, Neuspiel et al, 2008, Matheoud et al, 2016). Moreover, addition of GTPgS, a slowly hydrolysing GTP analog which kills Drp1 functions, was shown to not affect MDV generation *in vitro* from purified mitochondria indicating Drp1 or any Dynamin subfamily protein, likely, is not involved in the formation of these vesicles (Soubannier et al, 2012). This begs an interesting question about the identity of the membrane fission catalyst that helps in the formation of these vesicles from the mitochondria. In the later part of the thesis, I have tried to design a biochemical screen using Supported Membrane templates (SMrT) to identify and characterize the fission catalyst that likely is involved in the

formation of these transport carriers and also tried to understand the physiological significance of this fission reaction in the cell.

Chapter 2:

Supported membrane templates (SMrT) as an assay system to analyze CL and DAG-dependent membrane remodeling reactions

2.1 Introduction:

Mitochondria exists in a dynamic equilibrium between fused and fragmented states. As stated earlier, mitochondria need to undergo fission for efficient mitophagy to happen. While much is known about the role of protein assemblies that regulate fission, the influence of particular lipids in this process remains poorly understood. This is partly due to the significant challenges associated with changing lipid composition on an organellar surface and monitoring its effect on protein assemblies. Moreover, unlike most other organelles in a eukaryotic cell, mitochondria are made up of two membranes, outer and inner, having distinct lipid compositions and particularly enriched in unique glycerophospholipids like phosphatidylglycerol (PG) and cardiolipin (CL). CL accounts for about 20% of the total IMM lipids and 1-10% of OMM lipids (Horvath and Daum, 2013, Konig et al, 2021). CL is absolutely essential for mitochondrial functions including maintaining network morphology. Moreover, CL has been reported to have some unique roles in mitochondrial quality control mechanisms. CL externalization to the OMM has been shown to be necessary for mitochondrial clearance through mitophagy (Chu et al, 2013). Additionally, the autophagy adapter LC3 has been reported to directly bind CL suggesting CL externalization can act as potential 'eat-me' signal of the mitochondria. CL is also necessary for Drp1 functions. CL promotes membrane binding and stimulates GTPase activity of Drp1 (Bustillo-Zabalbeitia et al., 2014, Macdonald et al., 2014). CL is also essential for Drp1-catalyzed membrane fission (Kamerkar et al, 2019, Mahajan et al, 2021).

Other mitochondrial lipids like ceramide and sphingosine-1-phosphate (S1P) have also been implicated in mitophagy. S1P has been reported to directly bind to prohibitin 2 (PHB2) (Strub et al, 2011). PHB2 is a mitochondrial chaperone which also functions as a mitophagy adapter. Moreover, both ceramide and S1P has been shown to regulate the lipidation of LC3B (Sentelle et al, 2012). Being a center for phospholipid biosynthesis in the cell, mitochondria also contain low abundance regulatory glycerophospholipids like phosphatidic acid (PA) and diacylglycerol (DAG). These lipids are essential intermediates in lipid synthesizing pathways which have been reported to have regulatory roles in maintaining mitochondrial morphology (Frohman, 2015; Kameoka et al., 2018). PA has been shown to stimulate Mfn1/2-mediated mitochondrial fusion (Choi et al 2006, Zhang et al, 2016) and inhibit Drp1 functions in cells (Adachi et al, 2016). DAG, on the other hand, promotes mitochondrial fission (Huang et al., 2011, Adachi et al, 2016). DAG has been shown to be generated on mitochondria in response to addition of mitophagy-inducing agents (Lin et al., 2022). DAG generation is important for mitochondrial clearance through mitophagy since, loss of Lipin1 activity, the enzyme which

makes DAG from PA, leads to lesser clearance of the organelle. Together, these reports suggest that DAG is essential for mitophagy, however, the molecular mechanism remains to be understood.

DAG is a bioactive lipid which usually make up very small proportions of cellular membranes and often perform regulatory roles in diverse signalling pathways like lipid metabolism and neurotransmission (Goni and Alonso, 1999). *In vitro*, DAG has been shown to affect bilayer properties of the membrane. The spontaneous curvature of a lipid membrane decreases with increasing DAG content (Leikin et al, 1996). Moreover, increased DAG content increases the bending rigidity of a bilayer. Simulation studies have shown that at low relative concentration within the membrane, DAG behaves like other glycerophospholipids with their glycerol head-group facing water and the acyl chains tucked in the hydrophobic core of the membrane. However, in membranes containing high relative amount of DAG, it tends to form lens like phases within two leaflets of membranes leading to relatively lower DAG exposure on the membrane surface (Campomanes et al, 2019). The acyl chains of DAG also has been shown to be important for functioning of the protein. Saturated side chains of DAG has been shown to be ineffective for protein kinase C (PKC) activation whereas mono- or poly-unsaturated chains can cause PKC activation on phospholipid membranes *in vitro* (Mori et al, 1982). Together, these reports suggest that DAG is a unique lipid which not only is involved in mitophagy but also changes bulk membrane properties which can lead to recruitment and membrane remodelling by effector proteins. This led us to test if DAG is directly involved in regulating Drp1 functions.

To test the effects of DAG on Drp1 functions, we used a reconstitution setup aimed at directly relating changes in lipid composition to protein functions. Supported Membrane templates (SMrT) provide an unique advantage in this case as it helps to monitor these membrane remodelling reactions in real-time (Dar et al, 2017). SMrT are made up of an array of membrane tubes connected to a planar bilayer. As such, it mimics varied membrane topologies which proteins usually encounter on a mitochondria. Furthermore, SMrT has been utilised previously to follow membrane fission reactions catalyzed by Dynamin and Drp1 in real-time (Dar et al, 2015, Kamerkar et al 2019). These led us to utilise SMrT as an assay system to monitor DAG-dependent membrane remodelling reactions. Our goal was to set up a membrane assay system containing DAG and CL and test the effects of DAG addition/in-situ DAG generation on template properties.

2.2 Materials and Methods:

2.2.1 Cloning, expression and purification of proteins:

6xHis-mEGFP-*Mm*PKD^{C1a} (C1a domain (^{C1a}) of *Mus musculus* (*Mm*) protein kinase D (PKD), Residues 134-198) was used as a low-affinity DAG sensor. Bacillus cereus PI-PLC (6xHis-*Bc*PI-PLC) was used as the PI to DAG converting enzyme. Both were cloned into a pHGT-2 vector using BamHI and NotI restriction sites. Briefly, the pHGT-2 plasmid has been derived from the pRSFDuet-1 backbone (Novagen), additionally containing an N-terminal 6xHis-GB1 solubility tag along with a tobacco etch virus (TEV) cleavage site. Both the constructs were transformed in NiCo21 (DE3) competent cells and grown in suspension culture for 36-40 hours in autoinduction media at 18°C. Cells were pelleted down at 6000g and stored at 4°C for future use. Pellets were thawed and resuspended in lysis buffer (20mM HEPES pH 7.4, 500mM KCl, 1mM phenylmethanesulfonyl fluoride, 10mM imidazole), lysed by sonication and spun at 30000g for 20 minutes to get rid of un-lysed cells and insoluble contents. The soluble pool was loaded on HiTrap Chelating column (5ml), washed extensively with the lysis buffer and then exchanged for assay buffer (20mM HEPES pH 7.4, 150mM KCl). Elution was done using the assay buffer in a gradient of imidazole (10mM-300mM). The eluants were run on a gel and the fractions containing the relatively pure proteins were pooled together and stored at 4°C for 3-5 days during which all assays were carried out. All proteins were spun at 100,000g for 30 minutes to get rid of aggregates before using in assays.

2.2.2. Supported Membrane Templates (SMrT) assay:

Dioleoyl-phosphatidylcholine (DOPC) (Avanti Polar Lipids), bovine heart cardiolipin (CL; Avanti Polar Lipids), dioleoylglycerol (DOG; Avanti Polar Lipids), liver phosphatidyl inositol (PI; Avanti Polar Lipids) and Texas Red™ 1,2-dihexadecanoyl-*sn*-glycero-3-phosphoethanolamine (TR-DHPE; Invitrogen) were aliquoted in their desired respective molar ratios in chloroform to a final total lipid concentration of 1 mM. Supported Membrane templates were formed by spotting 2µl of the lipid mix on a pegylated glass coverslip (PEG 400 or PEG 8000). The coverslip was dried and assembled in an FCS2 chamber (Bioptechs). The chamber was attached to a pump and assay buffer was allowed to flow through. The flow of buffer spontaneously converts the lipids to membranes and the sheer force of buffer flow helps extrude tube. The region on the coverslip where the lipids were spotted initially forms the planar bilayer. For 6xHis-mEGFP-*Mm*PKD^{C1a} experiments, 10µM of the protein was flowed in, incubated for 10 minutes, excess protein washed off and images were recorded in both channels (membrane and protein). For experiments with *Mm*BcPI-PLC (WT and H32A),

templates were incubated with 1µM final concentration of the protein for 30mins followed by washing off excess unbound protein prior to addition of 10µM 6xHis-mEGFP-*Mm*PKD^{C1a}. The templates were incubated with 6xHis-mEGFP-*Mm*PKD^{C1a} for 10minutes, excess protein was washed off and templates were imaged both in the protein and membrane channel.

2.2.3 Fluorescence microscopy, statistical analyses and tube radius estimation:

All images were acquired in Olympus IX83 inverted fluorescence microscope attached to a stable LED light source (CoolLED) and an Evolve 512 EMCCD camera (Photometrics). Image acquisition was done using Micro-manager software and rendered using Fiji (version 2.1.0/1.53c). All graphical representations and statistical analyses were carried out on GraphPad Prism 9 using tests as mentioned in the figure legends. Tube size estimation was done as mentioned previously (Dar et al, 2017). Briefly, images were taken of the planar membrane patches and tubes before addition of protein. These unilamellar patches were used to calculate a calibration constant (K1) by equating membrane area with integrated fluorescence intensity. This calibration constant was then used to estimate radii of starting tubes assuming them to be a cylinder (Area=2.Π.r.l , where 'r' is the radius of the tube and 'l' is the length of the ROI on the tube). These starting tube radii estimates were then equated to maximum fluorescent intensity of the tube to get another calibration constant (K2). Pixels in fluorescent micrographs after the addition of the protein were divided by K2 to convert them to tube radii. For membrane density estimation of GFP-tagged proteins, after background correction of images, the mean fluorescence intensity of an identical line drawn on the membrane channel and protein channel along the tube was reported as a ratio.

2.3 Results:

2.3.1 Supported membrane templates to analyze DAG-dependent membrane remodeling reactions

Bulk estimation of total phospholipids in mammalian cells showed that PI constitutes about 5-10% of total phospholipids of the mitochondria. Unlike CL, PI is distributed preferentially on the OMM where it makes up ~9-13% of the total OMM lipids whereas IMM has relatively lesser PI content (~2-5% of total IMM lipids). In order to recreate the scenario of induced recruitment of PI-PLC to the OMM, we made SMrT containing moderate levels of 5% DAG or 5% PI in a background of 15% CL and rest dioleoyl phosphatidylcholine (DOPC). Lipid mixtures were doped with 1% of a fluorescent lipid probe (Texas Red™ 1,2-dihexadecanoyl-*sn*-glycero-3-phosphoethanolamine**;** TR-DHPE) for visualization under

fluorescence microscope. Notably, the lipid mixes were spotted on a PEGylated glass coverslip, allowed to evaporate the solvent and then assembled in a flow cell. Flow of buffer through the flow cell led to the generation of stable templates with characteristic planar bilayers at the source and an array of parallel membrane tubes connected with it (Fig 2.1 A, B, D). Thus, incorporation of PI or DAG did not interfere with the ability of the lipid mixture to get hydrated with a water-based buffer and formed stable templates for monitoring protein activity.

Next, we wanted to directly visualize DAG distribution on our templates. We utilised a well-known DAG sensor consisting of the C1a domain of protein kinase D tagged to mEGFP (mEGFP-MmPKD^{C1a}) as a DAG-sensor (Maeda et al., 2001; Baron and Malhotra, 2002). Addition of the sensor to both 5%PI and 5%DAG-containing templates showed that it selectively bound to DAG-containing membranes and not PI-containing membranes (Fig 2.1 B-E). Together, these results suggest two things: first, that the DAG sensor specifically recognizes DAG and does not passively associate with membranes containing any lipids. Second, it pointed to the fact that the DAG on these templates are accessible for protein binding.

2.3.2 In situ DAG generation and its effects on membrane properties:

DAG has been shown to affect bulk membrane properties like bending modulus and intrinsic curvature (Das and Rand, 1986; Leikin et al., 1996). This is attributed to the fact that DAG is a conical lipid owing to its smaller head-group and a relatively bulky acyl tail. This results in DAG inducing packing defects in membranes at low concentrations and phase separates to cause local membrane deformations at high concentrations (Vamparys et al., 2013; Campomanes et al., 2019). This led us to question if *in situ* generation of DAG can cause a spontaneous change in membrane curvature. For this we utilised a bacterial phosphatidyl inositol specific phospholipase C (Bacillus cereus (Bc)PI-PLC) to convert PI to DAG on SMrT. The purified protein was added to templates made of 5%PI , incubated for 30mins and then excess unbound protein was washed off (Fig 2.1 F, G). Subsequent addition of the DAG sensor showed that DAG was indeed produced on templates incubated with the wild-type BcPI-PLC and not with the catalytically inactive BcPI-PLC^{H32A} mutant. Importantly, the templates were stable after lipid head-group conversion reaction and were amenable for protein binding as indicated by the DAG-sensor binding. A paired analysis of tube sizes before and after formation of DAG showed a minute, but significant, 1.5 fold increase in tube dimension as compared to a condition which does not generate DAG (Fig 2.1 H). Thus, acute production of DAG on membrane tubes leads to a systemic expansion of tube radius. Together, these results indicate

that stable templates can be formed with DAG/PI and CL which are amenable to head-group modification reactions.

2. 4 Discussion:

DAG is an important regulatory lipid with proposed roles in mitochondrial quality control. Here, using a system of supported membrane templates (SMrT), we show that incorporation of DAG (with both chains monounsaturated: di-oleoyl glycerol) in lipid mixtures does not interfere with the formation of either planar bilayers or membrane tubes. This is expected because of the use of dioleoyl versions of the lipid which makes it fluidic in nature at RT. The templates generated stay stable even after protein addition and does not show any obvious defects in either bilayers or tubes. Previous reports have indicated that DAG at higher concentrations within membranes can phase separate and aggregate to form lens within the two leaflets of the bilayer (Campomanes et al., 2019). However, our experiments with the DAG sensor flown on 5%DAG-containing templates clearly showed that the DAG was exposed on the membrane tubes and bilayers and available for protein binding. However, if the acyl chain length of DAG can significantly alter its properties of solvent exposure remains to systematically tested.

DAG has been suggested to induce negative spontaneous curvature in membranes owing to its conical shape. However, our results with *in situ* DAG generation on the templates using BcPI-PLC showed that, DAG production causes a small but significant increase in tube dimension. It is important to mention that the design of the assay limits the accessibility of the enzyme only to the outer leaflet of the bilayer and, as such, the lipid head-group modification reaction only happens on that leaflet of the bilayer. Hence, after BcPI-PLC treatment, the tubes had DAG generated only on the outer leaflet making them quite different from tubes made of DAG which will likely have equal DAG distribution across both leaflets. Even though DAG has been reported to have a high rate of transbilayer flip-flop movement, how much of that happens in our assay system during 30 minutes of incubation with BcPI-PLC remains to be addressed (Bai and Pagano, 1997).

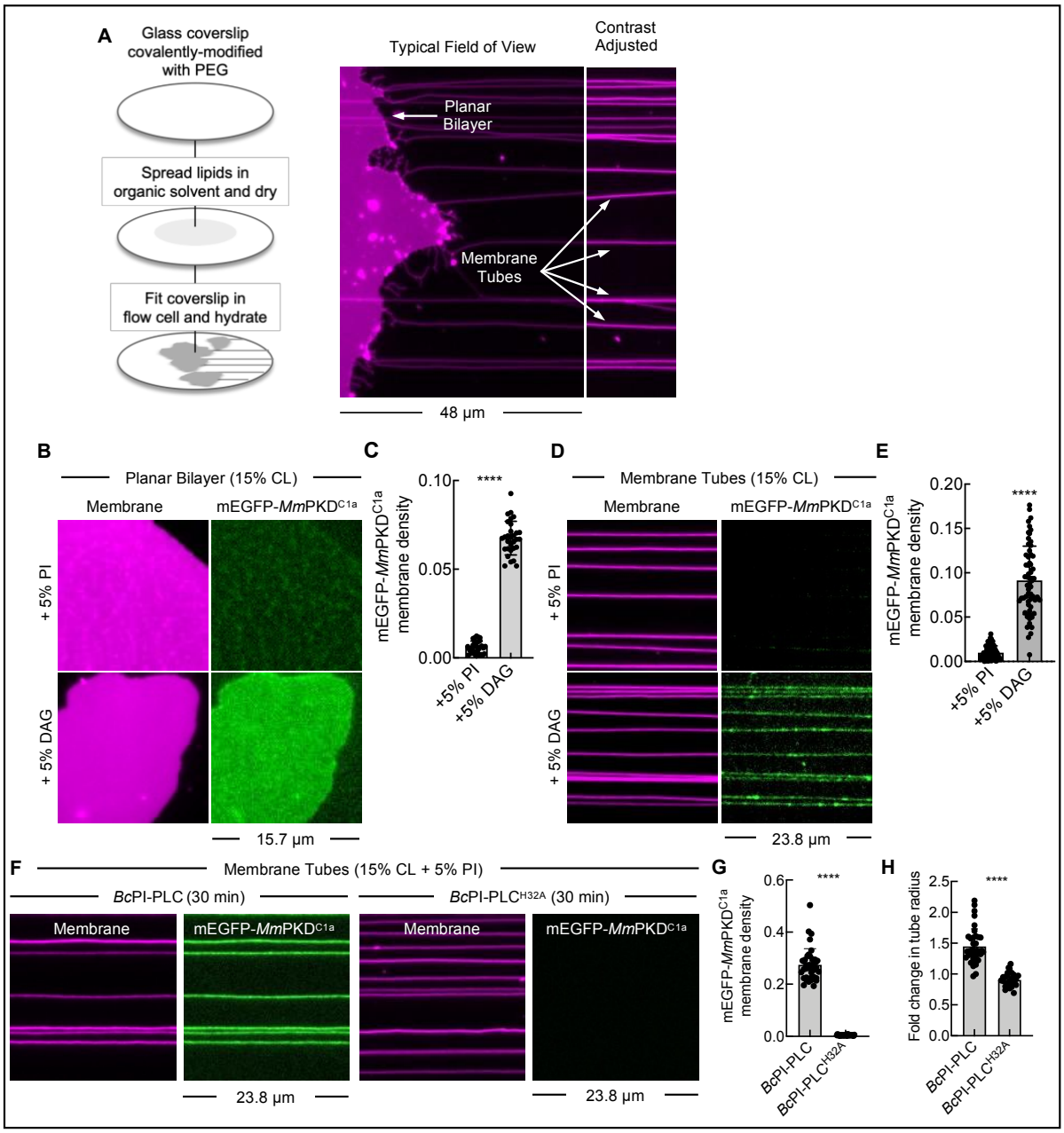

Figure 2.1- Supported Membrane templates as an assay to monitor DAG-dependent membrane remodeling reactions. (A) Schematic of supported membrane templates and a representative image of planar bilayers and curved tubes. Representative fluorescent images of planar membrane patches (magenta) (B) and curved membrane tubes (D) of the indicated lipid composition in the presence of the DAG sensor (mEGFP-*Mm*PKD^{C1a}) (green). Quantitation of DAG sensor membrane density on bilayers (C) and tubes (E). Data represents at least 30 patches of the planar bilayer and 60 tubes for each lipid composition. (F) Representative fluorescent images of tubes (magenta) of indicated lipid composition after 30 mins incubation with BcPI-PLC or BcPI-PLC^{H32A} followed by incubation with DAG sensor (green). (G) Quantitation of mEGFP-*Mm*PKD^{C1a} membrane density after incubating templates with wild-type or catalytically defective BcPI-PLC. Data represents mean ± SD of at least 30 tubes for each protein. (H) Fold change in tube radius after incubating tubes with BcPI-PLC or BcPI-PLC^{H32A}. Data represents mean ±SD of at least 26 tubes for each protein. All statistical significance is estimated using the Mann-Whitney test.

Chapter 3:

DAG facilitates Drp1-catalyzed membrane fission

3.1. Introduction:

Mitochondria undergo constant cycles of fission and fusion that are absolutely critical for the maintenance of organellar function. Fusion of mitochondria leads to the formation of a reticular network whereas fission leads to the fragmentation of the network. Mitochondrial fission is essential for organelle inheritance and stress responses (Ishihara et al, 2009). Moreover, mitochondrial fission has been shown to be absolutely critical for mitochondrial clearance during mitophagy both in yeast and mammalian cells.

Mitochondrial fission is brought about by the action of Dynamin-related protein 1 (Drp1) (Krauss et al, 2021). Loss of Drp1 leads to embryonic lethality in mice (Ishihara et al, 2009). Depletion of Drp1 in adult mice muscle cells leads to lack of energy production, swollen mitochondria and poor Ca2+ signalling making the muscles undergo atrophy and degeneration (Favaro et al., Nat Comms., 2019). Cultured mammalian cells can survive without Drp1, however, it leads to pronounced defects in several cellular functions including proliferation, secretion and anti-tumour responses (Hennings et al, Endocrinology, 2018, Simula et al, Cell Reports, 2018).

Drp1 acts in concert with multiple accessory partners to bring about mitochondrial fission. Most important among these are Drp1 adapters which are transmembrane resident OMM proteins that help recruit Drp1 to the mitochondrial membrane surface. In addition to adapter proteins, mitochondrial fission requires the concerted action of multiple organelle contact sites of the mitochondria like with the ER and lysosomes (Friedman et al., 2011, Wong et al, 2018). Cytoskeletal components like the actin machinery and its regulatory proteins have also been implicated in mitochondrial fission (Moore et al, 2016). All these factors come together and work in concert to define a constricted mitochondria which is acted upon by Drp1 to cause mitochondrial fission.

Drp1 is a member of the dynamin superfamily of large GTPases (Kraus et al, 2021). It has a N-terminal G domain followed by a stalk domain and an unstructured variable domain (VD). The G domain catalyses GTP hydrolysis; the stalk domain is essential for oligomerization on the membrane and the VD is necessary for membrane binding. *In vitro*, Drp1 has been shown to bind to the mitochondria-specific lipid CL. Upon membrane binding it oligomerizes with other subunits on the membrane leading to a stimulation of its GTPase activity like other dynamin superfamily proteins. Previous studies from our lab has shown that Drp1 is sufficient to cause fission of CL-containing membrane tubes (Kamerkar et al., 2019).

Given the importance of Drp1-catalyzed mitochondrial fission in mitophagy added to the fact that DAG generation causes robust mitochondrial fragmentation, we wondered if DAG can directly regulate Drp1 functions.

3.2 Materials and Methods:

3.2.1 Cloning, expression and purification of proteins:

Drp1 (*Homo sapiens*, Isoform 3)-StrepII and Drp1 (*Homo sapiens*, Isoform 3)-EGFP-StrepII, mitochondrial fission factor (StrepII-MFF(1-271 residues, without transmembrane domain)-6xHis) were all cloned in pET15B vector. The constructs were grown exactly as is mentioned in Chapter 2 of this thesis. For purification of Drp1 constructs, cells were lysed in lysis buffer (20mM HEPES pH 7.4, 500mM KCl, 1mM phenylmethylsulfonic acid) by sonication. The lysate was spun at 30000g and the supernatant was used for further purification. The supernatant was loaded on to a HiTrap Strep-tactin column (5ml, GE Lifesciences) and washed extensively with the lysis buffer. The buffer was exchanged with assay buffer (20mM HEPES pH 7.4, 150mM KCl) on the column. The bound protein was given an additional wash with 10mM EDTA in assay buffer to get rid of any bound nucleotide. The proteins were eluted using desthiobiotin in a final concentration of 2.5mM in the assay buffer. For MFF purification, the supernatant of the lysate was loaded on to a HiTrap Chelating column (5ml, GE Lifesciences) and eluted with 250mM imidazole in the lysis buffer. All elutions were pooled together and subsequently loaded on a HiTrap Strep-tactin column, washed extensively with lysis buffer, exchanged for assay buffer and finally eluted with 2.5mM final concentration of desthibiotin in assay buffer. The proteins were run on a gel and the pure fractions were pooled and kept on ice at 4°C for use within 3-5 days.

3.2.2. Supported Membrane Templates (SMrT) assay:

SMrT were made exactly as is mentioned in chapter 2 of this thesis. For assays using Drp1, 1µM of the protein was flowed in with 1mM GTP and 1mM $MgCl_2$, incubated for 10 minutes and images were captured in the membrane channel. Fission was calculated manually by estimating the number of tubes that showed at least one break. For Drp1-mEGFP experiments, 0.5µM of untagged Drp1 was mixed with 0.5µM of Drp1-mEGFP and flowed in with 1mM GppNHp and 1mM $MgCl_2$ and allowed to assemble on the membrane. Membrane density of the protein under different conditions were measured exactly like is stated in chapter 2 of this thesis. For MFF experiments, the lipid mix additionally had 5 mol% of DGS-Ni^{2+}-

NTA(1,2-dioleoyl-sn-glycero-3-[(N-(5-amino-1-carboxypentyl)iminodiacetic acid)succinyl]). MFF was flowed in at 1μM final concentration, allowed to incubate for 10 minutes before excess unbound protein was washed off prior to addition of Drp1 or Drp1/Drp1-mEGFP.

3.2.3 Bulk fission rates, kymograph analysis and parameters of fission:

Bulk fission rates were measured by flowing in Drp1 with 1mM GTP and 1mM $MgCl_2$ on membrane templates of indicated lipid composition and acquiring a time-lapse movie in the presence of oxygen scavenger cocktail (OSC) and 1mM DTT at 100ms interval between frames. The reason to have OSC and DTT is to reduce phototoxicity induced effects which interfere with Drp1 functions (Roy and Pucadyil, 2022). The first cut was marked and from then onwards the time of every subsequent cut was recorded and plotted as a cumulative frequency plot. For estimation of parameters of fission, Drp1 was assembled on tubes in the presence of GppNHp and $MgCl_2$ and a movie was recorded with the flow of 1mM GTP and 1mM $MgCl_2$ in the assay chamber. The movie was used to generate kymographs of individual fission events starting from a constricted assembled state. The line profile along the time-axis of the kymograph was used to generate the fission plot (tube radii versus time). Intensities were converted to tube sizes using the same in-situ calibration constants as mentioned in Chapter 2 of this thesis. The initial part of the plot was fitted to a plateau followed by exponential decay in Prism which indicated the scaffolded tube radius (plateau) and constricted tube radius (second plateau after exponential decay). The time between the start of the GTPase-induced constriction (start of the exponential decay) and eventual fission (total drop of membrane fluorescence) was recorded as the fission time for each event.

3.2.3 Fluorescent microscopy and statistical analyses:

All fluorescence images were acquired in Olympus IX83 inverted fluorescence microscope attached to a stable LED light source (CoolLED) and an Evolve 512 EMCCD camera (Photometrics). Image acquisition was done using Micro-manager software and rendered using Fiji (version 2.1.0/1.53c). All graphical representations and statistical analyses were carried out on GraphPad Prism 9 using tests as mentioned in the respective figure legends.

3.3 Results:

3.3.1. DAG facilitates Drp1-catalysed membrane fission of CL-containing membrane tubes:

Previous work from the lab has shown that Drp1 is sufficient to catalyse membrane fission of CL tubes (Kamerkar et al, 2019). Fission caused by Drp1 was dependent on the CL concentration in the membrane. In order to analyse the effects of DAG addition, we tested Drp1's ability to cause fission on templates containing a range of CL concentrations (0-20%) in a background of 5%DAG and DOPC. Templates made of 5%PI instead of DAG were used as a control. For these experiments, Drp1 was flowed in presence of GTP, incubated for 10 minutes and bulk fission was estimated by counting tubes that showed at least one cut. Notably, addition of 5%DAG showed a marked increase in bulk tube fission at an intermediate concentration of CL (10%) (Fig 3.1 A, B). Control experiments with 5%PI did not show any stimulation of membrane fission over and above what bare CL tubes showed. Together, these results emphasized the fact that inclusion of DAG in a membrane containing CL stimulates the bulk fission rate of Drp1.

Membrane binding is a prerequisite for fission. We wondered if the stimulation of fission activity on DAG-containing membranes is because of enhanced membrane binding by Drp1. We have previously reported that Drp1-mEGFP flowed in with an equimolar amount of untagged Drp1 can efficiently bind and cause fission of CL-containing membrane tubes in presence of GTP (Kamerkar et al, 2019). However, similar reactions carried out in the presence of GppNHp, a non-hydrolysable GTP analog, leads to the formation of stable protein scaffolds on the membrane. Underlying the protein scaffolds is usually a dimmer membrane fluorescence (Fig 3.1 C). Since these tubes are diffraction-limited, a change in fluorescence is directly proportional to a change in volume of the tube. Thus, a dimmer membrane fluorescence usually indicates thinning down of the tube which we refer to as constriction. The stable protein scaffolds also lets us measure the extent of protein binding on different templates taken as a ratio of protein to membrane fluorescence intensities. Measuring the protein density on membrane tubes, however, showed that DAG-containing membranes recruit much higher Drp1 across a range of tube sizes as compared to tubes made of PI (Fig 3.1 D). The data was consistent for tubes having both 10% and 15%CL. Together, these results indicate that DAG stimulates Drp1's ability to cause fission by recruiting more Drp1 to the membrane surface.

3.3.2 DAG facilitates Drp1 functions on OMM-mimetic templates:

Drp1 acts in concert with multiple other factors at the division site on the mitochondria to bring about fission. These include OMM adapters, ER and lysosome contacts and the cytoskeletal machinery. We have previously shown that SMrT can be re-engineered to make OMM-mimetic membrane templates by displaying the soluble portion of an OMM adapter

MFF through chelating lipids. To test the effects of coincident detection of both the adapter and the lipid, we lowered the CL concentration on the membrane to a point where we do not see any fission without the adapter protein (5%). Remarkably, flowing in Drp1-mEGFP along with GppNHp on these OMM-mimetic templates showed much higher protein density on membranes made of DAG than on membranes made of PI across a range of tube sizes (Fig 3.1 E, F). Flowing in Drp1 with GTP showed tubes undergoing fission pointing to the importance of adapter proteins in mediating this. Interestingly, fission was much higher on tubes made of DAG than with PI as indicated by the relative fraction of tubes showing multiple cuts (Fig 3.1 G, H). Evidently, fission was much less robust on these templates, likely, due to the limiting amounts of CL present. Together, these results indicate that DAG facilitates Drp1's ability to cause fission on membrane tubes having CL and also OMM-mimetic templates having an adapter protein displayed with limiting CL concentration.

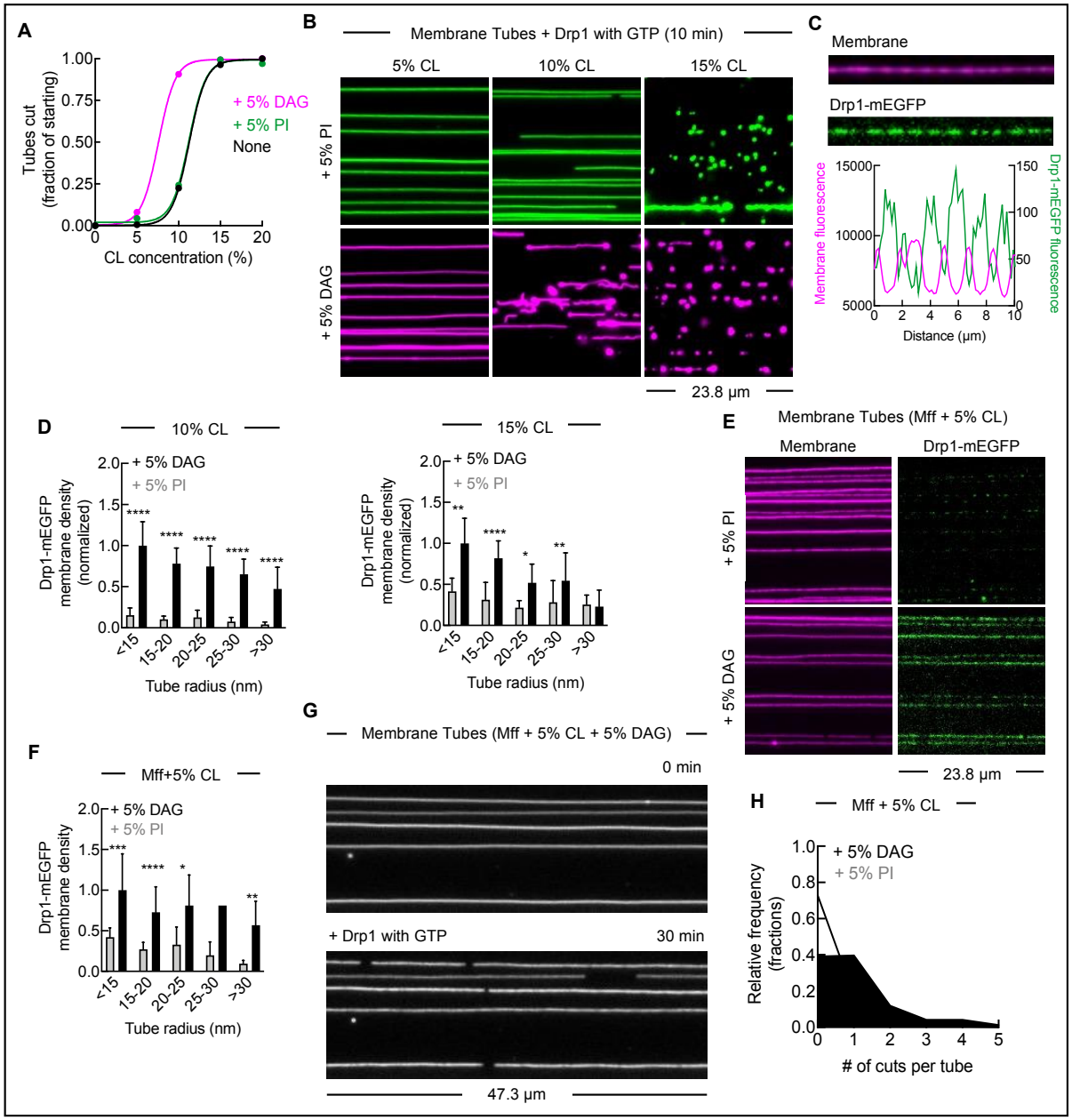

Figure 3.1- DAG facilitates Drp1-mediated membrane fission. (A) Plot showing fraction of tubes cut with Drp1+GTP when incubated with templates containing 5%DAG or 5%PI in a background of indicated CL concentration. At least 120 tubes for each condition was measured for the plot. (B) Representative fluorescent images of tubes of the indicated lipid composition (PI: green; DAG: magenta) after incubation with Drp1+GTP. (C) Representative fluorescent micrograph of a tube (magenta) having assembled Drp1-mEGFP (green) in the presence of GppNHp along with a line-scan profile where the line is drawn on the tube. (D) Plot showing Drp1-mEGFP membrane density on tubes containing either 10% or 15%CL. Data represents mean ± SD of at least 40 tubes. (E) Representative fluorescent images of tubes (magenta) containing Mff+5%CL with 5%PI or 5%DAG as indicated in the presence of Drp1-mEGFP (green). (F) Plot showing Drp1-mEGFP membrane density on tubes of indicated lipid composition. Data represents mean ± SD of at least 30 tubes for each condition tested. (G) Representative images of tubes having MFF+5%CL (gray scale) before and after flowing in Drp1+GTP. (H) Quantitation of relative frequency of cuts on tubes made of MFF+5%CL with 5%PI or 5%DAG in the presence of Drp1+GTP. Data represents mean ± SD of at least 280 tubes for each lipid composition. All statistical significances are measured using Mann-Whitney test.

3.3.3. DAG stimulates the mechanochemical activity of Drp1 resulting in accelerated membrane fission:

Membrane fission requires a concerted activity of fission proteins whereby the two opposing membranes of a tube are brought close together so as to have minimal hydrophobic effect within the luminal side. This results in lipids on the inner leaflets of both membranes to adopt non-bilayer conformations and spontaneously fuse with the opposing membrane resulting in fission. In such cases, lipids having a positive spontaneous curvature, like lysophospholipids, are known to delay the kinetics of fission (Morlot et al, 2012). DAG is a lipid which has a negative spontaneous curvature and as such should end up promoting the rate of fission. Our results with Drp1 on a range of CL concentrations showed a stimulation of bulk fission and fission rate at an intermediate concentration of CL (10%) (Fig 3.1 A, B). At very low CL concentration (5%), Drp1 did not show fission irrespective of the presence of DAG or PI suggesting the requirement of a minimal amount of CL in the background for this activity to manifest. At high CL concentrations (15% and 20%), there was virtually no difference in the extent of bulk fission irrespective of the lipids used. However, when fission rates were measured, even 15% CL containing tubes showed a marked stimulation in fission kinetics (Fig 3.2 A, B). Since fission is dependent on starting tube radii, we wondered if enhanced fission rate on DAG tubes is because of a systemic change in tube dimensions. However, measurement of tube radii distribution across DAG and PI-containing tubes showed no significant difference in tube size distributions suggesting that tube size is not the reason for faster fission kinetics on DAG membranes (Fig 3.2 C).

To test the effects of DAG on Drp1-catalysed fission post membrane binding, we resorted to monitoring individual fission events on tubes containing 15%CL where addition of DAG and PI leads to robust fission. First we assembled Drp1 on tubes in the presence of GppNHp. Stable protein scaffolds were formed as indicated by the intermittent dip in membrane fluorescence (Fig 3.2 D). Flowing in GTP on these tubes lead to fission which is evident from the kymograph analysis of each individual fission event (Fig 3.2 D). The tube fluorescence intensity can be equated to tube dimension using an in situ calibration method. A line profile along the time axis of the kymograph delineates the mechanical pathway to fission whereby Drp1 assembled with GppNHp constricts the tube to a particular radius (scaffolded tube radius), which upon GTP exchange and subsequent hydrolysis, constricts even further (pre-fission intermediate) ultimately leading to fission (Fig 3.2 E). Remarkably, analysis of multiple fission events showed that on DAG-containing tubes, the scaffolded tube radii were much smaller and uniform as compared to the tubes made of PI (DAG: 8.1 ± 1.6 nm; PI: 11.9

± 4.2 nm) (Fig 3.2 F). Thus, even before the onset of GTP driven constriction, Drp1 is able to constrict DAG-containing tubes to more narrower radius leading to fission. However, analysis of pre-fission radius showed that irrespective of the lipid, the tubes constrict to a similar extent before undergoing fission (DAG: 5.2 ± 0.8 nm; PI: 5.3 ± 0.8 nm) likely indicating that pre-fission radius is a characteristic of the process of fission rather than a variable dependent on the lipids or proteins involved (Fig 3.2 G). Fission time, which is defined as the time required by the protein from the moment it sees GTP to eventually causing fission, was markedly reduced for tubes made of DAG than with PI (DAG: 8.4 ± 1.3 s; PI: 14.2 ± 2.6 s) (Fig 3.2 H). Thus, after membrane binding and protein assembly, Drp1 takes much shorter time to cause fission on templates made of DAG than with PI. Together, these results indicate that DAG not only facilitates membrane binding of Drp1, but also stimulates the mechanochemical activity of the enzyme in subsequent steps leading to enhanced fission kinetics.

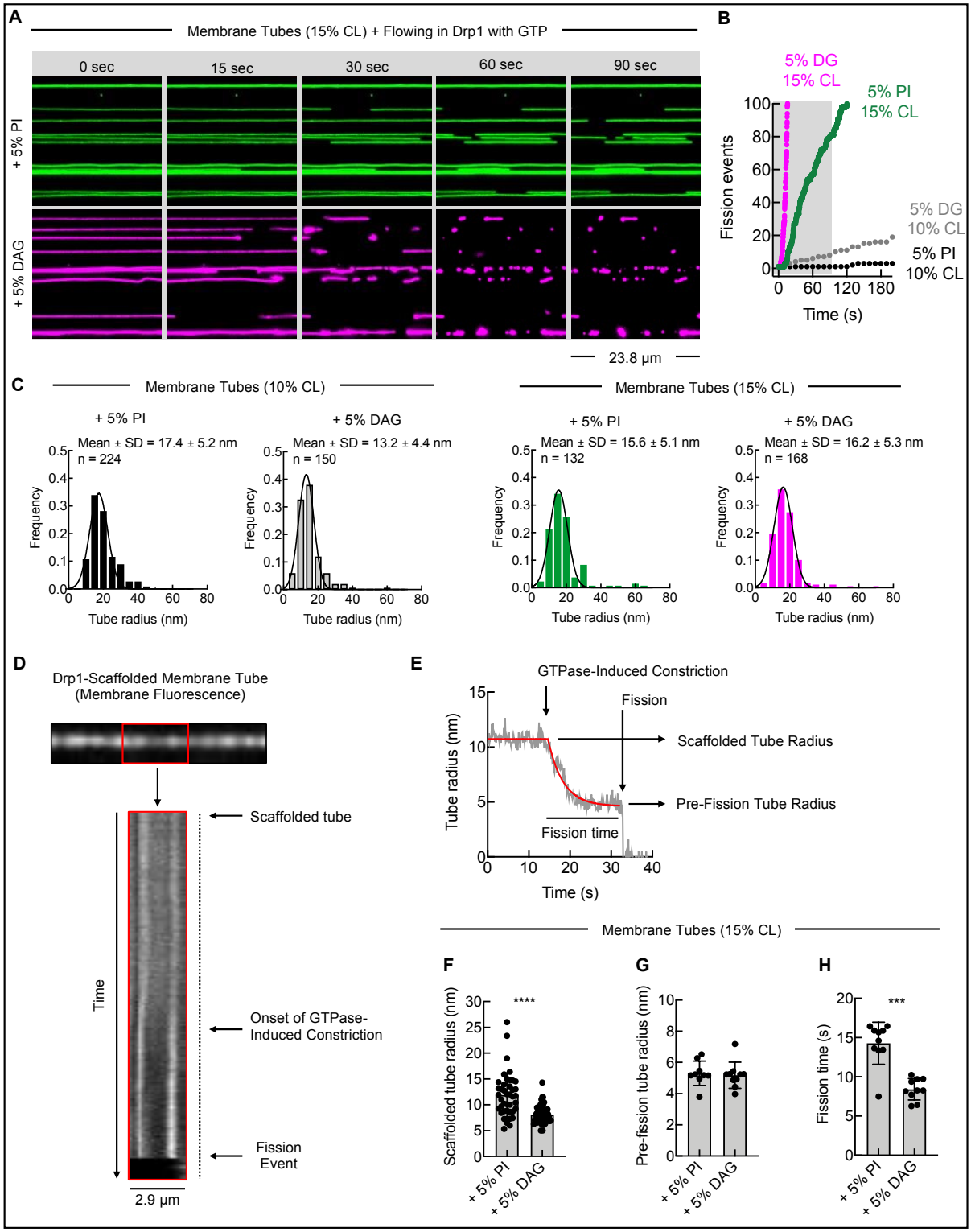
A
Membrane Tubes (15% CL) + Flowing in Drp1 with GTP
0 sec
15 sec
30 sec
60 sec
90 sec
+ 5% PI
+ 5% DAG
23.8 µm
B
5% DG
15% CL
5% PI
15% CL
5% DG
10% CL
5% PI
10% CL
Fission events
Time (s)
C
Membrane Tubes (10% CL)
Membrane Tubes (15% CL)
+ 5% PI
+ 5% DAG
Mean ± SD = 17.4 ± 5.2 nm
n = 224
Mean ± SD = 13.2 ± 4.4 nm
n = 150
Mean ± SD = 15.6 ± 5.1 nm
n = 132
Mean ± SD = 16.2 ± 5.3 nm
n = 168
Frequency
Tube radius (nm)
D
Drp1-Scaffolded Membrane Tube
(Membrane Fluorescence)
Scaffolded tube
Time
Onset of GTPase-
Induced Constriction
Fission
Event
2.9 µm
E
GTPase-Induced Constriction
Fission
Scaffolded Tube Radius
Pre-Fission Tube Radius
Fission time
Tube radius (nm)
Time (s)
Membrane Tubes (15% CL)
F
G
H
Scaffolded tube radius (nm)
Pre-fission tube radius (nm)
Fission time (s)
****
***
+ 5% PI
+ 5% DAG

Figure 3.2- DAG stimulates the mechanochemical activity of Drp1 resulting in accelerated fission. (A) Representative membrane fluorescence time-lapse images of Drp1+GTP flowed in on tubes containing 15%CL with 5%PI (green) or 5%DAG (magenta). (B) Bulk fission kinetics of Drp1 on indicated lipid compositions. (C) Tube radius estimation plotted as a frequency profile of the indicated lipid compositions. The histograms were fitted to a Gaussian distribution to estimate the mean and SD of the respective tube radii. (D) Representative fluorescent image of a tube having pre-assembled Drp1 with GppNHp which was followed in real-time. The marked red box has been used to generate a kymograph indicating GTPase induced constriction and fission. (E) Plot showing the fluorescence line profile of the kymograph (D) after conversion to of intensity to tube radius. (F-H) Plot of different fission parameters as indicated across 5%PI and 5%DAG containing tubes. Data represents the mean ± SD of 40 scaffolds for scaffolded tube radius, at least 9 events for pre-fission tube radius and at least 10 fission events for fission time estimation. Statistical significance was estimated using unpaired Mann-Whitney's test. **** denotes $p<0.0001$ and *** denotes $p=0.0007$.

3.4. Discussion:

Our efforts in reconstituting membrane fission mediated by Drp1 on mitochondrial surface in the presence of DAG shows that DAG enhances Drp1's ability to cause membrane fission on CL-containing tubes. Tubes having limiting CL concentration (5%) did not show any fission indicating that DAG on its own cannot recruit enough protein to the membrane surface to promote fission. Membrane tubes made up of DAG recruited higher amount of Drp1 on the membrane than tubes made of PI across a range of tube sizes. A minimum amount of CL is required for Drp1 to show fission even on DAG-containing tubes. This possibly alludes to the idea of initial requirement of CL for Drp1 to land and stably interact with the membrane. In fact, multiple studies have suggested the role of CL in promoting Drp1 interactions with the membrane (Bustillo-Zabalbeitia et al, 2014, Stepanyants et al, 2015, Mahajan et al, 2021). Thereafter, having DAG in the membrane makes the association between the protein and the membrane more tighter resulting in much higher equilibrium binding of the protein with the membrane.

Membrane fission is brought about by a concerted action of fission proteins to constrict a tube so much so that the lipids can take non-bilayer conformation leading to fission. Our results show that having DAG on the membrane leads to the formation of uniform thinner scaffolds of Drp1 as compared to on PI tubes. Thus, if fission is considered as a pathway in linear axis where it starts from a tube of 25nm radius which finally needs to come down to 5nm radius, having DAG in the membrane already gives a head-start to Drp1 by enabling it to constrict to a thinner radius even before GTPase-induced constriction. Moreover, this also leads to significant lowering of the time taken to complete the process as indicated by lesser fission time on DAG-containing tubes. Drp1 in mammalian cells exists in a dynamic equilibrium between soluble cytosolic fractions and tethered to the mitochondrial surface by adapter

proteins. DAG production during mitophagy has been shown to be absolutely essential for efficient clearance of the organelle. Our data indicate that, DAG production on the mitochondria can lead to (i) an increased recruitment of cytosolic Drp1 to the mitochondrial surface and (ii) potentiation of the membrane-anchored Drp1 already present on the mitochondria to proceed to fission.

Drp1's interaction with the membrane has long been thought to be brought about by electrostatic interactions between charged residues in the variable domain (VD) of Drp1 and anionic lipids in the membrane (Macdonald et al, 2014, Bustillo-Zabalbeitia et al, 2014). More recently, Drp1 has been reported to interact with various other membrane properties like lipid side-chain saturation (Adachi et al, 2016), lipid phases in membranes (Stepanyants et al, 2015) and hydrophobic interactions with CL in the membrane (Mahajan et al, 2021). These suggests that on top of known electrostatic interactions between charged residues in the VD with the membrane, Drp1 might also be interacting with the general membrane surface properties whereby it does come across membrane defects and acyl chain saturations. DAG is a non-ionic lipid. Since DAG incorporation in membranes does not cause a concomitant increase in membrane charge, an intriguing question is what exactly does DAG contribute for Drp1 to bind so efficiently? DAG is thought to induce packing defects in membranes owing to their conical shape (Vamparys et al, 2013). One testable hypothesis can be that Drp1 can sense membrane packing defects. Drp1 VD has been reported to dip inside the membrane to sense lipid acyl chain saturation and CL (Adachi et al, 2016, Mahajan et al, 2021). Thus, Drp1 can, in principle, have better access to the dip VD residues into the membrane if the membrane has many defects. However, a recent report suggested, a similar conical lipid PA, to inhibit Drp1-mediated mitochondrial fission both *in vitro* and in mammalian cells (Adachi et al, 2016). Interestingly, unlike DAG, PA is an anionic lipid and DAG and PA are known to have widely different roles in cellular physiology. How exactly does the presence of these regulatory lipids modulate Drp1 functions in cells remains to be systematically tested.

Chapter 4:

DAG promotes Endophilin B1/2-dependent membrane tubulation

4.1 Introduction:

In addition to Drp1, another protein that has been shown to be implicated in mitophagy and DAG production is the Bin-Amphiphysin-Rvs (BAR) domain-containing protein Endophilin B1 (EndoB1) (Lin et al, 2022). EndoB1 was originally discovered as a protein involved in maintenance of mitochondrial morphology (Karbowski et al, 2004). EndoB1 knockdown by RNAi led to global disruption of mitochondrial morphology including unusually inter-connected or rounded mitochondria and generation of OMM tubules in mammalian cells. Interestingly, however, over-expression of EndoB1 also caused a similar phenotype of highly inter-connected mitochondria with prominent OMM tubulation.

EndoB1/2 belongs to the family of Bin-Amphiphysin-Rvs (BAR) domain-containing proteins. Endophilins have a BAR domain at the N-terminus followed by a unstructured region and finally a Src homology 3 (SH3) domain at the C-terminus. In addition to these, the N-terminus of EndoB1 has two amphipathic helices (H_0 and H_{1i}) in close association with the BAR domain. The BAR domain of EndoB1 has been shown to be sufficient for membrane tubulation (Bhatt et al, 2021). The amphipathic helices are also important for membrane tubulation. H0 helix seems to be absolutely necessary for membrane binding whereas the H1i helix seems to only have a facilitatory role. The SH3 domain is thought to mediate protein-protein interactions.

EndoB1 is a closely related cousin of the relatively better known Endophilin A1 which has been implicated in clathrin-mediated endocytosis (CME) at the plasma membrane (Sundborger et al., 2011). EndoA1 has been widely studied for its protein-protein interactions via its SH3 domain binding to the proline-rich domain (PRD) of the endocytic dynamins, Dnm1 and Dnm2 (Micheva et al., 1997; Ringstad et al., 1997). However, if EndoB1 can directly bind to dynamin family proteins remain unknown, although, EndoB1 has been shown to bind the general scaffolding protein of the autophagic machinery UVRAG. EndoB1 has been shown to interact with Beclin via UVRAG and causes the activation of a specific class of phosphatidylinositol-3-kinase (PI3KC3) leading to the formation of autophagosomes (Takahashi et al, 2007). In fact, EndoB1 has also been reported to co-localize with known components of the general autophagic machinery like LC3, Atg5 and Atg9 vesicles (Takahashi et al, Autophagy, 2011). EndoB1 has also been implicated to regulate recycling of Atg9 vesicles during autophagy (Martorell-Riera et al, Bioarxiv, 2018).

EndoB1 has not only been implicated in general autophagy responses but has also been reported to be involved in organelle-specific autophagic responses like mitophagy. Even though majority of EndoB1 is cytosolic in cells, the protein gets recruited to the mitochondria

in response to apoptotic stimuli (Karbowski et al, 2004). Treating mammalian cells with CCCP a protonophore and a mitophagy inducer, recruits EndoB1 to the mitochondria (Lin et al, 2022). Moreover, EndoB1 knockdown has been shown to regulate DAG levels on the mitochondria undergoing mitophagy. Together, our data and these reports suggest that EndoB1 gets recruited to the mitochondria in response to acute DAG generation and also responds to mitophagic clearance of the organelle. These led us to question if DAG can directly regulate EndoB1 functions on membranes.

4.2 Materials and Methods:

4.2.1 Cloning, expression and purification of proteins:

6xHis-EndoB1 (Residues 1-365)-mEGFP, 6xHis-EndoB1$^{N\text{-}BAR}$ (residues 1-270)-mEGFP, and 6xHis-EndoB2$^{N\text{-}BAR}$ (Residues 1-292)-mEGFP were also all cloned into the pHGT-2 vector. EndoB1/2 constructs were transformed and grown in T7 Express competent cells. The transformants were grown in a 1L culture till O.D. of 0.4 after which induction was done using 0.1µM IPTG. The cells were grown at 18˚C for 12 hours post which they were pelted at 6000g and the pellets were stored in -40˚C for future use. For purification, bacterial pellets were resuspended in lysis buffer (20mM HEPES pH 7.4, 500mM KCl, 10mM imidazole, 1mM phenylmethanesulfonyl fluoride), lysed using sonication and spun at 30000g to get rid of un-lysed cells and membrane fraction. The supernatant was loaded on an equilibrated 5ml chelating column and washed extensively with the lysis buffer. Further, the buffer was exchanged to assay buffer (20mM HEPES pH 7.4, 150mM KCl). The proteins were eluted using a gradient of imidazole (10-300mM) in the assay buffer. The elution fractions were run on a gel and the pure protein containing fractions were pooled together, dialysed against assay buffer to get rid of the imidazole and kept on ice for 2-3 days during which all assays were done.

4.2.2. Supported Membrane Templates (SMrT) assay:

SMrT were made exactly as is mentioned in Chapter 2 of the thesis. For EndoB1/2 experiments, purified proteins were flown in at a final concentration of 1µM, incubated for 10 minutes and excess unbound proteins were washed off before acquiring images. For real-time analysis of membrane tubulation, EndoB1$^{N\text{-}BAR}$ was flown in along with oxygen scavenger cocktail (OSC) with 1mM DTT and images were acquired at 50ms interval. For tube size analysis, a line profile was drawn perpendicular to tubes at its nascent stage (to make sure these

are single tubules and not coiled) and the minimum fluorescence intensity (indicating the planar bilayer fluorescence) was subtracted from the maximum fluorescence intensity (indicating the fluorescence of planar bilayer and the tube) to get the tube intensity. This intensity was then converted to tube size using the same in situ calibration method reported in Chapter 2 of this thesis. For EndoB1+Drp1 experiments, 0.1μM of EndoB1 was flown in with 1μM of Drp1 with 1mM GTP and 1mM MgCl2 on to the templates along with OSC and DTT. The images were acquired in real-time with a time interval of 100ms.

4.2.3 Fluorescent recovery after photobleaching (FRAP):

For Fluorescent recovery after photobleaching (FRAP) experiments, 0.1μM of EndoB1 was flown in alone or with 1μM of Drp1 with 1mM GTP and 1mM MgCl2 on to the templates. This was incubated for 10 minutes upon which robust tubulation of the planar bilayer could be seen. Excess proteins were washed off post this and the templates were equilibrated with OSC and DTT in assay buffer. Area photobleaching was done by using highest possible LED intensity on an epifluorescence microscope (see below for microscope specifications) in the membrane channel until all fluorescence was lost. The field was then moved slightly and the recovery was monitored in real-time at 100ms interval between frames in both protein and membrane channels.

4.2.3 Fluorescent microscopy and statistical analyses:

All fluorescence images were acquired in Olympus IX83 inverted fluorescence microscope attached to a stable LED light source (CoolLED) and an Evolve 512 EMCCD camera (Photometrics). Image acquisition was done using Micro-manager software and rendered using Fiji (version 2.1.0/1.53c). All graphical representations and statistical analyses were carried out on GraphPad Prism 9 using tests as mentioned in the respective figure legends.

4.3. Results:

4.3.1. DAG enhances Endophilin B1's ability to bind planar membrane surfaces and subsequently tubulate them:

Results from our collaborative studies show that EndoB1 gets recruited to the OMM upon acute production of DAG and subsequently tubulates the membrane. We wanted to test if this translocation and tubulation activity is caused because DAG directly modulates EndoB1 functions. Like Drp1, EndoB1 is mostly cytosolic under basal conditions, however, unlike Drp1, EndoB1 does not get recruited or found associated with pre-constricted mitochondria.

Hence, the reported translocation, likely, happens on the planar surface of the mitochondria. In order to recreate this, we focussed on the planar bilayers for these subsequent experiments. Purified EndoB1-EGFP was passed on to membrane templates, incubated for 10 minutes and excess unbound protein was washed off before imaging. Interestingly, EndoB1-EGFP showed minimal binding to templates made up of 15%CL+5%PI (Fig 4.1 A). Remarkably, however, templates made up of 15%CL+5%DAG showed significantly higher EndoB1 getting recruited as estimated by the protein to membrane fluorescence ratio (Fig 4.1 B). The EndoB1-EGFP signal on the membrane was not uniform with some regions on the bilayer showing much higher fluorescence than others. Interestingly, these high protein intensity regions had a concomitant increase in membrane fluorescence as well, likely, representing tubulation of the underneath bilayer. The N-BAR domain of EndoB1 has been shown to be sufficient for tubulating liposomes (Bhatt et al, 2021). We wanted to see if the N-BAR domain of EndoB1 is capable of remodelling the bilayer on its own. Purified EndoB1$^{N\text{-}BAR}$-EGFP added to DAG-containing templates showed a similar DAG-specific membrane binding and tubulation activity on planar bilayers (Fig 4.1 C, E). Together, these results suggest that EndoB1 is able to bind and tubulate planar bilayers in a DAG-dependent manner.

4.3.2 Real-time analysis of tubulation mediated by EndoB1:

To better understand the process of membrane tubulation, we resorted to capturing the activity of EndoB1$^{N\text{-}BAR}$-EGFP on 5%DAG+15%CL bilayers at a high frame rate. Immediately after flowing in the purified protein, we could see numerous faint and spindle-like tubes emanating from the bilayer (Fig 4.1 F). These tubes grew both in size and intensity suggesting growth of the tubules. Subsequently, these spindle-like entities coalesced into bright stubs on the membrane. A closer look at the kinetics of a single tubulation reaction showed that the process begins with the formation of a tiny high intensity spot which is representative of a bud. These buds grow subsequently to form long thin tubes (Fig 4.1 F inset white arrows) which over time ends up acquiring varicosities along the length (Fig 4.1 F inset green arrows) of the tubes likely suggesting coiling of the tube (Fig 4.1 F inset yellow arrows). Subsequently, other such in the vicinities along with their varicosities seem to ‘merge’ to coalesce into single stub-like entities which we think represent an orientation of bundle of bundles. This, to our understanding, is the first report of real-time tubulation mediated by EndoB1.

A recent report, using cryo-EM, has put a size estimate of the tubes that are formed by EndoB1 from liposomes. They reported a tube lumen size of 12.5-14nm. Assuming the bilayer thickness to be ~5nm, the total tube radius (lumen + membrane) come to be about 12nm. We

estimated sizes of single tubes from images acquired at very early time points, likely, representing fluorescence intensity from a single tube using our *in situ* calibration method. The tube sizes generated by EndoB1N-BAR-EGFP came to be 15.5 ± 2.8 nm radius (n = 23). This is good accordance with the cryo-EM estimates of tube sizes. Thus, EndoB1 can bind and tubulate planar membranes containing DAG and sprouts out tubes which are about 15nm in radius.

4.3.3 EndoB1 is recruited to the membrane based on lipid composition and membrane curvature:

Given that EndoB1 binds planar membranes only in the presence of DAG, we wanted to check how does the protein behave on pre-formed tubes. Interestingly, EndoB1-EGFP showed binding to both DAG- and PI-containing tubes (Fig 4.1 D). Quantitation of EndoB1-EGFP fluorescence intensity on bilayers versus tubes made of 15%CL+5%DAG showed that EndoB1 bound both tubes and bilayers with equal affinity. However, binding was significantly improved for tubes made up of PI as compared to bilayers. Thus, two criteria seems to govern EndoB1 recruitment to the membrane: lipid identity and membrane curvature. On DAG-containing bilayers, EndoB1 gets recruited to the bilayer based on lipid specificity: its ability to bind DAG. On PI tubes it gets recruited based on the curvature as the bilayers in the same chamber does not show protein binding. Thus, EndoB1 gets recruited to membranes based on either lipid specificity or membrane curvature.

4.3.4 EndoB1 scaffolds do not impose a lipid-diffusion barrier on the underneath membrane:

Previous reports have suggested the effects of Endophilin scaffolds on the underlying membrane. Endophilin A, which is involved in the formation of endocytic transport vesicles at the plasma membrane has been shown to impose a lipid-diffusion barrier in the membrane (Simunovic et al, 2017). However, other proteins of the BAR family has been reported to only cluster and restrict movement of the specific phosphoinositides that they bind to and not change the diffusion properties of other bulk lipids in the membrane (Zhao et al, Cell Reports, 2013). These led us to question if EndoB1 scaffolds also impart a similar diffusion barrier on the membrane underneath. We analysed the bulk diffusion of tubules generated by EndoB1 by fluorescence recovery after photobleaching (FRAP) experiments. The rationale was to bleach the fluorescent lipid probe TR-DHPE in a large bilayer area and monitor recovery of fluorescence in both the EndoB1-generated tubes and the bilayer underneath. If the bilayer

recovers and not the tubes to the same extent, then there has to be a lipid-diffusion barrier because of the EndoB1 scaffold assembly on the tube. For the purpose of these experiments, we flowed in EndoB1$^{N\text{-}BAR}$-EGFP on bilayers made of 15%CL+5%DAG, incubate it for 10 minutes for the bilayer to undergo tubulation and then washed off excess unbound protein before bleaching the membrane fluorescence probe. Interestingly, bleaching of the TR-DHPE resulted in a recovery of fluorescence in both the bilayer and the tube over time suggesting no restriction in TR-DHPE movement across the tube (Fig 4.1 G). Thus, unlike EndoA2, EndoB1 scaffolds does not seem to create a lipid-diffusion barrier in the membrane underneath.

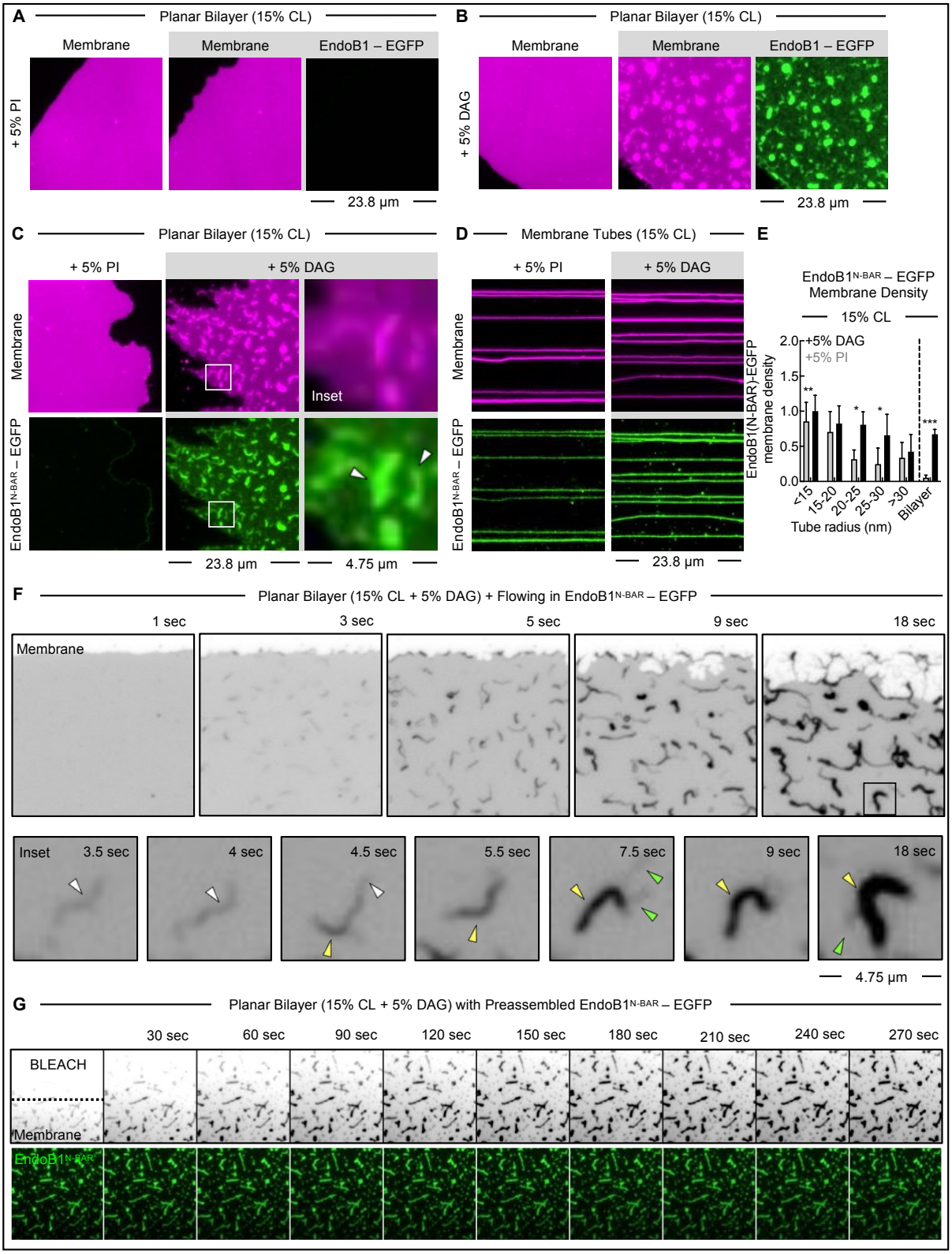
A
Planar Bilayer (15% CL)
Membrane
Membrane
EndoB1 – EGFP
+ 5% PI
23.8 µm
B
Planar Bilayer (15% CL)
Membrane
Membrane
EndoB1 – EGFP
+ 5% DAG
23.8 µm
C
Planar Bilayer (15% CL)
+ 5% PI
+ 5% DAG
Membrane
EndoB1N-BAR – EGFP
Inset
23.8 µm
4.75 µm
D
Membrane Tubes (15% CL)
+ 5% PI
+ 5% DAG
Membrane
EndoB1N-BAR – EGFP
23.8 µm
E
EndoB1N-BAR – EGFP
Membrane Density
15% CL
+5% DAG
+5% PI
EndoB1(N-BAR)-EGFP membrane density
2.0
1.5
1.0
0.5
0.0
**
*
*
***
<15
15-20
20-25
25-30
>30
Bilayer
Tube radius (nm)
F
Planar Bilayer (15% CL + 5% DAG) + Flowing in EndoB1N-BAR – EGFP
1 sec
3 sec
5 sec
9 sec
18 sec
Membrane
Inset
3.5 sec
4 sec
4.5 sec
5.5 sec
7.5 sec
9 sec
18 sec
4.75 µm
G
Planar Bilayer (15% CL + 5% DAG) with Preassembled EndoB1N-BAR – EGFP
30 sec
60 sec
90 sec
120 sec
150 sec
180 sec
210 sec
240 sec
270 sec
BLEACH
Membrane
EndoB1N-BAR

Figure 4.1- DAG-dependent membrane recruitment and tubulation mediated by EndoB1. (A-B) Representative fluorescent images of planar membranes (magenta) before and after incubation with EndoB1-mEGFP on 5%PI or 5%DAG-containing templates in a background of 15%CL. (C-D) Representative fluorescent images of planar membranes (C) and tubes (D) containing 5%PI or 5%DAG in a background of 15%CL incubated with EndoB1$^{N\text{-}BAR}$-EGFP. Boxes in the panels have been zoomed in to create the inset panel. White arrows mark the regions where increased protein fluorescence coincides with increased membrane fluorescence indicating membrane remodeling. (E) Plot showing EndoB1N-BAR-EGFP membrane density on bilayer and tubes with 5%PI or 5%DAG. Data represents the mean ± SD of 63 tubes and 31 different regions on planar bilayers for DAG-containing and 110 tubes and 35 different regions on planar bilayers for PI-containing membranes. Statistical significance was measured using Mann-Whitney test whereby **** denotes $p<0.0001$, ** denotes $p=0.074$, * denotes $p=0.0238$. (F) Representative time-lapse images of a planar membrane bilayer after addition of EndoB1$^{N\text{-}BAR}$-EGFP. Magnification of a single representative tubulation event is shown in the inset. Images are in the membrane fluorescence channel and are inverted in contrast for clarity. A single tubules is marked by white arrows, coiling tubes are marked as yellow arrows and coalescence of other single tubules in the near vicinity are marked with green arrows. **(G)** Representative time-lapse fluorescence images showing fluorescence recovery after photobleaching (FRAP) of the lipid probe (gray scale, inverted) in a large area of the planar membrane bilayer displaying EndoB1$^{N\text{-}BAR}$-EGFP-coated tubules (green). Region above which bleaching was done is marked with a black dotted line.

4.3.5 Tubes generated by EndoB1 are resistant to Drp1-mediated fission:

Endophilins contain a N-terminal BAR domain followed by a disordered stretch and an SH3 domain at the C-terminus. The SH3 domain have been shown to directly recruit Dynamin1 (Dnm1) and Dynamin 2 (Dnm2) via a SH3-PRD interaction to the endocytic sites to orchestrate the release of vesicles from the plasma membrane (Micheva et al, 1997, Ringstad et al, 1997, Sundborger et al, 2011). However, Dnm2 has been shown to vesiculate planar membrane in presence of EndoA1(N-BAR) suggesting that SH3-PRD interactions might not be necessary for these orchestrated cooperative events (Neuman et al, JBC, 2013). Our results suggest that both EndoB1 and Drp1 gets recruited to the membranes that contain DAG. Moreover, EndoB1 is able to generate tubes on the bilayer having a dimension of ~15nm in a DAG-dependent manner and the tubes do not seem to have a lipid diffusion barrier indicating that, likely, DAG and CL both gets partitioned into the tube. Given the tubes generated by EndoB1 were made of DAG and CL and within the size range where Drp1 can cause fission, we wondered in Drp1 will be able to cut these tubes. Flowing in EndoB1$^{N\text{-}BAR}$-EGFP on planar bilayers made of 15%CL and 5%DAG showed similar tubulation reaction irrespective of the presence of Drp1 added with GTP suggesting the presence of Drp1 had little to no effect on EndoB1$^{N\text{-}BAR}$-mediated tubulation (Fig 4.2 A). Fission although was not apparent in this case because of the coiled nature of tubes. In order to see if the tubes are actually separated from the bilayer because of fission, we resorted to FRAP experiments. Bulk area bleaching of TR-DHPE probe showed that the tubes generated by EndoB1$^{N\text{-}BAR}$ recovered fluorescence

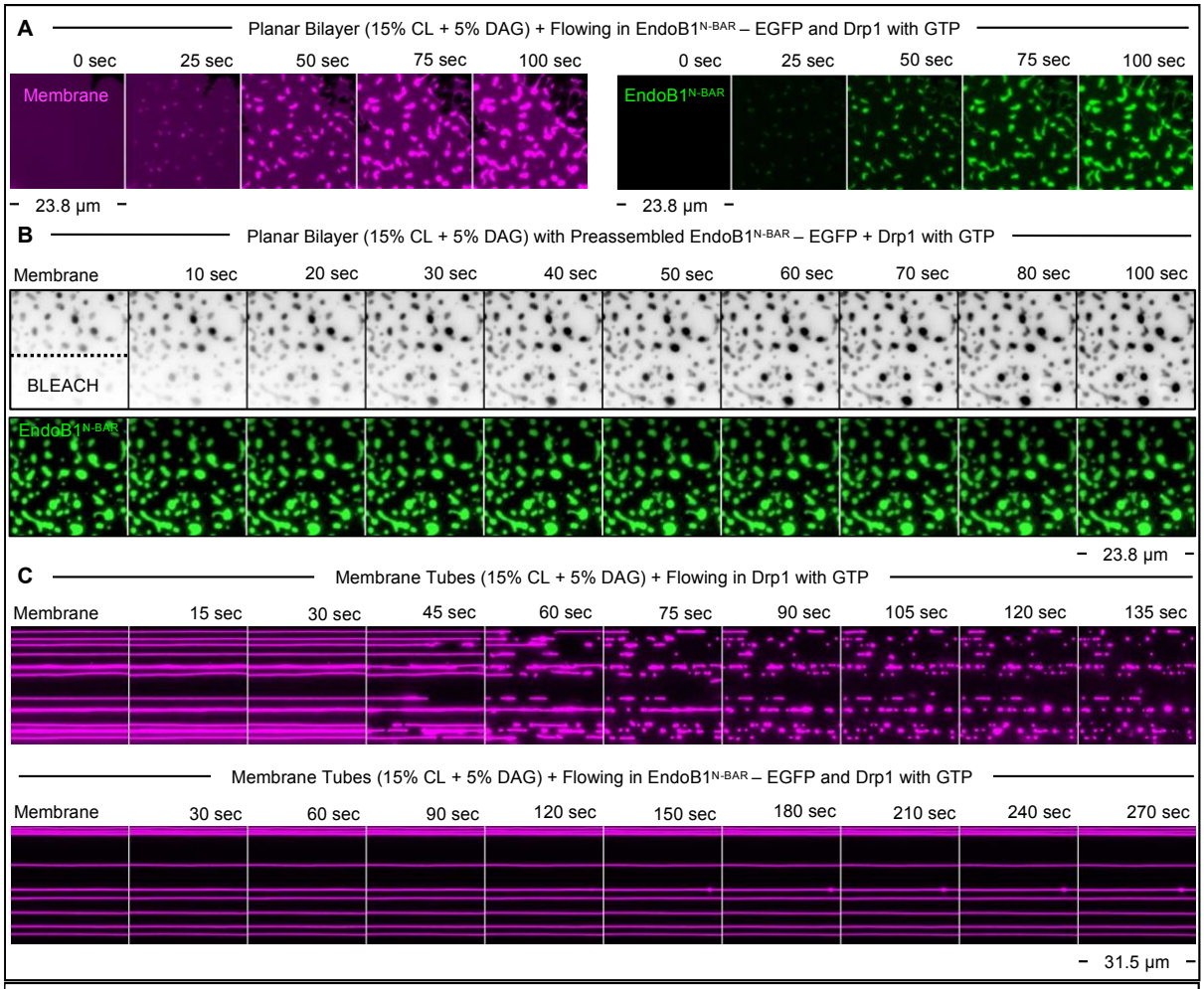

Figure 4.2- Drp1 is not able to cause fission of EndoB1-coated tubes. (A) Representative time-lapse images of planer bilayers (magenta) made of15%CL+5%DAG incubated with EndoB1$^{N\text{-}BAR}$-EGFP (green). (B) Representative time-lapse images of FRAP after incubation of 15%CL+5%DAG bilayers (gray scale inverted) with EndoB1$^{N\text{-}BAR}$-EGFP (green). The region below the black dotted line indicates the zone where the lipid probe was bleached. (C) Representative time-lapse images of membrane fluorescence (magenta) of the indicated lipid composition in the presence of Drp1+GTP or Drp1+GTP+ EndoB1$^{N\text{-}BAR}$-EGFP.

suggesting they were not detached form the underlying bilayer (Fig 4.2 B). Thus, Drp1 was not able to cause fission of the tubes generated on the bilayer.

Next, we wanted to see check if this inhibition of fission also holds true on pre-formed membrane tubes. Addition of EndoB1$^{N\text{-}BAR}$-EGFP along with Drp1 and GTP to tubes made of 15%CL and 5%DAG showed a dramatic reduction in fission mediated by Drp1 (Fig 4.2 C). Control experiments with just Drp1 and GTP on these templates showed robust fission suggesting the presence of EndoB1$^{N\text{-}BAR}$-EGFP severely compromised Drp1's ability to cut these pre-formed tubes. Given both these protein responds to DAG in the membrane, the inhibition of fission likely suggest that both the protein assemblies, likely, compete for the same binding sites on the membrane. Consistent with these observations, previous reports have indicated an inhibition of Dnm2 mediated membrane fission both in cells and in vitro by

endophilins (Hohendahl et al, 2017). Robust fragmentation of the mitochondrial network in response to acute DAG production can possibly happen by recruiting EndoB1 to the planar surfaces of the mitochondria for tubulation and restricting Drp1-mediated fission to constricted pre-assembled Drp1 sites on the mitochondria.

4.3.6 EndoB2 also shows DAG-dependent membrane binding and tubulation:

EndoB1 has a closely-related homologue EndoB2 expressed in mammalian cells having ~65% identity with EndoB1 (Pierrat et al, 2001). Remarkably, addition of EndoB2$^{N\text{-}BAR}$-EGFP to planar bilayers containing 15%CL+5%DAG showed protein binding and membrane deformations similar to seen with EndoB1. Consistent with EndoB1 data, EndoB2$^{N\text{-}BAR}$-EGFP did not get recruited to planar bilayers made of 15%CL+5%PI suggesting having DAG in the membrane is essential for EndoB2 to engage with planar bilayers (Fig 4.3 A). The extent of tubulation, however, was much lesser with EndoB2 than with EndoB1. The clusters were smaller and self-limited along with the fact that not every protein cluster showed equal extent of membrane remodelling. Interestingly, analysis of membrane binding on preformed tubes showed that EndoB2 binds only to DAG-containing tubes and not to PI-containing tubes indicating EndoB2 is likely more sensitive to lipid composition than membrane curvature as compared to EndoB1 (Fig 4.3 B, C). Together, these results bring about subtle quantitative differences between EndoB1 and EndoB2 in terms of membrane binding ability, oligomerization and remodelling the bilayer.

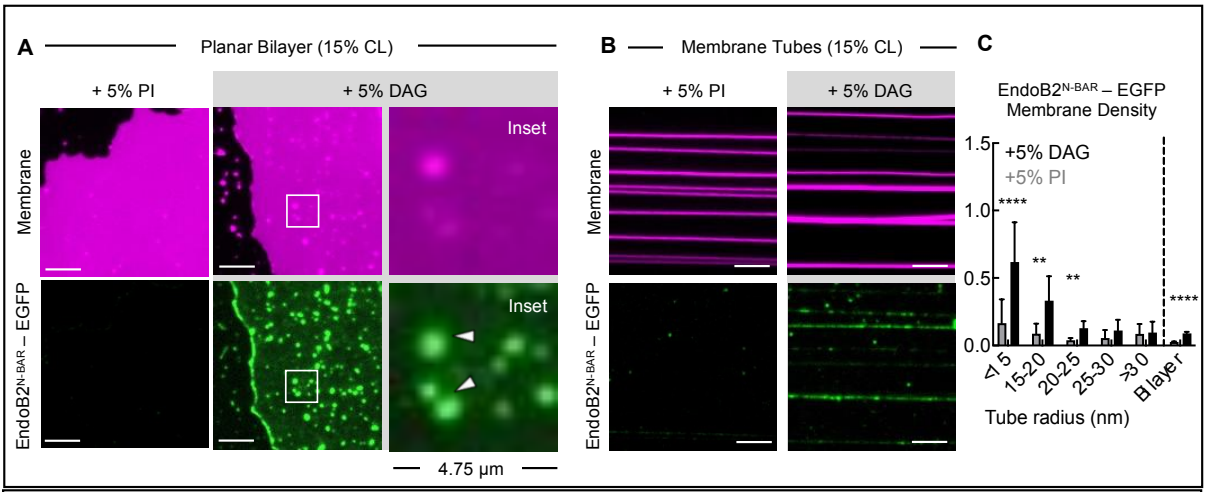

Figure 4.3- EndoB2 shows DAG-dependent membrane binding and remodeling. (A) Representative images of planar bilayers (magenta) after incubation with EndoB2N-BAR-EGFP (green). The white box in the panel have been zoomed in to create the inset. White arrows mark similar EndoB2 fluorescence with varied degrees of membrane remodeling in the membrane channel. (B) Representative fluorescence images of tubes (magenta) made of the indicated lipid composition incubated with EndoB2N–BAR-EGFP (green). (C) Plot showing EndoB2N-BAR-EGFP membrane density on tubes and bilayers. Data represents mean ± SD of at least 54 tubes and 36 different regions on planar bilayers for DAG-containing and 73 tubes and 28 different regions on planar bilayers for PI-containing membranes. Statistical significance is measured using Mann-Whitney test.

4.4 Discussion:

BAR domain containing proteins have long been studied for their roles in various cellular pathways. The unequivocal idea seems to be that BAR domain-containing proteins generate and stabilize curved membrane surfaces which act as important intermediates in a variety of cellular transport pathways (Simunovic et al, 2019). They usually are able to achieve this by responding to particular lipids on the membrane surface (Itoh et al, Dev Cell, 2005, Wu and Baumgart, 2014). Given that DAG is produced on the mitochondria during mitophagy and Endophilin B has prior literature suggesting it is able to interact with the general autophagic machinery, we wondered how would Endophilin B1/2 respond to the generation of DAG on the mitochondrial surface. Our efforts went into understanding the effect of DAG incorporation on EndoB1/2's activity. Our results show that Endophilin B1/2 both responds to the presence of DAG on a planar membrane. Both these proteins are able to bind to CL-containing planar membranes only in the presence of DAG. Upon binding, the proteins are able to oligomerize as seen by the formation of self-limited clusters in the protein channel. These clusters are associated with enhanced membrane fluorescence, as well, indicating remodelling of the underlying membrane. A closer look at the reaction showed us that the membrane remodelling reaction starts with the formation of thin spindly tubes on the bilayer which over time attains varicosities and finally coils with other tubes to form stub-like structures on the membrane. In our assays, EndoB1 was better in membrane binding and tubulation than EndoB2 indicating the subtle differences that these proteins have in terms of their ability to recognise and bind membranes, oligomerize on the membrane and finally remodel the membrane in spite of having a high degree of sequence identity.

On pre-formed membrane tubes, EndoB1 bound both DAG- and PI-containing tubes equally well suggesting that two criteria govern the recruitment of EndoB1 to a membrane surface: lipid specificity and curvature. These properties can be brought about in a temporally separated manner during the time course of a membrane remodelling reaction. Generation of DAG on the mitochondrial surface can lead to the recruitment of EndoB1 on the planar organelle surface and help generate tubes. These tubes can, in turn, recruit more EndoB1 from the cytosol to feed this process forward making it a DAG-dependent feed forward loop for tubulation reactions on organellar surface.

Endophilins have previously been reported to work in concert with Dynamin family proteins during endocytosis (Sundborger et al, 2011). Endophilin B1-generated tubes on the bilayer, however, were resistant to Drp1-mediated fission. The same was true for pre-firmed tubes as well. This was not surprising considering that Endophilins have previously been shown

to negatively regulate dynamin catalysed fission both *in vitro* and in cells in SH3-PRD dependent manner (Hohendahl et al, 2017). However, unlike dynamins, Drp1 does not have a PRD domain that can directly bind to Endophilin SH3. Given that Endophilin B1 does not impose a bulk lipid diffusion barrier in the membrane, the tubes generated must have 15%CL and 5%DAG in them and their dimension were also compliant with Drp1's ability to cause fission. This suggest that EndoB1 and Drp1 probably competes for the same binding sites on the membrane. Thus, Drp1's inability to cause fission probably reflects on the availability of membrane surface for Drp1 to bind and oligomerize after EndoB1 binding. Also, given that 10-fold excess of Drp1 could not hinder EndoB1's ability to tubulate the bilayer, but Drp1's ability to cause fission was severely compromised, indicates that EndoB1, likely, has a much higher binding affinity for these membranes as compared to Drp1.

BAR domain containing proteins have been suggested to bind to negatively charged lipids on the membrane surface (Itoh et al, Dev Cell, 2005, Wu and Baumgart, 2014). However, DAG is not a charged lipid. DAG is thought to be a conical lipid which imposes a negative spontaneous curvature on the membrane (Leikin et al, 1996). This leads to the generation of packing defects in the membrane (Vamparys et al, 2013). Endophilin B1 has two amphipathic helices in the vicinity of the of BAR domain which has been shown to be important for membrane binding and tubulation (Bhatt et al, 2021). On the other hand, amphipathic helices has been shown to be sensors of membrane packing defects (Vanni et al, 2013, Campelo and Kozlov, 2014). Whether Endophilin B can sense curvature through its amphipathic helices, however, remains to be tested.

Chapter 5:

A screen for Cardiolipin-dependent membrane fission catalysts identifies alpha-synuclein

5.1 Introduction:

Biological membranes are made up of lipids that in polar environments spontaneously associate together in the form of a bilayer. They are easily bendable but resists rupture, part of the reason why they were selected to serve the barrier function in cells. Membrane fission is the process by which two membrane-bound compartments are created from one. Membrane fission is required in multiple cellular processes like generation of transport carriers, division of an organelle or the cell itself. The process of fission requires the application of force on a tube-like membrane intermediate which causes it to constrict because of the radial curvature stress finally causing fission (Kozlovsky and Kozlov, 2003). Theoretically, it requires lipids to take up non-bilayer conformations which are thermodynamically unfavourable and hence the idea of 'catalysts' that manage this process (Chernomordik and Kozlov, 2003).

Finding proteins that manage the process of membrane fission has been a challenge in cell biology. The screens carried out in the 90's that looked at molecular players involved in the formation, transport and fusion of vesicular carriers did not yield a single gene involved in membrane fission (Schekman and Novick, 2004). The reason might be do with the essential nature of these genes in cellular physiology and mutations in these genes can, likely, lead to lethality. The most well established fission apparatus, dynamin, came from a genetic screen in Drosophila (Kelly and Suzuki, 1974). Research over years has led to the discovery of dynamin superfamily of proteins, soluble members of which have been implicated in membrane fission at different locations in the cell (Ramchandran and Schmid, 2018). However, dynamin family proteins have also been shown to not have any role in other fission reactions in the cell like fluid phase endocytosis and generation of VSVG carriers from Golgi bodies (Bonazzi et al, 2005). Moreover, cells lacking dynamin genes survives in culture from days to weeks suggesting that there are multiple other fission catalysts that are, likely, present in the cell (Ferguson et al, 2009, Park et al, JCS, 2013).

Mitochondria are double-membrane bound organelles which are not thought to be a part of secretory or endocytic pathways in the cell. Hence, the only kind of mitochondria-associated fission reactions that have been talked about in literature is that of division of the organelle. Mitochondrial fission is brought about by a dynamin family protein, Drp1 (Kamerkar and Krauss et al, 2019). However, recent insights into mitochondrial biology suggests that mitochondria actually cross-talk with multiple other organelles in the cell via the formation of mitochondria-derived vesicles (MDVs). MDVs are small transport carriers (~75-200nm in diameter) that transport mitochondrial proteins to different locations in the cell like peroxisomes, lysosomes and the plasma membrane (Neuspiel et al, 2008, Soubannier et al,

2012, Matheoud et al, 2016). Interestingly, however, formation of these transport carriers are generally considered Drp1-independent (Neuspiel et al, 2008, Soubannier et al, 2012). These led us to design a screen to look for novel membrane fission catalysts that might be involved in the formation of MDVs.

Assays systems that enable us to look at membrane fission reactions have been scarce. Experiments in cells are have helped us understand the functional implications of the fission catalysts, although, the resolution of imaging does not help us visualize the mechanical steps involved in the process. Reconstitution studies, on the other hand, have shed significant light on the abilities of protein/s to manage particular membrane remodelling reactions by defining the minimum machinery required for a particular process (Takei et al, Cell, 1998, Matsuoka et al, Cell, 1998). Traditionally, liposomes have been used to monitor membrane fission reactions *in vitro* (Lee et al, Cell, 2005, Boucrot et al, Cell, 2012). Although, liposome-based studies have been very insightful in discerning membrane binding properties of a protein, they are often limited by several drawbacks. Liposome-based assays are usually end-point read out and lack any real-time analysis of the steps involved in fission. Membrane templates with excess reservoir has also been used to study fission reactions but are limited by the planar nature of the membrane template (Pucadyil and Schmidt, 2008). Supported membrane templates (SMrT) have been previously used to monitor membrane fission reactions in real time (Dar et al, 2015, Kamerkar and Krauss et al, 2019). The templates provide unique advantages over other model membrane systems like, tube-like intermediates to assay for fission reactions, real-time analysis of the pathway to fission and are also robust and facile. These led us to design a screen for novel membrane fission catalysts using SMrT as an assay system.

5.2 Material and Methods:

5.2.1 Brain lysate preparation:

Goat brain lysate was prepared as previously described (Kamerkar et al, 2018). Briefly, goat brains were washed extensively using PBS and suspended in lysis buffer ((25 mM Tris pH 8.0, 500 mM KCl, 250 mM sucrose, 2 mM EGTA, and 1 mM DTT with EDTA-free protease inhibitor cocktail (Roche)). Lysis was done using an Waring blender and the lysate was spun at 160,000g for 2 hours to get a soluble fraction in the supernatant. The supernatant was subsequently loaded on a Hi-Trap 26/10 desalting column (GE Lifesciences) and desalted in assay buffer (20mM HEPES, 150mM KCl, 1mM DTT). The protein containing fractions

were pooled, flash frozen in liquid N2 and stored in -80˚C for future use. Protein estimation was done using BCA reagent kit (Takara).

5.2.2 Supported Membrane template assay and tube size estimation:

Supported Membrane template assay and tube size estimation were done exactly as is mentioned in Chapter 2 of this thesis. Proteins were flown in at 0.1mg/ml final concentration on templates made of different lipids and images were taken 5 minutes after protein was flown in without washing off excess unbound protein.

5.2.3 Pull-down using chelator beads:

0.1mg/ml of the brain lysate (400µl) was incubated with 5µl of bed volume of Co^{2+}-charged chelator beads (Takara), incubated for 30 minutes on a rotor to allow for uniform mixing and then spun at 3000g on a benchtop centrifuge for 5 minutes at RT. The supernatant was separated and used in SMrT assay. The pellet was washed thrice with assay buffer and subsequently processed for mass spectrometry. For incubation with uncharged beads, the same experiment was done in the presence of 10mM EDTA.

5.2.4 Depletion using antibody:

Purified α-Syn was used to generate a standard curve of protein amount to chemiluminescence signal on a blot. This was used to quantify the amount of α-Syn present in brain lysate which came up to ~50nM. To deplete α-Syn function from the lysate, the lysate was incubated with 3x monoclonal α-Syn antibody (Abcam 138501) for 30 minutes following which it was flown in on templates and images were recorded after 5 minutes without washing out excess unbound protein.

5.2.5 Mass spectrometry for identification of proteins:

For protein identification using mass spectrometry, the chelator beads bound to the protein of interest in 20mM HEPES, 150mM KCl was reduced with DTT (10mM) at 60 °C for 30 minutes. This was followed by addition of 20mM iodoacetamide (IAA) in dark at room temperature for 15mins for alkylation. Proteins were digested on-bead using 1µg trypsin (Sequencing grade modified trypsin, Promega V5111) in 100mM TEAB buffer at 37 °C for 16 hours (overnight). Next day, the solution was spun at 3000g for 10 mins to separate the supernatant containing peptides, desalted using C18 resin (Empore, 66883-U), dried and stored

in -80 °C. The stored peptides were resuspended in 0.1% formic acid (FA) and analyzed in a Sciex Triple-TOF6600 mass spectrometer interfaced with an Eksigent nano-LC 425. The trypsin-digested peptides (~3µg) were first flown thorough a Eksigent C18 trap column (to get rid of any common contaminants) and eluted onto an Eksigent C18 analytical column in a linear acetonitrile gradient. A typical LC run was of 120 mins at a flow rate of 300nL/min in the presence of a gradient of acetonitrile (0-100%) in 0.1% formic acid. The gradient for the run was kept as 5% acetonitrile for 10mins, followed by a linear gradient of 0-30% acetonitrile for 80 mins, 80 acetonitrile for 15mins and re-equilibration with 5% acetonitrile for 15mins. All proteomic data acquisition was done in an information-dependent acquisition (IDA) mode over a selected and specified mass range of 300-2000 *m/z*. Each MS survey was followed by a MS/MS scan of 10 peptides with the highest intensity. Peptide identification and quantitation was done using Protein Pilot software. A Refseq goat (*Capra hircus*) protein database (release no. 210) was used for peptide identification. In Protein Pilot, iodoacetamide was specified as the alkylating agent and identification was performed on peptides filtered with <1% FDR. For identification of the protein of interest, first, proteins were sorted based on the number of peptides (>1 peptides were taken for further analysis). The list of common proteins from all four independent runs were then collated and added to UNIPROT ID mapping to look for proteins that had) 'lipid-binding' (GO: 0008289) as a GO annotation (molecular function).

5.2.6 Cell culture and CRISPR-Cas9 mediated knock-out (KO) cell line generation:

SH-SY5Y cells were maintained in DMEM/F12 (1:1) media (Gibco) supplemented with Fetal bovine serum (FBS) (Gibco) at 10% final concentration and 100units/ml penicillin/streptomycin (Invitrogen) in a 5% CO_2 incubator maintained at 37°C. For routine maintenance and passaging, the existing media was first discarded and the cells were washed once with DPBS. 1xTrypsin-EDTA was added to cells and incubated at 37°C for 1 minute. Complete media was added to trypsinized cells and spun at 1000g for 5 minutes at 10°C. The pellet was further resuspended in complete media and 1/4th of the total volume was re-seeded in a new flask.

α-Syn KO cell lines were generated using CRISPR-Cas9 mediated gene knockout technology. Briefly, wild-type SH-SY5Y cells were grown in 35mm dishes and transfected with two gRNAs specific to α-Syn (5'-GTGGTGCATGGTGTGGCAAC-3' and 5'-AATTCTGGAAGATATTGCCTG-3'cloned in pLentiCRISPR v2) along with a co-transfection marker pEGFP-N1. The cells were grown for 72 hours post-transfection and sorted

for EGFP positive cells using a cell sorter (BD Aria Fusion Sorter). The EGFP-positive cells were sorted into 96-well plates having 5 cells in each well. The clones were grown further and KO lines were tested for using western blotting.

5.2.7 Cell lysis and Western Blotting:

Cells pellets were lysed in lysis buffer (20mM HEPES, 500mM KCl, 0.1% Triton X-100) in the presence of 1mM PMSF. Lysis was done by sonication and lysates were spun down at 1000g to get rid of un-lysed cells. Total protein estimation was done using BCA reagent kit (Takara). Equal amounts (15µg) of cell lysate were were boiled at 99˚C for 10 minutes in the presence of 1x Laemmli's buffer and run on an 15% SDS-PAGE. The proteins were transferred to a PVDF membrane overnight and blotted using primary antibodies according to the manufacturer's protocol. Beta-actin was used as a loading control (Santa Cruz Biotechnology, 47778).

5.3 Results:

5.3.1 Brain lysate shows a CL-specific membrane fission activity:

Based on the rationale that narrow tube-like intermediates mimic the late stages of any fission reaction, we employed SMrT to assay for novel fission catalysts in the brain cytosol. Goat brains were lysed, centrifuged to get rid of membrane fractions and desalted to get rid of any soluble small molecules or nucleotides. This soluble pool of proteins was used for further assays (Fig 5.1 A). Cardiolipin (CL) is a lipid that is present in the mitochondria and peroxisomes and have been shown to be important for multiple functions of the mitochondria including fission of the organelle (Kamerkar and Krauss et al, 2019, Macdonald et al, 2014, Bustilo-Zabalbeitia et al, 2014). Membrane templates were made of 15%CL (or any other phospholipid of choice for control experiments) in a background of dioleoylphosphatidyl choline (DOPC). Templates contained a small amount (1%) of a fluorescent lipid-probe (Texas red DHPE) that helped us visualize the templates by fluorescent microscopy. Brain lysate having a concentration of 0.1mg/ml was flown on to templates, incubated for 5 minutes and fission was scored as a fraction of the starting number of tubes that showed at least one cut. Remarkably, flowing in brain lysate on 15%CL tubes showed robust fission within 5 minutes of flowing in 0.1mg/ml protein (200µl) (Fig 5.1 B). Fission was CL-specific as tubes made of different other phospholipids did not show similar activity. Interestingly, fission happened without the requirement of any externally added nucleotides suggesting that dynamin super-family proteins are, likely, not involved in this activity. Fission was curvature-sensitive;

narrower tubes showed an increased tendency of undergoing fission that thicker tubes (Fig 5.1 C). Together, these results indicate the presence of a CL-specific, nucleotide-independent membrane fission catalyst in the brain cytosol.

5.3.2 Biochemical analysis and mass spectrometry identified the active component in brain lysate to be alpha-synuclein

Next, we wanted to know the protein/s in the brain lysate that are involved in this activity. We tried to biochemically fractionate the lysate but that did not yield fruitful results. Serendipitously we encountered that incubating the brain lysate with chelator beads functionalized with a metal ion (Co^{2+}) depleted the lysate of the membrane fission activity (Fig 5.1 D). The soluble fraction after incubation and pelleting down the beads did not show any membrane fission activity. As a control, beads not functionalized with the metal ion did not deplete the lysate of the activity (Fig 5.1 D). Subsequently, mass spectrometric analysis of the beads functionalized with Co^{2+} led to identification of 240 proteins of the brain lysate being bound to these beads. Membrane binding is a pre-requisite for membrane fission. Hence, we sorted the list based on proteins that have been reported to bind the membrane. Bioinformatic analysis of the list of proteins based on Gene Ontology (GO) annotations showed 8 proteins from the list to be 'lipid-binding' proteins (GO:0008289) (Table 5.1). Based on previous reports on membrane binding, membrane remodeling and association with cardiolipin and the mitochondria, we narrowed down our protein of interest to be alpha-synuclein (α-Syn). In order to test if α-Syn is actually necessary for the activity of the brain lysate, we incubated the lysate with a α-Syn monoclonal antibody and flowed in onto 15%CL-containing tubes. Remarkably, addition of the antibody dramatically hindered the robust fission that was otherwise seen with the brain lysate. If α-Syn in the brain lysate was responsible for causing fission, we argued, any other source of native α-Syn should also show a similar nucleotide-independent, CL-dependent membrane fission reaction. The human neuroblastoma cell line, SH-SY5Y, have been used extensively in looking at α-Syn functions (Xicoy et al, 2017). Lysates made from wildtype (WT) SH-SY5Y cells showed a similar membrane fission activity on CL tubes. Notably, the fission activity was not as robust as brain lysate, likely, because of the expression level of the protein in these cells. Next, we generated a α-Syn knock-out (KO) cell line using CRISPR-Cas9. Lysates from the KO cell line showed significantly reduced membrane fission activity cementing the idea that α-Syn is necessary for the CL-specific fission activity in lysates.

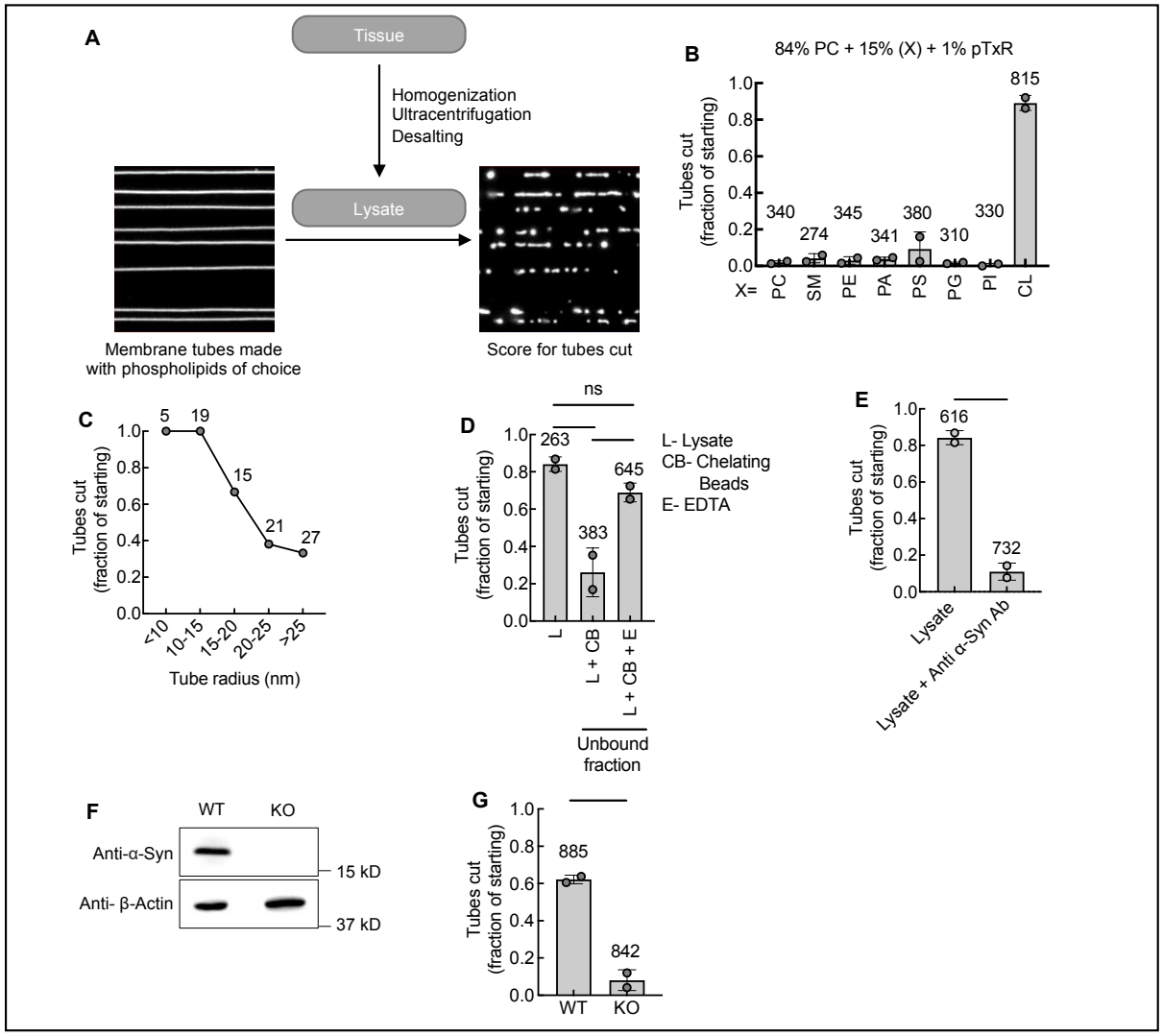

Figure 5.1. A screen for cardiolipin-dependent membrane fission catalysts identifies alpha-synuclein (α-Syn). (A) Schematic of steps involved in brain lysate preparation and use Supported Membrane Tubes (SMrT) assay system as a read-out for the biochemical screen. (B) Plot showing quantitation of tubes showing at least one cut represented as a fraction of starting number of tubes. Tubes were made of 15% of the indicated lipid in a background of DOPC (84%) and pTxR (1%). Data represents mean ± SD of 2 independent experiments. The number on top of each bar represents the number of tubes analysed for each lipid. (C) Quantitation showing 15%CL tubes cut as a function of tube radii. Data represents mean across all tubes analysed (numbers on top of each point) in that bin. (D) Quantitation showing 15%CL tubes undergoing fission when incubated with lysate (L), unbound fraction of Lysate + Chelating beads (Co^{2+}) and Lysate + Chelating beads (Co^{2+}) + EDTA. Data represents mean ± SD of 2 independent experiments while the number at the top of each bin represents the number of tubes analysed for that particular condition. (E) Plot showing 15%CL tubes cut as a fraction of starting number of tubes when incubated with Lysate and Lysate + Anti α-Syn Ab. Data represents mean ± SD of 2 independent experiments with number of tubes analysed indicated on top of each bar. (F) Representative Western Blot showing CRSIPR-Cas9-mediated knock-out (KO) of α-Syn in SHSY-5Y cells as probed with Anti-α-Syn Ab. Beta-actin is used as a loading control. (G) Plot showing number of tubes cut as a fraction of starting number of tubes upon incubation of 15%CL tubes with WT or α-Syn KO SHSY-5Y lysate. The number at the top of each bar represents the total number of tubes analyzed in that condition. Data represents mean ± SD of 2 independent experiments.

Table 5.1 Lipid-binding proteins in the brain lysate:

Table 5.1	GI accession	Official Gene Symbol	'Lipid-binding' proteins (GO:0008289)
1	1062948079	SPTBN2	spectrin beta, non-erythrocytic 2(SPTBN2)
2	1062910850	MAP1B	microtubule associated protein 1B(MAP1B)
3	1062941066	MBP	myelin basic protein(MBP)
4	1062990226	SPTBN1	spectrin beta, non-erythrocytic 1(SPTBN1)
5	1062881117	SNAP91	synaptosome associated protein 91(SNAP91)
6	1062980096	SH3GL2	SH3 domain containing GRB2 like 2, endophilin A1(SH3GL2)
7	926693681	SNCA	synuclein alpha(SNCA)
8	1062947650	SF1	splicing factor 1(SF1)

5.4 Discussion:

Membrane fission is a central theme in cellular physiology implicated in diverse cellular processes. However, deciphering proteins that are involved in membrane fission has been a challenge. This is, in part, due to a lack of assay systems that directly look at membrane fission reactions. Here, using a system of polyethylene glycol (PEG)-cushioned supported membrane templates (SMrT), we assayed for proteins that are involved in fission of cardiolipin tubes. Our results show that brain lysate has a robust cardiolipin-specific membrane fission activity. Furthermore, the fission activity was nucleotide-independent negating the involvement of any dynamin superfamily proteins, all of which have been shown to use nucleotide hydrolysis for their activities. The activity was curvature-sensitive indicating a bona-fide concerted membrane fission activity as has been reported for canonical fission catalysts and not just random rupture of membrane tubes (Dar et al, 2015, Kamerkar and Krauss et al, 2019). Biochemical analyses followed by mass spectrometry-based proteomics identified the active component to be alpha synuclein (α-Syn). We further confirmed this finding using antibodies and cell lines that express the protein.

Interestingly, α-Syn bound to chelator beads functionalized with a metal ion that helped us pull down the protein and identify it through mass spectrometry. Previous reports have showed that α-Syn binds to different divalent metal cations (Binolfi et al, JACS, 2006). Thus, in hindsight, α-Syn from the brain lysate binding to the chelator beads is not surprising.

Moreover, the same report narrowed down the site of binding to these metal ions as ^{119}PDNEA^{124} residues. Coincidentally, the monoclonal antibody that we used for depletion studies recognises almost the same epitope (^{118}VDPDNEA^{124}). A possible explanation for the antibody-mediated depletion of activity is that the antibody competed out the bound metal cations in the protein which resulted in drastic reduction of fission. However, whether metal ions have a definitive role to play in fission caused by α-Syn remains to be systematically tested.

α-Syn has mostly been studied in the context of Parkinson's Disease (PD)-associated neurodegeneration. α-Syn is the active component of Lewy bodies found in patients suffering from PD. Although, a lot is known about the mechanisms by which α-Syn aggregates in a cell under different conditions, very little is known about the function of the protein in a non-disease scenario. Given the unbiased nature of the biochemical screen carried out, our results, likely, indicate a native function of the protein which for a long time has remained elusive.

Chapter 6:

Alpha-synuclein binds to and causes fission of CL-containing membrane tubes

6.1 Introduction:

Alpha-synuclein (α-Syn) is a vertebrate-specific small 140 amino acids-containing protein abundantly present in the presynaptic terminals. It is both genetically and physiologically linked to a diverse range of neurodegenerative diseases called 'synucleopathies'. Parkinson's Disease (PD) is one such condition characterized by misfolded aggregation of the protein in different regions of the brain. Although, a lot is known about how the protein misfolds leading to accumulation and aggregation, relatively little is understood about the function of the protein in a cell in a no-disease condition.

6.1.1. History:

α-Syn was discovered as neuron-specific protein that is localized both in the nucleus and the pre-synaptic terminal from the Torpedo electric organ (Maroteaux et al, 1988). A few years later α-Syn was identified as a non-amyloid-β component (NAC) present in the neuronal plaques of patients suffering from Alzheimer's disease (Ueda et al, 1993). The discovery of α-Syn was closely followed by the discovery of two other genes of the synuclein family: β-synuclein and γ-synuclein (Jakes et al, 1994, Lavedan et al, 1998). Subsequently, α-Syn was reported to be present in Lewy bodies of patients suffering from PD (Spillantini et al, 1998). A genome-wide association study revealed the genetic risk of mutations in the α-Syn gene being causally linked to pathogenesis of PD (Simon-Sanchez et al, 2009). Over years α-Syn has been associated with multiple other neurodegenerative diseases as well like Lewy body-associated dementia, multiple system atrophy, amyotrophic lateral sclerosis, Krabbe disease among others (Burre, 2015).

6.1.2. Expression pattern:

α-Syn has been shown to be present ubiquitously in different parts of the central nervous system including neocortex, hippocampus, cerebellum and thalamus among others (Iwai et al, 1995). Although, initially thought to be a protein associated with only the nervous system, later studies indicated that α-Syn is actually present in most cell and tissue types in the human body. α-Syn has been reported to be present in abundance in red blood cells, in hematopoietic cells, in fetal liver, lungs, kidney, heart, muscles, adrenal gland and testes (Baltic et al, 2004, Shin et al, 2000). Thus, α-Syn expression is ubiquitous across multiple tissues and organs in humans.

Expression of α-Syn is developmentally regulated. α-Syn mRNA expression starts in late embryonic stages in rats, reaching a peak in the first few weeks postnatally and then is reduced again (Petersen et al, 1999). In humans, α-Syn proteins levels increase during the time

course of development and remains high during throughout adulthood (Chu et al, 2007). This suggests post-transcriptional regulation of α-Syn mRNA to produce desired quantities of the protein during different time points in development.

6.1.3 Structure:

α-Syn is thought to be an intrinsically disordered protein (IDP) in solution. It does not fold into any domain architecture. However, it is broadly classified to have three regions: N-terminal region (residues 1-60), non-amyloid-β component (NAC) (residues 61-95) and the C-terminal region (residues 96-140). The N-terminus of the protein is thought to interact with membranes whereby it adopts an α-helical conformation in the presence of lipids (Davidson et al, 1998). Furthermore, the N-terminus contain seven 11 residue repeats (KTKGEV) which helps in the formation of α-helix upon membrane binding (Bussels et al, 2003). In this context α-Syn is thought to be quite similar to apo-lipoproteins (Varkey et al, 2010). Interestingly, all known familial mutations associated with PD have been reported to be present in the N-terminus of the protein. The N-terminus of α-Syn has also been reported to undergo post-translational modifications like acetylation. Acetylation is thought to modulate several functions of the protein including membrane binding, protein-protein interactions and aggregation (Bartels et al, 2014). The amphipathic helix traverses not only the N-terminus but also covers the NAC region which has been reported to be important for aggregation of α-Syn in multiple diseased conditions (Ueda et al, 1993). The C-terminus of the protein has a lot of negatively charged residues which have been shown to be mobile both in α-Syn oligomeric species and in fibrils (Paslawski et al, 2014, Tuttle et al, 2016). α-Syn has been reported to bind to divalent metal cations through particular residues in the C-terminus (Binolfi et al, 2006). Moreover, phosphorylation of the serine at 129th position (S129) in the C-terminus of the protein is considered a dominant pathological modification of the protein in familial and sporadic PD. Thus, α-Syn has three distinct regions all of which perform unique functions for the proteins.

6.1.4. Reported functions:

Since its discovery α-Syn has been considered to be important for neuronal functions. However, knock-out of all three synuclein genes did not cause any drastic phenotypic change in mice. The mice had slightly lesser life span and along with some morphological changes in synapse and axonal structure (Greten-Harrison et al, 2010). α-Syn has been implicated to participate in multiple different processes in the cell. α-Syn is widely regarded as a protein that

can interact with membranes. Hence, it has been looked at in diverse processes that necessitate membrane binding and remodelling. *In vitro*, α-Syn has been shown to bind to vesicles containing anionic lipids (Jo et al, 2000). Moreover, α-Syn's interaction with membrane has been reported to be curvature-sensitive (Davidson et al, 1998, Pranke et al, 2011). Upon membrane binding, α-Syn has been shown to cause morphological changes to the membrane architecture. Incubation with high amounts of α-Syn transforms negatively charged vesicles into much smaller entities (Varkey et al, 2010). Moreover, depending on the protein to lipid ratio, α-Syn has been shown to induce extensive tubulation of negatively charged membranes. α-Syn has also been suggested to disrupt the integrity of membranes. Vesicle-leakage experiments confirm that α-Syn is able to cause leaks in highly anionic small unilamellar vesicles by its ability to form pores in the membrane (Volles et al, 2002, Jao et al, 2008, Tosatto et al, 2012). α-Syn binding to remodelling activity is dependent on the membrane binding affinity, the insertion depth of the protein into the bilayer and the interleaflet asymmetry of lipids in the membrane (Braun et al, 2017). α-Syn has also been suggested to impart and recognize membrane packing defects in bilayers (Kamp et al, 2006, Ouberai et al, 2013).

In neurons, α-Syn has been suggested to be involved in SNARE-mediated synaptic vesicle fusion. α-Syn has been shown to promote SNARE complex assembly during different steps like docking and fusion of transport carriers (Yoo et al, 2023). It has also been shown to be associated with synaptic vesicles, release of neurotransmitters and lipid metabolism. Furthermore, over-expression of α-Syn has been associated with basal and stimulated synaptic vesicle endocytosis in hippocampal neurons (Gedalya et al, 2009). Over-expression of synuclein has been shown to be disruptive for multiple organelles in cells like Golgi, mitochondria, lysosomes and nuclear membranes (Gosavi et al, 2002, Martin et al, 2006, Meredith et al, 2002, Stichel et al, 2007).

Extensive research have also suggested α-Syn to be associated with the mitochondria. α-Syn is mostly cytosolic in the cell but does associate with mitochondria minimally under basal conditions which goes up upon induction of stress (Cole et al, 2008). In fact, α-Syn has been suggested to be associated with both the inner and outer membranes of the mitochondria. (Cole et al, 2008, Devi et al, JBC, 2008). FRET-based biochemical assays show that α-Syn interacts with the mitochondria much better than other organelles including the ER, plasma membrane and vesicle fractions (Nakamura et al, 2008). Over-expression of α-Syn has been shown to cause fission of the mitochondria as well (Nakamura et al, JBC, 2011). Additionally, mitochondrial dysfunction is considered one of the earliest hallmarks of PD.

Our results from a biochemical screen suggested that α-Syn is necessary to cause fission of CL templates in a nucleotide-independent manner. Although, α-Syn has been reported to be associated with a wide variety of cellular functions, its molecular role in a cell still remains elusive. This led us to test the biochemical properties of synuclein in isolation.

6.2 Materials and Methods:

6.2.1 Cloning, expression and purification:

Human α-Syn cloned in pRK172 vector was a generous gift from Prof. Jayant Udgaonkar. The construct was transformed in BL21(DE3) competent cells and grown at 37˚C till it reached an O.D. of 0.6 upon which cultures were induced with 100nM IPTG, grown for 5 hours at 37˚C and pelleted down at 6000g. 1L bacterial culture pellets were resuspended in 30ml of osmotic shock buffer ((30mM Tris-HCl, 40% w/v sucrose and 2mM EDTA (pH 7.2)) and incubated for 15-20 minutes at RT with occasional vortexing. It was then spun at 15000g for 20 minutes. The supernatant was discarded and the pellet was further resuspended in ice-cold 30ml Millipore water containing 37µl of saturated MgCl2 with occasional vortexing. The solution was then centrifuged at 15000g for 20 minutes at 4˚C. The supernatant of this step was carefully taken out and dialysed against 20mM HEPES pH 7.4, 150mM KCl, 1mM DTT for 12 hours at 4˚C. The dialyzed supernatant was loaded on a pre-equilibrated Hi-Trap CaptoQ column (5ml, GE Lifesciences) and washed extensively with buffer. The protein was eluted in a gradient of salt (150mM-1000mM KCl) in background of 20mM HEPES and 1mM DTT. The elutions were run on a gel and the fractions containing pure proteins were pooled together and dialysed against 20mM HEPES pH 7.4, 150mM KCl and 1mM DTT. The pure protein after dialysis was kept on ice for 2-3 days and all assays were performed within that time. For all assays the protein was spun down at 100,000g for 30 minutes at 4˚C to get rid of any aggregates. For heat-denatured purification, the bacterial pellet was lysed using sonication, spun down at 30000g to get rid of the membrane fraction and then the supernatant was subjected to heat precipitation at 99˚C in a water-bath for 10 minutes, followed by another spin at 30000g and the supernatant from that was used for further anion-exchange purification like mentioned above. For heat-denaturation of the lysate, 0.1mg/ml of the lysate was incubated in a water bath at 99˚C for 10 minutes followed by a spin at 30000g to get rid of aggregated proteins. The supernatant was used for assay.

6.2.2. Liposome preparation and Proximity-based labelling of Membrane Associated Proteins (PLiMAP):

Lipids in desired amounts were aliquoted in chloroform stocks and added to the bottom of a clean glass test tube to a final concentration of 1mM. In addition to lipids of choice, for PLiMAP, liposomes contained 1 mol% of a bi-functional lipid probe Bodipy-Diazirine phosphatidyl ethanolamine (BDPE). The chloroform mixture was dried to generate a thin film in the bottom of the test tube, kept for drying under vacuum for 3 hours. Required amount of filtered Millipore water was added to the glass test tube and kept for hydrating in a water-bath for 30 minutes at 50°C. The mixture was then vortexed vigorously and extruded using an extrusion apparatus through a 50nm polycarbonate filter unless mentioned otherwise.

For experiments, 10μM of purified protein was incubated with 100μM of desired liposomes in a final volume of 30μl for 30 minutes at RT. The mix was then UV-irradiated for 1 minute using a 365nm UV lamp (Analyticjena, UVP crosslinker CL-1000L) at an intensity of 200mJ cm^{-2}. The reaction mixture was boiled in 1x Laemmli's buffer for 10 minutes at 99°C and run on a 15% SDS-PAGE. The gels were first imaged for Bodipy fluorescence and then stained with Coomassie brilliant blue to check for equal sample loading. Images of the fluorescence channel were analysed exactly as mentioned previously (Jose and Pucadyil, 2020).

6.2.3 SMrT assay and image analysis:

SMrT assay system was made exactly as is stated in Chapter 2 of this thesis. For experiments with α-Syn, 1μM of the purified protein was flown in assay buffer (20mM HEPES pH 7.4, 150mM KCl, 1mM DTT), incubated for 10 minutes before acquiring images. For real-time analysis, the assay buffer was supplemented with oxygen scavenger cocktail and recorded with 0 sec interval and an exposure of 100ms. All image analysis and statistical analysis was done as is mentioned in Chapter 2 of this thesis.

6.3 Results:

6.3.1 Alpha-synuclein preferentially binds to CL-containing membrane templates

α-Syn has been reported to bind to membranes containing anionic lipids (Davidson et al, 1998). However, a systematic investigation of the lipid specificity of α-Syn has been lacking. We have previously reported Proximity-based Labelling of Membrane-Associated Proteins (PLIMAP) as an assay system to look at lipid binding specificities of protein. Briefly,

proteins are incubated with liposomes containing a bifunctional lipid probe (Bodipy-Diazirine phosphatidylethanolamine (BDPE)) which gets covalently conjugated to any protein molecule which is in proximity to the membrane upon UV irradiation. This causes proteins to get covalently fluorescent labelled because of Bodipy attached to the lipid and can be separated on a gel. Extent of fluorescent signal is an indicator of amount of protein being bound to that particular liposome. We tested the lipid binding specificity of α-Syn using this assay. Recombinantly purified α-Syn was added to different liposomes containing 15% of the lipid of choice in a background of DOPC (84%) and BDPE (1%), incubated for 30 minutes to attain equilibrium binding, UV irradiated and then run on SDS-PAGE. Fluorescent blot analysis showed α-Syn bound to CL liposomes better than any other phospholipid (Fig 6.1 A, B). In fact, α-Syn bound better to CL liposomes even compared to all phosphatidyl inositols (Fig 6.1 C, D). This was quite interesting since α-Syn has been thought to engage with the membrane based on charge alone (Davidson et al, 1998). Consistent with this, our results does show that α-Syn engages with membranes having negative charge (PA, PS, PG) better than membranes made of zwitterionic lipids (PC, SM, PE). However, our results also indicate that α-Syn recognizes lipid head-groups in addition to charge since most of the phosphoinositides had similar or higher charge densities than CL (Fig 6.1 E). Next, we wanted to test if this protein has any curvature preference for membrane binding. Incubation of the protein with CL liposomes of increasing dimensions (30nm-400nm) suggested that α-Syn preferentially binds to liposomes having smaller diameter indicating it prefers binding to membranes having high curvatures (Fig 6.1 F, G). Together, these results suggest that both charge and lipid head-group-specific binding recruits α-Syn to the membrane surface.

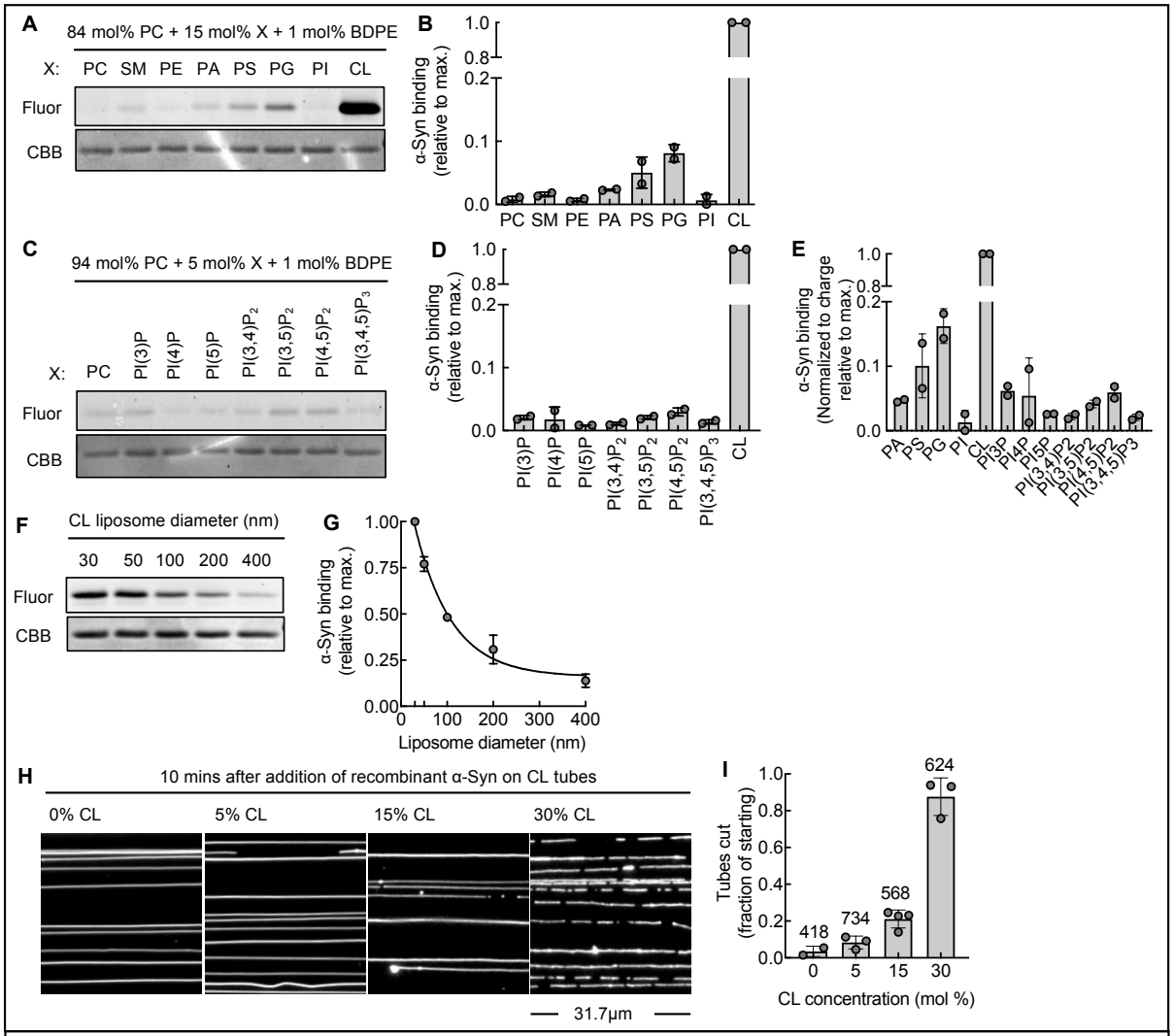

Figure 6.1. Recombinantly purified α-Syn is sufficient to cause membrane fission. (A, C) Representative PLiMAP images showing fluorescence (top) and Coomassie Brilliant Blue (CBB) (bottom) staining of α-Syn incubated with liposomes of the indicated phospholipid composition. (B, D) Quantitation of fluorescence signal in (A) and (C) respectively. Data has been normalized to the maximal binding condition (CL). Data represents mean ± SD of two independent experiments. (E) Plot showing extent of binding of α-Syn to liposomes containing indicated anionic lipids normalized to the charge of the lipid. Data represents mean ± SD of two independent experiments. (F) Representative PLiMAP fluorescence and CBB images of 15%CL liposomes of the indicated diameter. (G) Quantitation of fluorescence signal in (F). Data has been normalized to the highest fluorescence signal for each experiment. Data represents mean ± SD of two independent experiments. (H) Representative fluorescent micrographs showing SMrT made of the indicated lipid composition in a background of DOPC after incubation for 10mins with purified α-Syn. (I) Plot showing tubes cut as a function of increasing CL concentration. Data represents mean ± SD of at least 2 experiments for each condition and the number of tubes analysed indicated at the top of each bar.

6.3.2. Recombinant alpha-synuclein is sufficient to catalyze fission of CL-containing membrane tubes:

α-Syn has been implicated in multiple kinds of membrane remodelling reactions (Varkey et al, 2010, Jao et al, 2008). Our results from a biochemical screen suggested that α-Syn is necessary for CL-specific fission caused by brain lysate. Moreover, recombinantly

purified α-Syn preferentially binds to CL-containing liposomes suggesting it does have lipid specificity. Next, we wanted to test if purified α-Syn is sufficient to cause membrane fission. Purified α-Syn was added to SMrT containing increasing amounts of CL, incubated for 10 minutes and tubes having at least one cut were scored. Remarkably, purified α-Syn showed robust fission of tubes containing 30%CL (Fig 6.1 H, I). Tubes containing lesser amounts of CL (5% and 15%) showed significantly lesser cuts. It is important to mention here that the screen was done with 15%CL tubes which showed robust fission after 10 minutes of incubation. However, purified α-Syn showed robust fission only on 30%CL tubes with 15%CL tubes showing significantly lesser fission. This can be due to the presence of post-translational modifications in native α-Syn which is lacking in the protein made from heterologous sources (Zhang et al, 2019). Alternatively, this can also be due to the difference in the oligomeric state of the native protein as compared to the one purified recombinantly. α-Syn has been reported to be a tetramer in native state in cells, whereas, recombinant α-Syn is widely regarded as monomeric in solution (Bartels et al, 2011). Thus, one or a combination of multiple things mentioned above can render the protein purified from heterologous source lesser active.

Next, we monitored the fission reaction in real-time to understand the mechanism of fission. Real-time imaging of α-Syn on CL tubes showed that milliseconds before fission happens, the tube shows a dimming in fluorescence in the membrane channel at the site of fission (Fig 6.2 A, B). Since these tubes are diffraction limited and imaged under epi-fluorescence microscope, dimming in fluorescence indicates a reduction in tube dimension. Thus, the tube constricts before it undergoes fission. Whether α-Syn is localized on the constriction or adjacent to the constriction remains to be seen since our efforts with a fluorescently-labelled/tagged protein did not show fission.

Notably, we also saw differences in fission activity of α-Syn based on the method of purification. α-Syn has been widely reported to be intrinsically disordered in solution and hence one method of purifying the protein involves heat denaturation of lysates containing the protein. Alternatively, α-Syn has been reported to go the periplasm of E. *coli* making it easier to isolate the protein and do chromatographic separation (Huang et al, 2005). We purified the protein using both these methods. Interestingly, α-Syn purified by heat-denaturation showed significantly reduced fission of CL tubes as compared to the protein purified from periplasmic space (Fig 6.2 C, D). Moreover, the fission activity of the brain lysate also showed heat susceptibility since heat denaturation of the lysate rendered it inactive (Fig 6.2 E). Heat denaturation of the protein has been reported to cause multiple C-terminal truncations of the protein. Whether truncations contributes to the heat-denatured protein being inactive in assays,

however, remains to be tested. Together, these results indicate that, although, multiple methods are reported in literature for the purification of α-Syn, they may not lead to identical functional output by the protein in reconstitution assays.

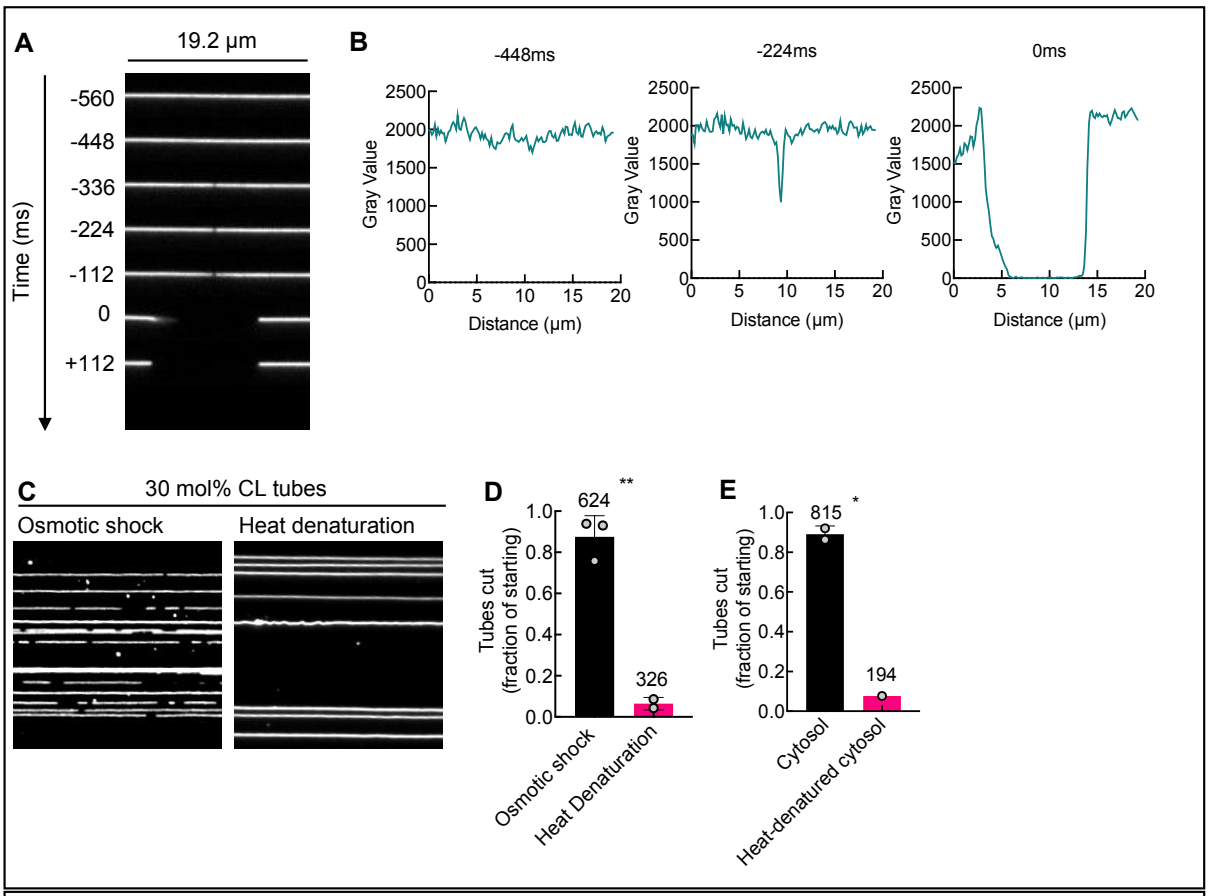

Figure 6.2 Alpha synuclein mechanism of fission. (A) Representative montage of a tube incubated with recombinant α-Syn and monitored over time. (B) Representative line profiles drawn on the tube at different time points during the fission reaction. (C) Representative fluorescent images of 30%CL tubes incubated with differentially purified α-Syn as indicated. (D) Plot showing number of 30%CL tubes cut as a function of starting number of tubes (indicated on top of each bar) upon incubation with osmotic shock purified or heat denatured α-Syn. Data represents mean ± SD of at least 2 experiments for each condition. (E) Plot showing 30%CL tubes cut as a fraction of starting number of tubes (indicated at the top of each bar) upon incubation with brain lysate or heat-denatured brain lysate. Data represents mean ± SD of at least 2 independent experiments. Statistical analyses are done using Mann-Whitney test.

6.4. Discussion:

α-Syn is small, abundant pre-synaptic protein which has been widely studied in the context of neurodegenerative diseases like PD. Our results from a biochemical screen suggested that α-Syn is important for CL-specific fission activity of lysates. We wanted to characterize the protein biochemically to understand what the protein is capable of doing in isolation. α-Syn has been widely reported to bind to membranes containing anionic lipids (Davidson et al, 1998, Cholak et al, 2020). However, given the protein is mostly cytosolic in

the cell, recruitment to a particular organelle/vesicle will be determined by the ability of the protein to interact with the lipids in that membrane. Biochemical characterization of purified protein showed that it preferentially binds to membranes having CL. CL is a mitochondria-specific lipid. Our results show that, given a choice, α-Syn will preferentially bind to mitochondria than any other member. One thing to consider here is the amount of CL present usually on the OMM. Lipidomic analysis of isolated OMM has reported a CL content of about 10% of total phospholipid in the membrane (Konig et al, 2021). However, CL has been shown to externalized under multiple stress-related conditions in the cell (Chu et al, 2013). Thus, α-Syn can bind to mitochondria, likely, minimally under basal conditions which can go up under conditions which increases CL-content on the OMM like mitophagy.

CL is an unique anionic phospholipid. It has four acyl chains and a charged head-group. CL has been shown to be dibasic at physiological pH (Olofsson and Sparr, 2013). Interestingly, our membrane binding data shows α-Syn has a higher affinity for CL membranes than it has for other phospholipids and phosphoinositides. All the mono-phosphoinosidites should behave dibasic at physiological pH with di- and tri-phosphoinositides having one or two more charges, respectively (Quarteng et al, 2021). Thus, clearly even though some of these phosphoinositides have higher charge density, α-Syn showed higher affinity to CL membranes indicating binding is determined by sites which does not solely rely on charge. We speculate, α-Syn can possibly detect head-group chemistry of different phospholipids once it interacts with the membrane. CL is, likely, a preferred head-group which lets α-Syn bind these membranes with higher affinity.

Our results show that α-Syn's prefers binding to membranes with higher curvature. The N-terminal of α-Syn is known to form an amphipathic α-helix after binding to the membrane. The amphipathic helix has a poorly arranged hydrophobic face which gets inserted into the membrane and has been implicated to be helpful in sensing membrane curvature (Jensen et al, 2011, Pranke et al, 2011). Given these findings, it is likely that α-Syn binds to the parts of the mitochondria that have higher curvatures. Mitochondria-derived vesicles have been shown to define a 'neck' of a budding vesicle which is about 30-50nm wide (Soubannier et al, 2012). It is possible that α-Syn gets recruited to these sites on the mitochondria and help in the release of these vesicles form the parent membrane.

Our results show that purified α-Syn is able to catalyse fission of CL tubes. Interestingly, the tubes underwent constriction before fission. α-Syn is known to oligomerize better in the presence of membranes (Lee et al, JBC, 2002). However, the exact mechanism by which α-Syn monomers will be able to oligomerize on the membrane to impart forces on the

membrane to constrict it and finally cause fission remains unclear. Membrane fission is brought about by forces being imparted on the bilayer circumferentially that leads to constriction of the tube and subsequently fission (Morlot and Roux, 2013). In all models of fission, there has been a necessity of an external energy currency that is brought about by nucleotide hydrolysis. However, unlike, canonical membrane fission catalysts, α-Syn does not have any nucleotide hydrolysis domain/motif. One possibility is that the nature of oligomerization on the membrane surface itself causes deformations on the membrane. The energy requirement, in this case, can be brought about by the propensity of α-Syn to oligomerize and the subsequent bond-energies released that drive the process forward. However, if this is actually the case remains to systematically tested.

Chapter 7:

Parkinsonian mutants of alpha-synuclein are incapable of causing membrane fission

7.1 Introduction:

α-Syn has mostly been studied in the context of Parkinson's Disease (PD). Parkinson's Disease is a chronic degenerative disease affecting both motor and non-motor functions associated with the central nervous system. There is usually a slow build-up of symptoms which worsens over age and is characterized by disruptive motor neuron functions like tremors, rigidity and difficulty in walking. Non-motor functions like memory loss or dementia are associated with the advanced stages of the disease.

Pathologically, PD is characterized by the development of Lewy bodies or Lewy neurites which are aggregates of proteins, lipids and other molecules at different regions within the brain of a PD-suffering individual. Interestingly, α-Syn was found to be a key constituent of the Lewy bodies (Spillantini et al, 1998). Almost at the same time, an Italian kindred was discovered having a pattern of familial aggregation and associated symptoms (Polymeropoulos et al, 1997). The family had a mutation in the α-Syn gene providing the first evidence of a genetic control of the disease. Subsequently, multiple point mutations in the α-Syn have been reported which causes early-onset familial PD. A few of these mutations are associated with mild clinical symptoms (A18T, A29S and A30P) whereas others have been shown to cause rapidly progressing clinical phenotypes (E46K, H50Q, G51D, A53E, A53T) (Guan et al, Frontier cell neuroscience, 2020).

In vitro, PD-associated α-Syn mutations have been shown to accelerate the aggregation kinetics of α-Syn and *in vivo*, induce cell death through apoptosis (Narhi et al, 1998, El-Agnaf et al, 1998). α-Syn can form aggregates in solution and the aggregation process is faster in the presence of lipids (Perrin et al, JBC, 2001). However, not all Parkinsonian mutants behave similarly in cells and *in vitro*. α-Syn (A30P) has been shown to be defective in binding to vesicles in rodent brains (Jensen et al, JBC, 1998). In solution NMR data suggests that α-Syn (WT) and α-Syn (A53T) have indistinguishable structure and kinetics of aggregation in the presence of micelles whereas the α-Syn (A30P) seems to be quite different (Ulmer and Bax, 2005). The reason for this difference is suggested to be a break in the extended helix that happens due to the presence of a proline residue. This results in defective membrane binding as due to loss of particular contacts between the protein and micelle surface that are present otherwise. Site-directed spin labelling EPR studies too suggested that α-Syn (A30P) is defective in membrane binding. However, the same study also suggested that α-Syn (A53T) is defective in membrane binding too, albeit not to the extent of A30P. Simulation studies have indicated that α-Syn (A53T) to have multiple stabilizing hydrogen bonds with the membrane increasing its membrane occupancy (Perlmutter et al, 2009). Our results show that α-Syn (WT)

can bind to CL membranes and can cause fission of membrane tubes in a Cl-dependent manner. We wanted to test how the parkinsonian mutants of α-Syn behave in terms of membrane binding and fission.

7.2 Materials and Methods:

7.2.1 Expression and Purification

The mutants of α-Syn were expressed and purified exactly like the wild-type protein mentioned in Chapter 6 of this thesis.

7.2.2 PLiMAP and SMrT assays:

PLiMAP and SMrT assays and subsequent image analyses were done exactly as is stated in Chapter 6 of this thesis.

7.3 Results:

7.3.1 Parkinsonian mutants of α-Syn show varied membrane binding but are incapable of causing fission:

The first two mutants in the α-Syn gene reported to cause familial PD were the alanine to threonine substitution at 53rd position (A53T) and an alanine to proline mutation at the 30th position (A30P) (Fig 7.1 A). We wanted to test their ability to bind CL membranes as compared to the WT protein using PLIMAP. Both the mutants were purified along with the WT protein under identical conditions. Further, they were incubated with 15%CL liposomes containing the bi-functional lipid probe BDPE in a background of DOPC, incubated for 30 minutes to attain equilibrium binding and then UV irradiated and run on SDS-PAGE. Fluorescence band intensity measurements showed that as compared to the WT protein, α-Syn (A30P) had significantly reduced equilibrium binding (Fig 7.1 B, C). Interestingly, α-Syn (A53T) showed better binding to CL membranes than the WT protein. These results are consistent with previous simulation studies showing A30P to have reduced membrane binding due to helix-break caused by proline and A53T to have enhanced membrane binding because of additional hydrogen bonding due to threonine (Ulmer et al, 2005, Perlmutter et al, 2009).

Next, we wanted to test how these mutants perform in fission assays. 1μM of the protein was passed on to tubes made of 30%CL in a background of DOPC, incubated for 10 minutes and tubes which showed at least one break were scored for cut. As expected, as compared to the WT protein, α-Syn (A30P) showed significantly reduced membrane fission activity (Fig

7.1 D, E) . This, likely, is due to the inability of the protein to engage with the membrane. Remarkably, however, α-Syn (A53T) also displayed inability to cause fission of CL tubes (Fig 7.1 D, E). This was surprising considering α-Syn (A53T) shows good binding to membranes as reported by us and others previously. α-Syn binds membranes in a curvature-sensitive manner. We wondered if differences in fission activity across the mutants is due to the size of tubes. Random tubes from the experiments picked for radius estimation showed no significant difference between tube radii of experiments indicating difference in tube size cannot be the reason for diminished fission activity of the mutants (Fig 7.1 F-H). Together, these results show that the Parkinsonian mutants of α-Syn have varied abilities to bind membranes but are unable to cause fission of CL-containing membrane tubes.

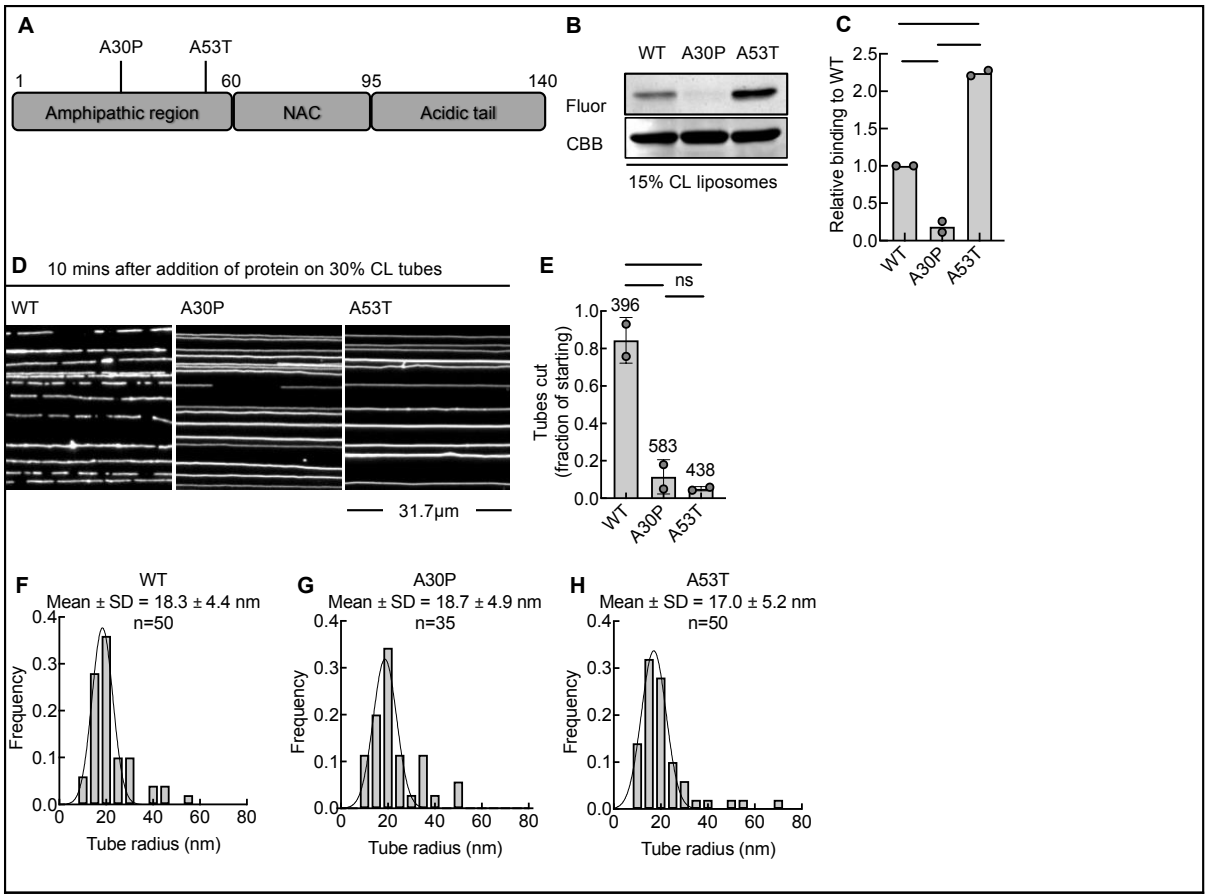

Figure 7.1. Parkinsonian mutants of α-Syn are incapable of causing fission of CL-containing membrane tubes. (A) Domain architecture of α-Syn showing different regions in the protein and the position of Parkinsonian point mutants (A30P and A53T). (B) Representative PLiMAP fluorescence (top) and CBB (bottom) images of α-Syn (WT), α-Syn (A30P) and α-Syn (A53T) with 15%CL liposomes in a background of DOPC (84%) and BDPE (1%). (C) Quantitation of normalized fluorescence signal relative to WT in (B). Data represents mean ± SD of two independent experiments. (D) Representative images of membrane channel of 30%CL tubes after incubation for 10mins with α-Syn (WT), α-Syn (A30P) and α-Syn (A53T). (E) Quantitation of 30%CL tubes cut by α-Syn (WT), α-Syn (A30P) and α-Syn (A53T) after 10mins of incubation. The number at the top of each bin indicates the number of tubes analysed in that bin. Data represents mean ± SD of at least 2 experiments for each condition. (F-H) Estimated tube size distribution for templates from a combination of two experiments formed of 30%CL in a background of DOPC (84%) and pTxR (1%) for α-Syn (WT), α-Syn (A30P) and α-Syn (A53T).

7.4 Discussion:

Since their discovery, the Parkinsonian mutants of α-Syn have long been studied for their effects on aggregation dynamics of the protein. However, very little is known about how these proteins might affect the native function of the protein. This is, in part, due to a lack of assays that directly look at α-Syn functions in an isolated setup. Our in vitro data suggests that α-Syn is able to bind and catalyze fission of CL-containing tubes. Comparative binding analysis suggested that the two mutants tested have markedly different ability to bind with the membrane. α-Syn (A30P) showed reduced membrane binding ability whereas, α-Syn (A53T) showed enhanced membrane binding. α-Syn (A30P) has previously been suggested to have

reduced membrane binding because of a break in the extended helix that happens because of a proline substitution (Ulmer et al, 2005, Robotta et al, 2017). Consistent with this, α-Syn (A30P) also shows binding to native vesicles isolated from rodent brains (Jensen et al, 1998). Since membrane binding is a pre-requisite for membrane fission, unsurprisingly, α-Syn (A30P) failed to cause fission of CL-containing membrane tubes.

α-Syn (A53T) was initially discovered from an Italian kindred showing symptoms of familial PD. Subsequently, α-Syn (A53T) has been shown to bind to large unilamellar vesicles (LUVs) equally well as that of the WT protein (Narayanan et al, 2001). Our assays confirm the same that α-Syn (A53T) can bind membranes. Importantly, we do see enhanced equilibrium binding. Whether that is because of a lower binding constant (K_d) or a higher number of binding sites (B_{max}) remains to be investigated. Previously, simulation studies indicated that a threonine in the 53rd position can increase hydrogen bonds with the membrane which can increase the residence time of each protein molecule on the membrane showing enhanced binding.

Interestingly, α-Syn (A53T) did not show membrane fission. Although, we do not have a clear understanding of the mechanism by which this happens, a hypothesis for this would be that the mutation causes changes to the oligomerization property of the protein on a membrane. Molecular dynamics simulations along with theoretical predictions suggest a difference in structure and dynamics of aggregation due to A53T mutation (Coskuner et al, 2013). Moreover, A53T has been shown to cause defects in site-specific microenvironments leading to differences in conformational flexibility of the protein (Sahay et al, JBC, 2015). These variations can lead to a different nature of oligomerization and force transduction on the membrane causing the inability of the protein to cause membrane fission. However, if this is actually the case remains to be tested.

Chapter 8:

Alpha-synuclein is required for normal mitochondrial respiratory functions

8.1 Introduction:

Maintenance of mitochondrial health and integrity is central for cell survival and growth. Mitochondria performs essential cellular functions like ATP generation, maintenance of redox equilibria, Ca2+ homeostasis and apoptosis. As such, cells have employed dedicated quality-control (QC) pathways that selectively rid the network of damaged/dysfunctional mitochondria. However, mitochondrial damage or dysfunction have been associated with multiple neurodegenerative diseases including PD (Thorne and Tumbarello, 2022). Several genes involved in recessive parkinsonism is associated with mitochondrial quality control. These include PINK1 and Parkin which are central players in mitophagy and mutations in these genes are associated with PD (McCoy and Cookson, 2011). Even though the exact mechanism by which mutations in specific genes are linked to cell death and neurodegeneration are not known, defects in mitochondrial QC pathways are usually considered the potential basis for such dysfunctions.

α-Syn has been shown to be associated with the mitochondria in both tissues derived from animal models and mammalian cells in culture (Parihar et al, 2008, Devi et al, 2008, Ludtman et al, 2016). Deletion studies revealed that first 32 residues in the protein are critical to get associated with the mitochondria (Devi et al, 2008). Moreover, α-Syn has been reported to regulate several processes at the mitochondria. α-Syn can regulate Ca2+ signalling from the mitochondria and has been shown to regulate ER-mitochondria contact (Cali et al, 2012, Guardia-Laguarta et al, 2013). α-Syn has also been reported to regulate the morphological dynamics of mitochondria. Mitochondrial fragmentation has been observed during over-expression of the wild-type protein as well as multiple PD-associated mutants like A53T and E46K (Kamp et al, 2010, Guardia-Laguarta et al, 2013). Moreover, selective targeting of wild-type α-Syn or α-Syn (A53T) to the mitochondria has been shown to cause mitochondrial fragmentation whereas the membrane binding mutant α-Syn (A30P) does not. Additionally, mitochondrial motility was shown to be reduced in mammalian cell lines and neurons derived from embryonic stem cells expressing α-Syn (Xie and Chung, 2012). Endogenous α-Syn is required for the activity of respiratory chain complexes of the mitochondrial inner membrane. Over-expression of α-Syn has been shown to cause impairment in Complex I activity. Consistent with this, inhibitors of Complex I of the ETC pathway has been reported to cause PD (Davies et al, 1979).

There is considerable debate about the localization of α-Syn on the mitochondria. α-Syn is majorly a cytosolic protein and technically should bind to only the OMM. However, multiple reports claim that α-Syn does go inside the mitochondria and interact with the IMM.

α-Syn has been shown to be imported in the mitochondria in a potential-dependent manner (Devi et al, 2008). Moreover, the TOM40 subunit of the import complex at the OMM is critical for α-Syn import into the mitochondria. Additionally, post-translationally modified α-Syn has been shown to affect the dynamics of the mitochondria import complex by regulating the functions of TOM22.

Together these pieces of evidences suggest that α-Syn is associated with the mitochondria. However, most of these studies were done in a condition where the wild-type protein or PD-associated mutants were over-expressed in the cells which itself has been associated with PD-like symptoms. Our results suggest that α-Syn can bind to and remodel CL-containing membranes. Given this, we wanted to analyse the effects of α-Syn on mitochondrial functions.

8.2 Materials and Methods:

8.2.1. Oxygen consumption rate measurements:

Oxygen consumption rates (OCR) were measured in a Seahorse XFp analyser (Agilent biosciences) using Mito-Stress test kit according to manufacturer's instructions. Briefly, the XFp sensor cartridge was hydrated with sterile water and kept in a dehumidified incubator at 37 °C overnight for equilibration overnight. An hour prior to the experiment, the water was aspirated and the calibrant solution was added to the wells of the chamber, incubated at 37 °C in a non-CO_2 incubator for equilibration. The system was calibrated using this plate before the start on any experimental run. Each plate had 8 wells out of which three were used for WT cells and 3 for KO cells. Each well was seeded with $2.5x10^4$ cells and kept for 16 hours in a CO2 incubator for them to adhere and grow. An hour before the experiment, the existing media was discarded and new XFp media (phenol red-, serum-, bicarbonate-, glucose-, puruvate- and L-glutamine-free DMEM) supplemented with 10mM glucose, 1mM pyruvate and 2mM glutamine was added to the plate and incubated in a non-CO_2 incubator for 1 hour for equilibration. Respiratory rates (oxygen consumption and extracellular acidification) were estimated under basal conditions and upon injection of oligomycin (Complex V inhibitor, 1.5 μM), carbonyl cyanide-p-trifluoromethoxy-phenylhydrazone (FCCP, Mitochondrial membrane potential inhibitor, 0.5μM) and Rotenone/Antimycin A (Complex I and III inhibitor respectively, 0.5μM each) at indicated time points.

8.2.2 Cell viability assays:

Cell viability was measured using thiazolyl blue tetrazolium bromide reagent (MTT, Sigma) assay. Briefly, for each experiment 10 wells of a 96-well plate was seeded with $5x10^4$ WT and KO cells respectively. 5 wells were used for glucose and 5 wells for galactose treatment respectively. 12 hour post seeding, the existing media was discarded and cells were washed thoroughly before incubating with glucose-free DMEM/F12 (1:1) (Elabsciences) supplemented with 4.5g/l glucose or 0.9 g/l galactose respectively for glucose and galactose conditions additionally supplemented with 10% fetal bovine serum and 100units/ml Penicillin/Streptomycin. At desired time points, final concentration of 0.5mg/ml of MTT in DMEM/F12 was added to the cells and left in the incubator for 4 hours for development of formazan crystals. The media was carefully aspirated out from the top leaving the formazan crystals at the bottom. 200µl of anhydrous DMSO was added to each well and the plate was incubated at 37 °C for 5 mins. Absorbance was measured at 570nm using Infinite M200Pro (Tecan) and analysed using Magellan 7.

8.2.3 Mitochondria isolation:

Mitochondria isolation from wildtype and α-Syn knock-out cells was carried out according to the protocol published previously (Liao et al., 2020). Briefly, a confluent 10cm dish of WT and KO SH-SY5Y cells were harvested by scraping in PBS. The cell suspension was spun at 3000g for 3 minutes, the existing DPBS discarded and the cells were resuspended in mitochondria isolation buffer (0.25 M sucrose, 20 mM HEPES-KOH, pH 7.5, 10 mM KCl, 1.5 mM MgCl2, 1 mM EDTA, 1 mM EGTA, 1 mM dithiothreitol, 1 mM PMSF, 1x protease inhibitor cocktail). Homogenization was done using sonication (2 on, 3 off at 25% amplitude, done 3-5 times with intermittently incubating on ice for 30s before next round). The cell suspension was centrifuged at 1000g for 10 minutes following which the supernatant was carefully aspirated without disturbing the pellet and put in a fresh 1.5ml tube. This step was repeated once more. The pooled supernatant was spun at 10000g for 20mins to pellet down mitochondria. The pellet was washed 3 times with isolation buffer to get a purer mitochondria preparation. Protein concentration was estimated using BCA reagent kit (Takara) after digesting the pellet with PBS containing 1% SDS. Equal amount of WT and KO mitochondria was then either boiled with 1x Laemmli's buffer to run on an SDS-PAGE for western blotting or was processed for quantitative mass spectrometry.

8.2.4 Quantitative proteomics of isolated mitochondria:

Quantitative proteomics was done exactly as is mentioned for identification proteomics in Chapter 5 of this thesis except with the following modifications. For quantitative mass spectrometry, equal amounts of mitochondria (20µg each of WT and KO) were first precipitated using chloroform/methanol to get rid of all non-polar components like lipids. The supernatant after precipitation was carefully aspirated and the pellet was resuspended into 100mM TEAB buffer containing 8M urea. Reduction, alkylation and trypsin digestion was done exactly as is mentioned previously. After overnight trypsin digestion, the peptides were labelled with heavy (CD_2O) (WT mitochondria) and light (CH_2O) (KO mitochondria) formaldehyde in the presence of sodium cyanoborohydride ($NaBH_3CN$) as described previously (Kamat et al, NCB 2015). Desalting, drying and running of the samples was done exactly as is mentioned previously. For quantification of WT and KO proteins, proteins were first sorted based on number of peptides detected across all 6 runs (>1 peptides) and then common proteins from all 6 runs were analyzed using gene ontology (GO) annotation to sort them into mitochondrial proteins and non-mitochondrial proteins. The proteins were then sorted based on their Heavy: Light (H:L) score to identify proteins enriched (H:L value less than 1) or depleted in KO mitochondria (H:L value more than 1). The mitochondrial proteins enriched in KO were further clustered using STRING database based on biological function to annotate proteins involved in particular biochemical pathways.

8.3 Results:

8.3.1 Alpha synuclein KO cells show reduced mitochondrial respiration and over-dependence on glycolysis:

Mitochondria produces ATP through oxidative phosphorylation which involves the transport of electrons through multiple multi-protein complexes in the IMM. The electron transport starts from Complex I and ends in Complex IV where molecular oxygen is reduced to form water. All these complexes, except complex II, drive protons across the IMM from the matrix to the inter-membrane space. Finally, Complex V uses this proton gradient to phosphorylate ADP to form ATP.

Previously, α-Syn has been suggested to inhibit complex I function (Reeve et al, 2015). Given the propensity of α-Syn to bind to CL membranes, we wanted to analyse the effects of the loss of α-Syn on mitochondrial respiratory functions. We used SH-SY5Y cells which express α-Syn endogenously and has been used extensively in α-Syn research (Xicoy et al, 2017). We used wild-type (WT) and α-Syn knock-out (KO) cell line to test the effects of loss of α-Syn in mitochondrial functions. Seahorse is an instrument that helps analyse mitochondrial

respiratory function by detecting oxygen consumption under basal and different drug-treatment conditions. Measurement of oxygen consumption rates (OCR) showed that under basal conditions KO cells show significantly reduced oxygen consumption (Fig 8.1 A-D). Addition of oligomycin to cells, which inhibits complex V showed a smaller drop in OCR in KO cells indicating ATP production-linked respiration is much lower in these cells. Addition of FCCP, which is an uncoupler of the proton gradient across IMM, showed much higher maximal rate of respiration for WT cells as compared to KO cells. Thus, under conditions of stress, the KO cells have significantly lesser spare capacity of respiration. Addition of Rotenone/Antimycin A which blocks complex I and III showed that both cells have similar non-mitochondrial oxygen consumption. Together these data suggest that OCR is significantly reduced in cells not having synuclein both under basal and stimulated conditions indicating severe defects in respiratory functions of the mitochondria.

In addition to oxygen consumption, Seahorse experiments also monitors the extracellular acidification rates (ECAR) of the media where the cells are grown. Plotting OCR vs ECAR generates an energy map of the cell which helps us understand the biological processes from which the cells derive energy. The energy plot of WT cells showed that it is reliant on both mitochondrial oxidative phosphorylation and glycolysis for its energy output (energetic quadrant) (Fig 8.1 E) . However, the KO cells were dependent more on glycolysis than oxidative phosphorylation in the mitochondria compared to WT cells (glycolytic quadrant). This, likely, suggests how the KO cells utilise glycolysis as a compensation mechanism to generate energy because of a sub-optimally functioning mitochondria. To confirm this, we grew WT and KO cells in media containing galactose as a carbon-source instead of glucose. Galactose in the cells gets converted into glucose which further gets processed by glycolytic enzymes. However, the energy that is required to convert galactose to glucose is exactly the same that is generated from glucose through glycolysis. Hence, upon using galactose, the net energy output from glycolysis becomes zero necessitating the cells to depend on mitochondria for energy output. Cells grown on glucose media showed an increase in viable cell mass over time (Fig 8.1 F) however, WT cells fared better than the KO cells. Interestingly, WT cells grown on galactose media showed an initial bout of cell death but over time got used to the media and survived fine as determined by measuring the extent of formazan production from MTT. However, unsurprisingly, the KO cells were highly susceptible to galactose-containing media and all cells died within 72 hours of treatment (Fig 8.1 G). Thus, indeed, the KO cells are reliant on glycolysis and not mitochondrial energy generation for survival.

8.3.2 AS KO cells have an altered mitochondrial proteome:

We wondered if lesser OCR in cells lacking α-Syn is due to lesser mitochondrial mass. We analyzed bulk mitochondrial mass in WT and KO cells using western blotting. Probing lysates with antibodies against mitochondrial proteins (ATP5A for IMM and Mid51 for OMM) suggested that these proteins are not significantly altered in KO cells (Fig 8.1 H). Thus, steady-state number of mitochondria cannot be the reason for reduced mitochondrial activity. This led us to do a quantitative proteomic analysis of isolated mitochondria from both WT and KO cells to figure out why the KO mitochondria perform sub-optimally. Proteins were isolated from purified mitochondria, digested with trypsin and labelled with heavy or light formaldehyde before running on LC-MS/MS (Fig 8.1 I). Our MS analyses resulted in identifying 1132 proteins out of which 372 were mitochondrial (Fig 8.1 J). Interestingly, analyzing the mitochondrial proteins showed that out of the 372 proteins, 250 were enriched in mitochondria (Fig 8.1 K). This was quite surprising given that OCR analyses suggested a loss of function of KO mitochondria whereas MS analyses showed most of the mitochondrial proteins are more in KO compared to WT mitochondria. This led us to look at the identity of these proteins which are enriched in the KO mitochondria.

Since our in vitro assays suggested that α-Syn is required for fission, we wondered if loss of α-Syn leads to the accumulation of unwanted proteins in the mitochondria. STRING analysis of the list of protein enriched in the KO mitochondria showed that proteins involved in a diverse array of biochemical pathways were enriched (Fig 8.1 L). The gene ontology (GO) network based on biological processes classified the proteins majorly in four distinct clusters. This included proteins involved in aerobic respiration (electron transport chain and TCA cycle) (GO:0009060), mitochondrial gene expression (GO:0140053), fatty acid beta oxidation (GO:0006635) and proteins involved in mitochondrial transport (GO: 0006839). The first cluster was especially interesting. Proteins involved in aerobic respiration were enriched in the KO cells compared to WT, however, the oxygen consumption rate of the cells were lower than WT. This apparent discrepancy can be because of a build-up of non-functional proteins in the KO cells which otherwise would have been evicted from the mitochondria in a α-Syn-dependent manner. The build-up of non-functional mitochondrial proteins can be because of variety of stress like aggregation and oxidation in the absence of α-Syn. Mitochondria are known to have multiple internal quality control mechanisms to rid the organelle of these stresses. These include upregulation of multiple quality control proteins within the mitochondria which act both as chaperones and proteases. Consistent with these, our MS

analysis shows the upregulation of multiple quality control proteases in the mitochondria (LONP1, CLPP, YME1L1, PITRM1 and PMPCB) together with proteins that are involved in regulating their activities (PMPCA and UQCRC1) (Quiros et al, 2015) (Table 8.1). Moreover, we also detected multiple proteins involved in mitophagy to be upregulated in the KO cells indicating again that the improper functioning of the mitochondria targets them for mitophagy. Another pathway of getting rid of the oxidised cargo has been shown to be via the formation of mitochondria-derived vesicles (MDVs) (Soubannier et al, 2012, Vasam et al, 2021). Interestingly, our MS analyses showed the build-up of multiple proteins within the KO mitochondria that have been shown to be cargos of oxidised MDVs. Together, these results show that α-Syn is necessary for normal mitochondrial respiratory functions in absence of which there is a, likely, build-up of non-functional proteins within the mitochondria which leads to upregulated quality control surveillance mechanisms.

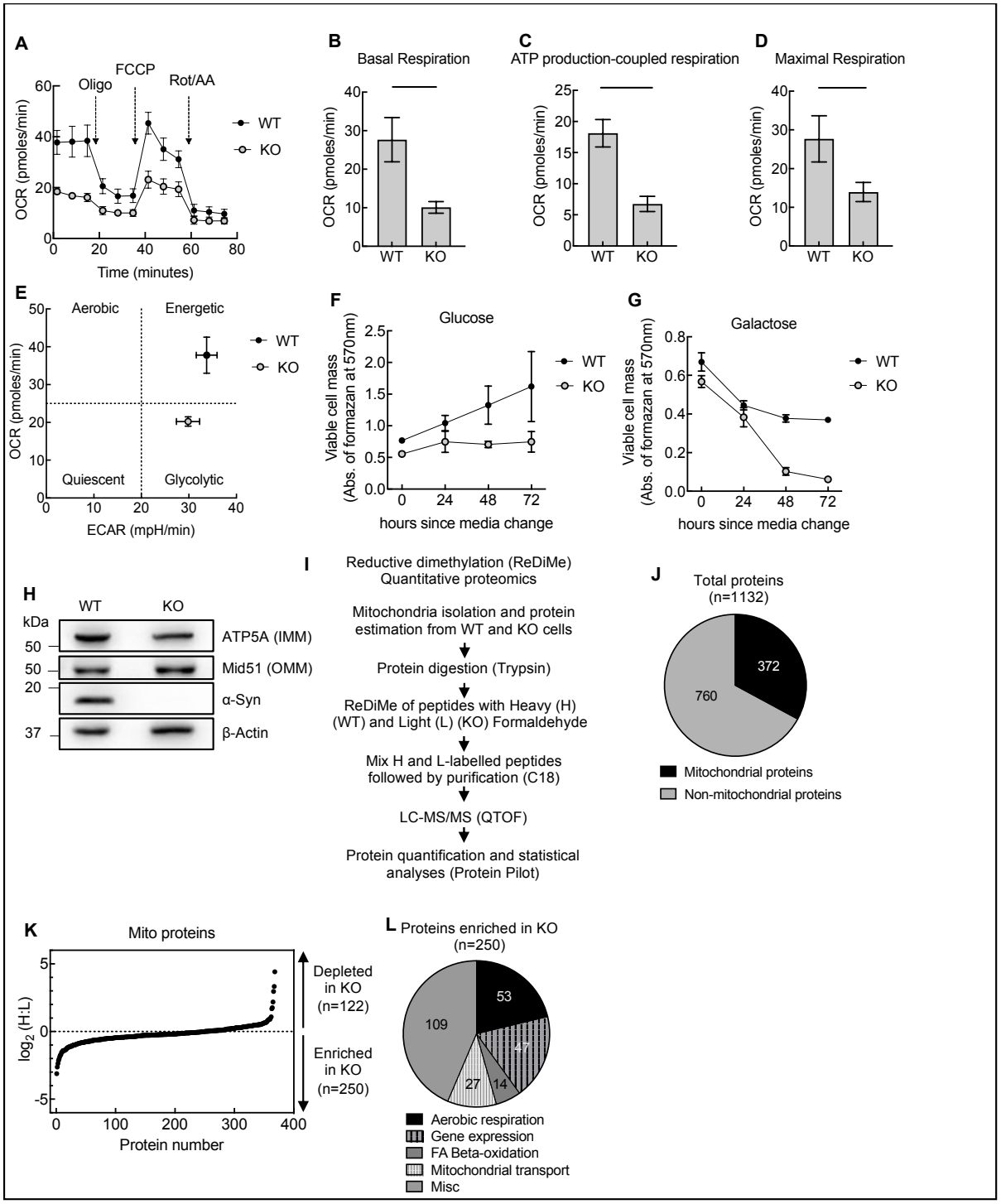
A
FCCP
Oligo
Rot/AA
OCR (pmoles/min)
Time (minutes)
WT
KO
B
Basal Respiration
C
ATP production-coupled respiration
D
Maximal Respiration
E
Aerobic
Energetic
Quiescent
Glycolytic
ECAR (mpH/min)
F
Glucose
Viable cell mass (Abs. of formazan at 570nm)
hours since media change
G
Galactose
H
kDa
ATP5A (IMM)
Mid51 (OMM)
α-Syn
β-Actin
I
Reductive dimethylation (ReDiMe) Quantitative proteomics
Mitochondria isolation and protein estimation from WT and KO cells
Protein digestion (Trypsin)
ReDiMe of peptides with Heavy (H) (WT) and Light (L) (KO) Formaldehyde
Mix H and L-labelled peptides followed by purification (C18)
LC-MS/MS (QTOF)
Protein quantification and statistical analyses (Protein Pilot)
J
Total proteins (n=1132)
372
760
Mitochondrial proteins
Non-mitochondrial proteins
K
Mito proteins
log2 (H:L)
Protein number
Depleted in KO (n=122)
Enriched in KO (n=250)
L
Proteins enriched in KO (n=250)
53
109
27
14
Aerobic respiration
Gene expression
FA Beta-oxidation
Mitochondrial transport
Misc

Figure 8.1. α-Syn is required for normal mitochondrial respiratory functions. (A) Oxygen consumption rate (OCR) measurements using Seahorse xFp Analyzer under basal or different stress conditions like Oligomycin, FCCP and Rotenone/Antimycin A. Data represents mean ± SD of two independent experiments (B-D) Basal, ATP-linked and maximal respiration as calculated from the OCR data in (A). Data represents mean ± SD of two independent experiments each. (E) Energy profile of WT and KO cells based on OCR and extracellular acidification rate (ECAR) measured. (F) Viable cell mass measured as a function of formazan absorbance at 570nm for cells grown in glucose (F) or galactose (G)-containing media as the primary carbon source. Data represents mean ± SD of two independent experiments. (H) Western blot analysis of WT and KO SH-SY5Y lysate blotted for ATP5A (Inner mitochondrial membrane; IMM), Mid51 (Outer mitochondrial membrane; OMM) and α-Syn. β-Actin is used as a loading control. (I) Flow chart showing the steps involved in quantitative proteomics of isolated mitochondria. (J) Pie chart showing the number of mitochondrial proteins detected as compared to non-mitochondrial proteins from 6 independent MS/MS runs. (K) Plot showing fold enrichment of different mitochondrial proteins detected across 6 runs. WT and KO peptides were labelled with heavy (H) and light (L) formaldehyde, respectively. (L) Pie chart showing distribution of proteins enriched in KO cells functioning in different biological pathways based on Gene Ontology (GO) : Biological processes.

Table 8.1:

List of proteins involved in quality control of the mitochondria that are significantly enriched in the mitochondria of KO cells:

Mitochondrial Proteases	Mitophagy-associated proteins
PMPCA	PARK7
PMPCB	PHB1
LONP1	PHB2
CLPP	NIPSNAP1
CLPX	NIPSNAP2
YME1L	TOM22
UQCRC1	PGAM5
PITRM1	NIPSNAP3A
	TOM70
	MFN1

8.4. Discussion:

α-Syn has long been implicated to be regulating different mitochondrial functions. However, a direct molecular mechanism by which α-Syn might be doing these remained elusive. Here, using SH-SY5Y cells which have been knocked out for the α-Syn gene using CRISPR, we show that mitochondrial respiratory functions are defective in these cells lacking α-Syn. The cells consume lesser oxygen as compared to their WT counterparts under both basal and drug-treated conditions. Our respiratory analyses also showed that the cells utilize glycolysis more than oxidative phosphorylation within the mitochondria to derive energy. This begged us to question the reason for such differences in the KO cells in absence of α-Syn. Bulk mitochondrial mass analysis showed that none of the proteins tested are significantly lower in KO cells indicating that lower mitochondrial mass cannot be the reason for sub-optimal functioning or lower oxygen consumption of the mitochondria. Quantitative proteomic analysis showed that most of the proteins associated with mitochondrial respiration

are actually enriched in the KO cells. Thus, the KO cells have more of the proteins that are required for oxidative phosphorylation, yet their functional output is lower compared to the WT cells. Moreover, the mitochondria in KO cells showed upregulation of multiple proteins associated with quality control of the organelles (proteases and mitophagy-related proteins).

Mitochondria has ~1500 proteins most of which are made from nuclear DNA and imported post-translation into the mitochondria. Imported proteins are usually proteolytically processed in the mitochondria to form functional proteins. Moreover, they undergo folding and maturation within the mitochondria with the help of multiple chaperones and proteases. Subsequently, mis-folded or aggregated proteins are selectively processed within the mitochondria by multiple proteases and are thought to be taken out of the mitochondria. A very likely cause of such mis-folding and aggregation is oxidation of the proteins (Mirzaei and Regnier, 2008). Mitochondria performs several redox reactions which generate reactive oxygen species (ROS) as a by-product. ROS can covalently modify different biomolecules and lead to the formation of aggregates or a build-up of non-functional proteins and lipids within the mitochondria. How these proteins are selectively gotten rid of from the mitochondria is not well understood. Ubiquitin-proteasome system takes care of majority of these mis-folded proteins from the OMM. However, how proteins from the IMS and matrix are gotten rid of remains elusive. One possible mechanism of removal of oxidised biomolecules is through the formation of mitochondria-derived vesicles (MDVs). MDVs are small 75-200nm vesicles that are released from the mitochondria in a Drp1-independent manner. MDVs are generated from the mitochondria in response to oxidative stress (Soubannier et al, 2012). These MDVs have been shown to contain multiple cargos which are proteins prone to oxidation like Fe-S cluster containing proteins (Vasam et al, 2021). Our MS analysis indicated a build-up of these proteins in the mitochondria of the KO cells. Thus, one possible molecular mechanism of α-Syn function is that it helps in the release of damaged cargo (proteins/lipids) from the mitochondria in response to oxidative stress. In the absence of α-Syn, these damaged components are not taken out of the mitochondria which leads to the build-up of non-functional proteins ultimately leading to respiratory defects of the mitochondria.

Summary and Future Perspectives

Mitochondria serve a crucial role in cellular homeostasis and as such are needed to maintain in an optimally functional form. Different stressors affect mitochondrial health and function and hence non-functional mitochondria need to be degraded by the cell to maintain a heathy functional network. Cells have multiple ways to get rid of such non-functional mitochondria. Mitophagy is the most well-known pathway that helps rid the network of damaged mitochondria and targets it to the lysosome for degradation. Drp1 has been implicated to have a crucial role in mitophagy whereby it helps to detach the dysfunctional parts from the entire network. However, how exactly Drp1 manages that was unclear. The data in this thesis suggests that the phospholipid diacylglycerol (DAG) helps Drp1 to cause fission of cardiolipin (CL)-containing tubes. DAG has previously been shown to be critical for mitophagy, however, the exact role it plays during mitophagy remained unclear (Lin et al, 2022). . Our data suggests that formation of DAG on the mitochondrial surface by Lipin1 during mitophagy is, likely, to recruit DAG-dependent effector molecules to the mitochondria. DAG helps recruit Drp1 to cardiolipin tubes, *in vitro*. Moreover, it simulates the mechanochemical activity of Drp1 post membrane binding leading to fission. Together, this enhances the bulk fission rate catalysed by Drp1 on CL tubes. Drp1 has been shown to exist in the form of puncta on the mitochondria. However, not all the puncta undergo fission all the time. These, likely, represent pre-assembled Drp1 on the mitochondria which are waiting to receive the final cue for fission which might come in the form of a lipid modification.

Drp1 is known to get recruited to the membrane surface based on membrane charge whereby lysine residues in the V-domain is thought to interact with negatively charged lipid head-groups (Bustillo-Zabalbeitia et al., 2014). DAG is a non-ionic lipid. This poses an interesting question regarding how DAG manages to recruit Drp1 efficiently on the membrane surface. A possible explanation for that is DAG causes the formation of packing defects in the membrane which helps Drp1 insert its unstructured membrane binding domain into the membrane. Thus, according to this hypothesis, DAG does not increase the k_{on} of protein but rather lowers the k_{off} rate of the protein on the membrane leading to enhanced equilibrium binding. The same can be the reason for uniform stable scaffolds of Drp1 on DAG tubes which can efficiently transduce forces leading to lesser fission time. One interesting avenue of research in future would be to systematically monitor fission reaction on membrane templates containing other known packing-defect inducing lipids to see if indeed packing defects is the only thing DAG contributes in Drp1 catalysed membrane fission.

DAG also helps Endophilin B1/2 (EndoB1/2) recruitment on CL-containing planar bilayers. Upon recruitment they show a DAG-dependent membrane tubulation reaction from

planar bilayers. In our understanding, this is the first report of real-time analysis of EndoB1-mediated tubulation from a planar bilayer. However, what is the need for the tubulation reaction which likely happens on the mitochondria in response to DAG generation remains elusive. Analysis of binding on curved membrane tubes suggested that EndoB1 gets recruited to tubes irrespective of DAG or PI being present. Thus, EndoB1, likely gets recruited to a membrane in response to two factors: lipid specificity and membrane curvature. This is interesting given that mitochondria usually never exists in the form of tubes which are about 20-50 nm in diameter. Hence, one possible way this manifests in the cell is that upon tubulation from the planar bilayer in a DAG-dependent manner, more EndoB1 from the cytosol can get recruited to these nascent tubules in a cooperative manner. Endo B1/2 have been shown to bind to UVRAG, an autophagic scaffolding protein, through its SH3 domain. Our data suggests Endophilin B1/2 are thus, likely, to recruit the general autophagic machinery to the mitochondria in response to DAG generation.

DAG has been shown to be generated by Lipin 1 from dephosphorylation of phosphatidic acid on the mitochondrial surface (Lin et al, 2022). Lipin 1 can directly get recruited through Parkin and hence will, likely, be clustered around the non-functional regions of the mitochondria. Thus, DAG production happens only on the non-functional part of the mitochondria which then can recruit Drp1 and Endophilin B1/2 to the mitochondria.

Mitochondria-derived vesicles is another way by which cells get rid of damaged products from the mitochondria. MDVs are generated by the mitochondria under different conditions, however, the membrane fission catalyst that helps in the release of these vesicles remained unknown. Electron micrographs suggested that the buds of MDV defined a neck about 30-50 nm which matches really well with the size of tubes in a SMrT assay. Hence, using SMrT, we screened brain lysate for a possible membrane fission catalyst. Brain lysate showed the presence of a CL-specific membrane fission reaction. Biochemical fractionation and subsequent proteomic analyses revealed the active component of the brain lysate to be alpha-synuclein (α-Syn). Recombinantly purified α-Syn bound CL-containing liposomes better than any other phospholipid or phosphoinositide tested suggesting a lipid-binding preference. Moreover, purified α-Syn was able to catalyse fission of tubes in a CL-dependent manner indicating it is sufficient for fission. One interesting avenue of research would be to model the structural changes that monomeric α-Syn undergoes on the membrane surface to oligomerize and transduce forces on a tube to bring about fission. From the modelling studies, specific regions/residues that are important can be tested in *in vitro* assays for membrane binding and fission which will help postulate the mechanistic pathway to fission.

Interestingly, mutants of α-Syn which are known to cause early-onset Parkinson's Disease (PD) showed varied affinity for CL liposomes but were defective in catalysing fission. In this context, α-Syn (A53T) is particularly interesting. The mutant binds CL membranes better than the wild-type protein, however, is incapable of causing fission. Thus, the mutant is a naturally occurring defective protein modelling which on a CL membrane can provide insights into the pathway to oligomerization to finally undergoing fission. Independently, the disease-associated mutants are considered to be more likely to aggregate and hence there is an early onset of the disease in such patients. However, our data suggests that these mutants are essentially loss-of-function derivatives thus linking inability to cause membrane fission to neurodegeneration.

Mammalian cells lacking α-Syn showed significantly reduced respiratory functions of the mitochondria under basal and stressed conditions. The cells were also over-dependent on glycolysis for their energy generation as compared to the wild-type cells. Proteomic analysis revealed markedly altered proteome of the α-Syn KO cells with an increase in levels of proteins involved in aerobic respiration and other biochemical pathways. Lesser functional output but higher protein amount can be due to accumulation of non-functional proteins in the mitochondria which otherwise would have been evicted out in α-Syn-dependent manner. Our proteomic analyses hints at possible cargos that are likely taken out by α-Syn. This involves multiple proteins involved in aerobic respiration/proteins having Fe-S clusters. One possible line of enquiry could be to follow such cargos and monitor if they are taken out of the cell through MDV formation in a α-Syn dependent manner.

References

1. Spinelli, J. B., & Haigis, M. C. (2018). The multifaceted contributions of mitochondria to cellular metabolism. *Nature cell biology*, *20*(7), 745-754.
2. Solaini, G., Baracca, A., Lenaz, G., & Sgarbi, G. (2010). Hypoxia and mitochondrial oxidative metabolism. *Biochimica et Biophysica Acta (BBA)-Bioenergetics*, *1797*(6-7), 1171-1177.
3. Samluk, L., Chroscicki, P., & Chacinska, A. (2018). Mitochondrial protein import stress and signaling. *Current Opinion in Physiology*, *3*, 41-48.
4. Ruan, L., Wang, Y., Zhang, X., Tomaszewski, A., McNamara, J. T., & Li, R. (2020). Mitochondria-associated proteostasis. *Annual review of biophysics*, *49*, 41-67.
5. Kitada, T., Asakawa, S., Hattori, N., Matsumine, H., Yamamura, Y., Minoshima, S., ... & Shimizu, N. (1998). Mutations in the parkin gene cause autosomal recessive juvenile parkinsonism. *nature*, *392*(6676), 605-608.
6. Valente, E. M., Abou-Sleiman, P. M., Caputo, V., Muqit, M. M., Harvey, K., Gispert, S., ... & Wood, N. W. (2004). Hereditary early-onset Parkinson's disease caused by mutations in PINK1. *Science*, *304*(5674), 1158-1160.
7. Ye, X., Sun, X., Starovoytov, V., & Cai, Q. (2015). Parkin-mediated mitophagy in mutant hAPP neurons and Alzheimer's disease patient brains. *Human molecular genetics*, *24*(10), 2938-2951.
8. Khalil, B., El Fissi, N., Aouane, A., Cabirol-Pol, M. J., Rival, T., & Liévens, J. C. (2015). PINK1-induced mitophagy promotes neuroprotection in Huntington's disease. *Cell death & disease*, *6*(1), e1617-e1617.
9. Lee, J. J., Sanchez-Martinez, A., Zarate, A. M., Benincá, C., Mayor, U., Clague, M. J., & Whitworth, A. J. (2018). Basal mitophagy is widespread in Drosophila but minimally affected by loss of Pink1 or parkin. *Journal of Cell Biology*, *217*(5), 1613-1622.
10. Diwan, A., Koesters, A. G., Odley, A. M., Pushkaran, S., Baines, C. P., Spike, B. T., ... & Dorn, G. W. (2007). Unrestrained erythroblast development in Nix−/− mice reveals a mechanism for apoptotic modulation of erythropoiesis. *Proceedings of the National Academy of Sciences*, *104*(16), 6794-6799.
11. Takano-Ohmuro, H., Mukaida, M., Kominami, E., & Morioka, K. (2000). Autophagy in embryonic erythroid cells: its role in maturation. *European journal of cell biology*, *79*(10), 759-764
12. Tracy, K., & Macleod, K. F. (2007). Regulation of mitochondrial integrity, autophagy and cell survival by BNIP3. *Autophagy*, *3*(6), 616-619.

13. Shitara, H., Kaneda, H., Sato, A., Inoue, K., Ogura, A., Yonekawa, H., & Hayashi, J. I. (2000). Selective and continuous elimination of mitochondria microinjected into mouse eggs from spermatids, but not from liver cells, occurs throughout embryogenesis. *Genetics*, *156*(3), 1277-1284.
14. Sekine, S., & Youle, R. J. (2018). PINK1 import regulation; a fine system to convey mitochondrial stress to the cytosol. *BMC biology*, *16*, 1-12.
15. Yoo, S. M., & Jung, Y. K. (2018). A molecular approach to mitophagy and mitochondrial dynamics. *Molecules and cells*, *41*(1), 18.
16. Ney, P. A. (2015). Mitochondrial autophagy: Origins, significance, and role of BNIP3 and NIX. *Biochimica et Biophysica Acta (BBA)-Molecular Cell Research*, *1853*(10), 2775-2783.
17. Youle, R. J., & Van Der Bliek, A. M. (2012). Mitochondrial fission, fusion, and stress. *Science*, *337*(6098), 1062-1065.
18. Kraus, F., Roy, K., Pucadyil, T. J., & Ryan, M. T. (2021). Function and regulation of the divisome for mitochondrial fission. *Nature*, *590*(7844), 57-66.
19. Kanki, T., Wang, K. E., Baba, M., Bartholomew, C. R., Lynch-Day, M. A., Du, Z., ... & Klionsky, D. J. (2009). A genomic screen for yeast mutants defective in selective mitochondria autophagy. *Molecular biology of the cell*, *20*(22), 4730-4738.
20. Tanaka, A., Cleland, M. M., Xu, S., Narendra, D. P., Suen, D. F., Karbowski, M., & Youle, R. J. (2010). Proteasome and p97 mediate mitophagy and degradation of mitofusins induced by Parkin. *Journal of Cell Biology*, *191*(7), 1367-1380.
21. Twig, G., Elorza, A., Molina, A. J., Mohamed, H., Wikstrom, J. D., Walzer, G., ... & Shirihai, O. S. (2008). Fission and selective fusion govern mitochondrial segregation and elimination by autophagy. *The EMBO journal*, *27*(2), 433-446.
22. Wu, W., Lin, C., Wu, K., Jiang, L., Wang, X., Li, W., ... & Feng, D. (2016). FUNDC 1 regulates mitochondrial dynamics at the ER–mitochondrial contact site under hypoxic conditions. *The EMBO journal*, *35*(13), 1368-1384.
23. Lin, C. C., Yan, J., Kapur, M. D., Norris, K. L., Hsieh, C. W., Huang, D., ... & Yao, T. P. (2022). Parkin coordinates mitochondrial lipid remodeling to execute mitophagy. *EMBO reports*, *23*(12), e55191.
24. Sugiura, A., McLelland, G. L., Fon, E. A., & McBride, H. M. (2014). A new pathway for mitochondrial quality control: mitochondrial-derived vesicles. *The EMBO journal*, *33*(19), 2142-2156.

25. Soubannier, V., McLelland, G. L., Zunino, R., Braschi, E., Rippstein, P., Fon, E. A., & McBride, H. M. (2012). A vesicular transport pathway shuttles cargo from mitochondria to lysosomes. *Current Biology*, *22*(2), 135-141.
26. Soubannier, V., Rippstein, P., Kaufman, B. A., Shoubridge, E. A., & McBride, H. M. (2012). Reconstitution of mitochondria derived vesicle formation demonstrates selective enrichment of oxidized cargo. *PloS one*, *7*(12), e52830.
27. Neuspiel, M., Schauss, A. C., Braschi, E., Zunino, R., Rippstein, P., Rachubinski, R. A., ... & McBride, H. M. (2008). Cargo-selected transport from the mitochondria to peroxisomes is mediated by vesicular carriers. *Current Biology*, *18*(2), 102-108.
28. Matheoud, D., Sugiura, A., Bellemare-Pelletier, A., Laplante, A., Rondeau, C., Chemali, M., ... & Desjardins, M. (2016). Parkinson's disease-related proteins PINK1 and Parkin repress mitochondrial antigen presentation. *Cell*, *166*(2), 314-327.
29. Vasam, G., Nadeau, R., Cadete, V. J., Lavallée-Adam, M., Menzies, K. J., & Burelle, Y. (2021). Proteomics characterization of mitochondrial-derived vesicles under oxidative stress. *The FASEB Journal*, *35*(4).
30. Horvath, S. E., & Daum, G. (2013). Lipids of mitochondria. *Progress in lipid research*, *52*(4), 590-614.
31. König, T., Nolte, H., Aaltonen, M. J., Tatsuta, T., Krols, M., Stroh, T., ... & McBride, H. M. (2021). MIROs and DRP1 drive mitochondrial-derived vesicle biogenesis and promote quality control. *Nature cell biology*, *23*(12), 1271-1286.
32. Chu, C. T., Ji, J., Dagda, R. K., Jiang, J. F., Tyurina, Y. Y., Kapralov, A. A., ... & Kagan, V. E. (2013). Cardiolipin externalization to the outer mitochondrial membrane acts as an elimination signal for mitophagy in neuronal cells. *Nature cell biology*, *15*(10), 1197-1205.
33. Bustillo-Zabalbeitia, I., Montessuit, S., Raemy, E., Basañez, G., Terrones, O., & Martinou, J. C. (2014). Specific interaction with cardiolipin triggers functional activation of dynamin-related protein 1. *PloS one*, *9*(7), e102738.
34. Macdonald, P. J., Stepanyants, N., Mehrotra, N., Mears, J. A., Qi, X., Sesaki, H., & Ramachandran, R. (2014). A dimeric equilibrium intermediate nucleates Drp1 reassembly on mitochondrial membranes for fission. *Molecular biology of the cell*, *25*(12), 1905-1915.
35. Kamerkar, S. C., Kraus, F., Sharpe, A. J., Pucadyil, T. J., & Ryan, M. T. (2018). Dynamin-related protein 1 has membrane constricting and severing abilities sufficient for mitochondrial and peroxisomal fission. *Nature communications*, *9*(1), 5239.

36. Mahajan, M., Bharambe, N., Shang, Y., Lu, B., Mandal, A., Madan Mohan, P., ... & Ramachandran, R. (2021). NMR identification of a conserved Drp1 cardiolipin-binding motif essential for stress-induced mitochondrial fission. *Proceedings of the National Academy of Sciences*, *118*(29), e2023079118.
37. Strub, G. M., Paillard, M., Liang, J., Gomez, L., Allegood, J. C., Hait, N. C., ... & Spiegel, S. (2011). Sphingosine-1-phosphate produced by sphingosine kinase 2 in mitochondria interacts with prohibitin 2 to regulate complex IV assembly and respiration. *The FASEB Journal*, *25*(2), 600.
38. Sentelle, R. D., Senkal, C. E., Jiang, W., Ponnusamy, S., Gencer, S., Panneer Selvam, S., ... & Ogretmen, B. (2012). Ceramide targets autophagosomes to mitochondria and induces lethal mitophagy. *Nature chemical biology*, *8*(10), 831-838.
39. Frohman, M. A. (2015). Role of mitochondrial lipids in guiding fission and fusion. *Journal of molecular medicine*, *93*, 263-269.
40. Kameoka, S., Adachi, Y., Okamoto, K., Iijima, M., & Sesaki, H. (2018). Phosphatidic acid and cardiolipin coordinate mitochondrial dynamics. *Trends in cell biology*, *28*(1), 67-76.
41. Choi, S. Y., Huang, P., Jenkins, G. M., Chan, D. C., Schiller, J., & Frohman, M. A. (2006). A common lipid links Mfn-mediated mitochondrial fusion and SNARE-regulated exocytosis. *Nature cell biology*, *8*(11), 1255-1262.
42. Adachi, Y., Itoh, K., Yamada, T., Cerveny, K. L., Suzuki, T. L., Macdonald, P., ... & Sesaki, H. (2016). Coincident phosphatidic acid interaction restrains Drp1 in mitochondrial division. *Molecular cell*, *63*(6), 1034-1043.
43. Huang, H., Gao, Q., Peng, X., Choi, S. Y., Sarma, K., Ren, H., ... & Frohman, M. A. (2011). piRNA-associated germline nuage formation and spermatogenesis require MitoPLD profusogenic mitochondrial-surface lipid signaling. *Developmental cell*, *20*(3), 376-387.
44. Goñi, F. M., & Alonso, A. (1999). Structure and functional properties of diacylglycerols in membranes. *Progress in lipid research*, *38*(1), 1-48.
45. Leikin, S., Kozlov, M. M., Fuller, N. L., & Rand, R. P. (1996). Measured effects of diacylglycerol on structural and elastic properties of phospholipid membranes. *Biophysical journal*, *71*(5), 2623-2632.
46. Campomanes, P., Zoni, V., & Vanni, S. (2019). Local accumulation of diacylglycerol alters membrane properties nonlinearly due to its transbilayer activity. *Communications Chemistry*, *2*(1), 72.

47. Dar, S., Kamerkar, S. C., & Pucadyil, T. J. (2017). Use of the supported membrane tube assay system for real-time analysis of membrane fission reactions. *Nature protocols*, *12*(2), 390-400.
48. Das, S., & Rand, R. P. (1986). Modification by diacylglycerol of the structure and interaction of various phospholipid bilayer membranes. *Biochemistry*, *25*(10), 2882-2889.
49. Vamparys, L., Gautier, R., Vanni, S., Bennett, W. D., Tieleman, D. P., Antonny, B., ... & Fuchs, P. F. (2013). Conical lipids in flat bilayers induce packing defects similar to that induced by positive curvature. *Biophysical journal*, *104*(3), 585-593.
50. Bai, J., & Pagano, R. E. (1997). Measurement of spontaneous transfer and transbilayer movement of BODIPY-labeled lipids in lipid vesicles. *Biochemistry*, *36*(29), 8840-8848.
51. Ishihara, N., Nomura, M., Jofuku, A., Kato, H., Suzuki, S. O., Masuda, K., ... & Mihara, K. (2009). Mitochondrial fission factor Drp1 is essential for embryonic development and synapse formation in mice. *Nature cell biology*, *11*(8), 958-966.
52. Favaro, G., Romanello, V., Varanita, T., Andrea Desbats, M., Morbidoni, V., Tezze, C., ... & Sandri, M. (2019). DRP1-mediated mitochondrial shape controls calcium homeostasis and muscle mass. *Nature communications*, *10*(1), 2576.
53. Hennings, T. G., Chopra, D. G., DeLeon, E. R., VanDeusen, H. R., Sesaki, H., Merrins, M. J., & Ku, G. M. (2018). In vivo deletion of β-cell Drp1 impairs insulin secretion without affecting islet oxygen consumption. *Endocrinology*, *159*(9), 3245-3256.
54. Simula, L., Pacella, I., Colamatteo, A., Procaccini, C., Cancila, V., Bordi, M., ... & Campello, S. (2018). Drp1 controls effective T cell immune-surveillance by regulating T cell migration, proliferation, and cMyc-dependent metabolic reprogramming. *Cell reports*, *25*(11), 3059-3073.
55. Friedman, J. R., Lackner, L. L., West, M., DiBenedetto, J. R., Nunnari, J., & Voeltz, G. K. (2011). ER tubules mark sites of mitochondrial division. *Science*, *334*(6054), 358-362.
56. Wong, Y. C., Ysselstein, D., & Krainc, D. (2018). Mitochondria–lysosome contacts regulate mitochondrial fission via RAB7 GTP hydrolysis. *Nature*, *554*(7692), 382-386.
57. Moore, A. S., Wong, Y. C., Simpson, C. L., & Holzbaur, E. L. (2016). Dynamic actin cycling through mitochondrial subpopulations locally regulates the fission–fusion balance within mitochondrial networks. *Nature communications*, *7*(1), 12886.
58. Roy, K., & Pucadyil, T. J. (2022). Is Drp1 sufficient to catalyze membrane fission?. *Proceedings of the National Academy of Sciences*, *119*(27), e2201709119.

59. Morlot, S., Galli, V., Klein, M., Chiaruttini, N., Manzi, J., Humbert, F., ... & Roux, A. (2012). Membrane shape at the edge of the dynamin helix sets location and duration of the fission reaction. *Cell*, *151*(3), 619-629.
60. Stepanyants, N., Macdonald, P. J., Francy, C. A., Mears, J. A., Qi, X., & Ramachandran, R. (2015). Cardiolipin's propensity for phase transition and its reorganization by dynamin-related protein 1 form a basis for mitochondrial membrane fission. *Molecular biology of the cell*, *26*(17), 3104-3116.
61. Sundborger, A., Soderblom, C., Vorontsova, O., Evergren, E., Hinshaw, J. E., & Shupliakov, O. (2011). An endophilin–dynamin complex promotes budding of clathrin-coated vesicles during synaptic vesicle recycling. *Journal of cell science*, *124*(1), 133-143.
62. Karbowski, M., Jeong, S. Y., & Youle, R. J. (2004). Endophilin B1 is required for the maintenance of mitochondrial morphology. *The Journal of cell biology*, *166*(7), 1027-1039.
63. Bhatt, V. S., Ashley, R., & Sundborger-Lunna, A. (2021). Amphipathic motifs regulate N-BAR protein endophilin B1 auto-inhibition and drive membrane remodeling. *Structure*, *29*(1), 61-69.
64. Ringstad, N., Nemoto, Y., & De Camilli, P. (1997). The SH3p4/Sh3p8/SH3p13 protein family: binding partners for synaptojanin and dynamin via a Grb2-like Src homology 3 domain. *Proceedings of the National Academy of Sciences*, *94*(16), 8569-8574.
65. Ramjaun, A. R., Micheva, K. D., Bouchelet, I., & McPherson, P. S. (1997). Identification and characterization of a nerve terminal-e
66. Takahashi, Y., Coppola, D., Matsushita, N., Cualing, H. D., Sun, M., Sato, Y., ... & Wang, H. G. (2007). Bif-1 interacts with Beclin 1 through UVRAG and regulates autophagy and tumorigenesis. *Nature cell biology*, *9*(10), 1142-1151
67. Takahashi, Y., Meyerkord, C. L., Hori, T., Runkle, K., Fox, T. E., Kester, M., ... & Wang, H. G. (2011). Bif-1 regulates Atg9 trafficking by mediating the fission of Golgi membranes during autophagy. *Autophagy*, *7*(1), 61-73.
68. Riera, A. M., Martinez, C. I., Itskanov, S., Steffen, J., Roach, B., Koehler, C. M., & Van der Bliek, A. M. (2018). Dynamin-2 facilitates Atg9 recycling from nascent autophagosomes. *bioRxiv*, 241901.
69. Simunovic, M., Manneville, J. B., Renard, H. F., Evergren, E., Raghunathan, K., Bhatia, D., ... & Callan-Jones, A. (2017). Friction mediates scission of tubular membranes scaffolded by BAR proteins. *Cell*, *170*(1), 172-184.

70. Zhao, H., Michelot, A., Koskela, E. V., Tkach, V., Stamou, D., Drubin, D. G., & Lappalainen, P. (2013). Membrane-sculpting BAR domains generate stable lipid microdomains. *Cell reports*, *4*(6), 1213-1223.
71. Neumann, S., & Schmid, S. L. (2013). Dual role of BAR domain-containing proteins in regulating vesicle release catalyzed by the GTPase, dynamin-2. *Journal of Biological Chemistry*, *288*(35), 25119-25128.
72. Hohendahl, A., Talledge, N., Galli, V., Shen, P. S., Humbert, F., De Camilli, P., ... & Roux, A. (2017). Structural inhibition of dynamin-mediated membrane fission by endophilin. *Elife*, *6*, e26856.
73. Cleland, M. M., Norris, K. L., Karbowski, M., Wang, C., Suen, D. F., Jiao, S., ... & Youle, R. J. (2011). Bcl-2 family interaction with the mitochondrial morphogenesis machinery. *Cell Death & Differentiation*, *18*(2), 235-247.
74. Simunovic, M., Evergren, E., Callan-Jones, A., & Bassereau, P. (2019). Curving cells inside and out: roles of BAR domain proteins in membrane shaping and its cellular implications. *Annual review of cell and developmental biology*, *35*, 111-129.
75. Itoh, T., Erdmann, K. S., Roux, A., Habermann, B., Werner, H., & De Camilli, P. (2005). Dynamin and the actin cytoskeleton cooperatively regulate plasma membrane invagination by BAR and F-BAR proteins. *Developmental cell*, *9*(6), 791-804.
76. Wu, T., & Baumgart, T. (2014). BIN1 membrane curvature sensing and generation show autoinhibition regulated by downstream ligands and PI (4, 5) P2. *Biochemistry*, *53*(46), 7297-7309.
77. Vanni, S., Vamparys, L., Gautier, R., Drin, G., Etchebest, C., Fuchs, P. F., & Antonny, B. (2013). Amphipathic lipid packing sensor motifs: probing bilayer defects with hydrophobic residues. *Biophysical journal*, *104*(3), 575-584.
78. Campelo, F., & Kozlov, M. M. (2014). Sensing membrane stresses by protein insertions. *PLoS computational biology*, *10*(4), e1003556.
79. Kozlovsky, Y., & Kozlov, M. M. (2003). Membrane fission: model for intermediate structures. *Biophysical journal*, *85*(1), 85-96.
80. Chernomordik, L. V., & Kozlov, M. M. (2003). Protein-lipid interplay in fusion and fission of biological membranes. *Annual review of biochemistry*, *72*(1), 175-207.
81. Schekman, R., & Novick, P. (2004). 23 genes, 23 years later. *Cell*, *116*, S13-S15.
82. Kelly, L. E., & Suzuki, D. T. (1974). The effects of increased temperature on electroretinograms of temperature-sensitive paralysis mutants of Drosophila melanogaster. *Proceedings of the National Academy of Sciences*, *71*(12), 4906-4909.

83. Ramachandran, R., & Schmid, S. L. (2018). The dynamin superfamily. *Current Biology*, *28*(8), R411-R416.
84. Bonazzi, M., Spanò, S., Turacchio, G., Cericola, C., Valente, C., Colanzi, A., ... & Luini, A. (2005). CtBP3/BARS drives membrane fission in dynamin-independent transport pathways. *Nature cell biology*, *7*(6), 570-580.
85. Park, R. J., Shen, H., Liu, L., Liu, X., Ferguson, S. M., & De Camilli, P. (2013). Dynamin triple knockout cells reveal off target effects of commonly used dynamin inhibitors. *Journal of cell science*, *126*(22), 5305-5312.
86. Ferguson, S., Raimondi, A., Paradise, S., Shen, H., Mesaki, K., Ferguson, A., ... & De Camilli, P. (2009). Coordinated actions of actin and BAR proteins upstream of dynamin at endocytic clathrin-coated pits. *Developmental cell*, *17*(6), 811-822
87. Takei, K., Slepnev, V. I., Haucke, V., & De Camilli, P. (1999). Functional partnership between amphiphysin and dynamin in clathrin-mediated endocytosis. *Nature cell biology*, *1*(1), 33-39.
88. Matsuoka, K., Orci, L., Amherdt, M., Bednarek, S. Y., Hamamoto, S., Schekman, R., & Yeung, T. (1998). COPII-coated vesicle formation reconstituted with purified coat proteins and chemically defined liposomes. *Cell*, *93*(2), 263-275.
89. Lee, M. C., Orci, L., Hamamoto, S., Futai, E., Ravazzola, M., & Schekman, R. (2005). Sar1p N-terminal helix initiates membrane curvature and completes the fission of a COPII vesicle. *Cell*, *122*(4), 605-617.
90. Emmanuel Boucrot [1], Adi Pick, Gamze Çamdere, Nicole Liska, Emma Evergren, Harvey T McMahon, Michael M Kozlov (2012). Membrane fission is promoted by insertion of amphipathic helices and is restricted by crescent BAR domains. *Cell*. 149(1):124-36.
91. Pucadyil, T. J., & Schmid, S. L. (2008). Real-time visualization of dynamin-catalyzed membrane fission and vesicle release. *Cell*, *135*(7), 1263-1275.
92. Dar, S., Kamerkar, S. C., & Pucadyil, T. J. (2015). A high-throughput platform for real-time analysis of membrane fission reactions reveals dynamin function. *Nature cell biology*, *17*(12), 1588-1596.
93. Xicoy, H., Wieringa, B., & Martens, G. J. (2017). The SH-SY5Y cell line in Parkinson's disease research: a systematic review. *Molecular neurodegeneration*, *12*, 1-11.
94. Binolfi, A., Rasia, R. M., Bertoncini, C. W., Ceolin, M., Zweckstetter, M., Griesinger, C., ... & Fernández, C. O. (2006). Interaction of α-synuclein with divalent metal ions reveals key differences: A link between structure, binding specificity and fibrillation enhancement. *Journal of the American Chemical Society*, *128*(30), 9893-9901.

95. Maroteaux, L., Campanelli, J. T., & Scheller, R. H. (1988). Synuclein: a neuron-specific protein localized to the nucleus and presynaptic nerve terminal. *Journal of Neuroscience*, *8*(8), 2804-2815.
96. Jakes, R., Spillantini, M. G., & Goedert, M. (1994). Identification of two distinct synucleins from human brain. *FEBS letters*, *345*(1), 27-32.
97. Lavedan, C., Leroy, E., Dehejia, A., Buchholtz, S., Dutra, A., Nussbaum, R. L., & Polymeropoulos, M. H. (1998). Identification, localization and characterization of the human γ-synuclein gene. *Human genetics*, *103*, 106-112.
98. Spillantini, M. G., Crowther, R. A., Jakes, R., Hasegawa, M., & Goedert, M. (1998). α-Synuclein in filamentous inclusions of Lewy bodies from Parkinson's disease and dementia with Lewy bodies. *Proceedings of the National Academy of Sciences*, *95*(11), 6469-6473.
99. Simon-Sanchez, J., Schulte, C., Bras, J. M., Sharma, M., Gibbs, J. R., Berg, D., ... & Gasser, T. (2009). Genome-wide association study reveals genetic risk underlying Parkinson's disease. *Nature genetics*, *41*(12), 1308-1312.
100. Burré, J. (2015). The synaptic function of α-synuclein. *Journal of Parkinson's disease*, *5*(4), 699-713.
101. Iwai, A., Masliah, E., Yoshimoto, M., Ge, N., Flanagan, L., De Silva, H. R., ... & Saitoh, T. (1995). The precursor protein of non-Aβ component of Alzheimer's disease amyloid is a presynaptic protein of the central nervous system. *Neuron*, *14*(2), 467-475.
102. Baltic, S., Perovic, M., Mladenovic, A., Raicevic, N., Ruzdijic, S., Rakic, L., & Kanazir, S. (2004). α-Synuclein is expressed in different tissues during human fetal development. *Journal of Molecular Neuroscience*, *22*, 199-203.
103. Shin, E. C., Cho, S. E., Lee, D. K., Hur, M. W., Paik, S. R., Park, J. H., & Kim, J. (2000). Expression patterns of α-synuclein in human hematopoietic cells and in Drosophila at different developmental stages. *Molecules and cells*, *10*, 65-70.
104. Petersen, K., Olesen, O. F., & Mikkelsen, J. D. (1999). Developmental expression of α-synuclein in rat hippocampus and cerebral cortex. *Neuroscience*, *91*(2), 651-659.
105. Chu, Y., & Kordower, J. H. (2007). Age-associated increases of α-synuclein in monkeys and humans are associated with nigrostriatal dopamine depletion: is this the target for Parkinson's disease?. *Neurobiology of disease*, *25*(1), 134-149.
106. Bussell Jr, R., Ramlall, T. F., & Eliezer, D. (2005). Helix periodicity, topology, and dynamics of membrane-associated α-synuclein. *Protein Science*, *14*(4), 862-872.

107. Varkey, J., Isas, J. M., Mizuno, N., Jensen, M. B., Bhatia, V. K., Jao, C. C., ... & Langen, R. (2010). Membrane curvature induction and tubulation are common features of synucleins and apolipoproteins. *Journal of Biological Chemistry*, *285*(42), 32486-32493.
108. Bartels, T., Kim, N. C., Luth, E. S., & Selkoe, D. J. (2014). N-alpha-acetylation of α-synuclein increases its helical folding propensity, GM1 binding specificity and resistance to aggregation. *PloS one*, *9*(7), e103727.
109. Ueda, K., Fukushima, H., Masliah, E., Xia, Y. U., Iwai, A., Yoshimoto, M., ... & Saitoh, T. (1993). Molecular cloning of cDNA encoding an unrecognized component of amyloid in Alzheimer disease. *Proceedings of the National Academy of Sciences*, *90*(23), 11282-11286.
110. Paslawski, W., Mysling, S., Thomsen, K., Jørgensen, T. J., & Otzen, D. E. (2014). Co-existence of two different α-synuclein oligomers with different core structures determined by hydrogen/deuterium exchange mass spectrometry. *Angewandte Chemie*, *126*(29), 7690-7693.
111. Tuttle, M. D., Comellas, G., Nieuwkoop, A. J., Covell, D. J., Berthold, D. A., Kloepper, K. D., ... & Rienstra, C. M. (2016). Solid-state NMR structure of a pathogenic fibril of full-length human α-synuclein. *Nature structural & molecular biology*, *23*(5), 409-415.
112. Greten-Harrison, B., Polydoro, M., Morimoto-Tomita, M., Diao, L., Williams, A. M., Nie, E. H., ... & Chandra, S. S. (2010). αβγ-Synuclein triple knockout mice reveal age-dependent neuronal dysfunction. *Proceedings of the National Academy of Sciences*, *107*(45), 19573-19578.
113. Jo, E., McLaurin, J., Yip, C. M., George-Hyslop, P. S., & Fraser, P. E. (2000). α-Synuclein membrane interactions and lipid specificity. *Journal of Biological Chemistry*, *275*(44), 34328-34334.
114. Davidson, W. S., Jonas, A., Clayton, D. F., & George, J. M. (1998). Stabilization of α-synuclein secondary structure upon binding to synthetic membranes. *Journal of Biological Chemistry*, *273*(16), 9443-9449.
115. Pranke, I. M., Morello, V., Bigay, J., Gibson, K., Verbavatz, J. M., Antonny, B., & Jackson, C. L. (2011). α-Synuclein and ALPS motifs are membrane curvature sensors whose contrasting chemistry mediates selective vesicle binding. *Journal of Cell Biology*, *194*(1), 89-103.
116. Volles, M. J., & Lansbury, P. T. (2002). Vesicle permeabilization by protofibrillar α-synuclein is sensitive to Parkinson's disease-linked mutations and occurs by a pore-like mechanism. *Biochemistry*, *41*(14), 4595-4602.

117. Jao, C. C., Hegde, B. G., Chen, J., Haworth, I. S., & Langen, R. (2008). Structure of membrane-bound α-synuclein from site-directed spin labeling and computational refinement. *Proceedings of the National Academy of Sciences*, *105*(50), 19666-19671.
118. Tosatto, L., Andrighetti, A. O., Plotegher, N., Antonini, V., Tessari, I., Ricci, L., ... & Dalla Serra, M. (2012). Alpha-synuclein pore forming activity upon membrane association. *Biochimica et Biophysica Acta (BBA)-Biomembranes*, *1818*(11), 2876-2883.
119. Braun, A. R., Lacy, M. M., Ducas, V. C., Rhoades, E., & Sachs, J. N. (2017). α-Synuclein's uniquely long amphipathic helix enhances its membrane binding and remodeling capacity. *The Journal of membrane biology*, *250*, 183-193.
120. Kamp, F., & Beyer, K. (2006). Binding of α-synuclein affects the lipid packing in bilayers of small vesicles. *Journal of Biological Chemistry*, *281*(14), 9251-9259.
121. Ouberai, M. M., Wang, J., Swann, M. J., Galvagnion, C., Guilliams, T., Dobson, C. M., & Welland, M. E. (2013). α-Synuclein senses lipid packing defects and induces lateral expansion of lipids leading to membrane remodeling. *Journal of Biological Chemistry*, *288*(29), 20883-20895.
122. Yoo, G., Shin, Y. K., & Lee, N. K. (2023). The role of α-synuclein in SNARE-mediated synaptic vesicle fusion. *Journal of Molecular Biology*, *435*(1), 167775.
123. Ben Gedalya, T., Loeb, V., Israeli, E., Altschuler, Y., Selkoe, D. J., & Sharon, R. (2009). α-Synuclein and Polyunsaturated Fatty Acids Promote Clathrin-Mediated Endocytosis and Synaptic Vesicle Recycling. *Traffic*, *10*(2), 218-234.
124. Gosavi, N., Lee, H. J., Lee, J. S., Patel, S., & Lee, S. J. (2002). Golgi fragmentation occurs in the cells with prefibrillar α-synuclein aggregates and precedes the formation of fibrillar inclusion. *Journal of Biological Chemistry*, *277*(50), 48984-48992.
125. Martin, L. J., Pan, Y., Price, A. C., Sterling, W., Copeland, N. G., Jenkins, N. A., ... & Lee, M. K. (2006). Parkinson's disease α-synuclein transgenic mice develop neuronal mitochondrial degeneration and cell death. *Journal of Neuroscience*, *26*(1), 41-50.
126. Meredith, G. E., Totterdell, S., Petroske, E., Santa Cruz, K., Callison Jr, R. C., & Lau, Y. S. (2002). Lysosomal malfunction accompanies alpha-synuclein aggregation in a progressive mouse model of Parkinson's disease. *Brain research*, *956*(1), 156-165.
127. Stichel, C. C., Zhu, X. R., Bader, V., Linnartz, B., Schmidt, S., & Lübbert, H. (2007). Mono-and double-mutant mouse models of Parkinson's disease display severe mitochondrial damage. *Human molecular genetics*, *16*(20), 2377-2393.

128. Cole, N. B., DiEuliis, D., Leo, P., Mitchell, D. C., & Nussbaum, R. L. (2008). Mitochondrial translocation of α-synuclein is promoted by intracellular acidification. *Experimental cell research*, *314*(10), 2076-2089.
129. Devi, L., Raghavendran, V., Prabhu, B. M., Avadhani, N. G., & Anandatheerthavarada, H. K. (2008). Mitochondrial import and accumulation of α-synuclein impair complex I in human dopaminergic neuronal cultures and Parkinson disease brain. *Journal of Biological Chemistry*, *283*(14), 9089-9100.
130. Nakamura, K., Nemani, V. M., Wallender, E. K., Kaehlcke, K., Ott, M., & Edwards, R. H. (2008). Optical reporters for the conformation of α-synuclein reveal a specific interaction with mitochondria. *Journal of Neuroscience*, *28*(47), 12305-12317.
131. Nakamura, K., Nemani, V. M., Azarbal, F., Skibinski, G., Levy, J. M., Egami, K., ... & Edwards, R. H. (2011). Direct Membrane Association Drives Mitochondrial Fission by the Parkinson Disease-associated Protein α-Synuclein*♦. *Journal of Biological Chemistry*, *286*(23), 20710-20726.
132. Zhang, J., Li, X., & Li, J. D. (2019). The Roles of Post-translational Modifications on α-Synuclein in the Pathogenesis of Parkinson's Diseases. *Frontiers in neuroscience*, *13*, 381.
133. Bartels, T., Choi, J. G., & Selkoe, D. J. (2011). α-Synuclein occurs physiologically as a helically folded tetramer that resists aggregation. *Nature*, *477*(7362), 107-110.
134. Huang, C., Ren, G., Zhou, H., & Wang, C. C. (2005). A new method for purification of recombinant human α-synuclein in Escherichia coli. *Protein expression and purification*, *42*(1), 173-177.
135. Cholak, E., Bugge, K., Khondker, A., Gauger, K., Pedraz-Cuesta, E., Pedersen, M. E., ... & Kragelund, B. B. (2020). Avidity within the N-terminal anchor drives α-synuclein membrane interaction and insertion. *The FASEB Journal*, *34*(6), 7462-7482.
136. Olofsson, G., & Sparr, E. (2013). Ionization constants pKa of cardiolipin. *PloS one*, *8*(9), e73040.
137. Kwarteng, D. O., Putta, P., & Kooijman, E. E. (2021). Ionization properties of monophosphoinositides in mixed model membranes. *Biochimica et Biophysica Acta (BBA)-Biomembranes*, *1863*(11), 183692.
138. Jensen, M. B., Bhatia, V. K., Jao, C. C., Rasmussen, J. E., Pedersen, S. L., Jensen, K. J., ... & Stamou, D. (2011). Membrane curvature sensing by amphipathic helices: a single liposome study using α-synuclein and annexin B12. *Journal of Biological Chemistry*, *286*(49), 42603-42614.

139. Lee, H. J., Choi, C., & Lee, S. J. (2002). Membrane-bound α-synuclein has a high aggregation propensity and the ability to seed the aggregation of the cytosolic form. *Journal of Biological Chemistry*, *277*(1), 671-678.
140. Morlot, S., & Roux, A. (2013). Mechanics of dynamin-mediated membrane fission. *Annual review of biophysics*, *42*, 629-649
141. Polymeropoulos, M. H., Lavedan, C., Leroy, E., Ide, S. E., Dehejia, A., Dutra, A., ... & Nussbaum, R. L. (1997). Mutation in the α-synuclein gene identified in families with Parkinson's disease. *science*, *276*(5321), 2045-2047.
142. Narhi, L., Wood, S. J., Steavenson, S., Jiang, Y., Wu, G. M., Anafi, D., ... & Citron, M. (1999). Both familial Parkinson's disease mutations accelerate α-synuclein aggregation. *Journal of Biological Chemistry*, *274*(14), 9843-9846.
143. El-Agnaf, O. M., Jakes, R., Curran, M. D., Middleton, D., Ingenito, R., Bianchi, E., ... & Wallace, A. (1998). Aggregates from mutant and wild-type α-synuclein proteins and NAC peptide induce apoptotic cell death in human neuroblastoma cells by formation of β-sheet and amyloid-like filaments. *FEBS letters*, *440*(1-2), 71-75.
144. Perrin, R. J., Woods, W. S., Clayton, D. F., & George, J. M. (2001). Exposure to long chain polyunsaturated fatty acids triggers rapid multimerization of synucleins. *Journal of Biological Chemistry*, *276*(45), 41958-41962.
145. Perrin, R. J., Woods, W. S., Clayton, D. F., & George, J. M. (2000). Interaction of human α-synuclein and Parkinson's disease variants with phospholipids: structural analysis using site-directed mutagenesis. *Journal of Biological Chemistry*, *275*(44), 34393-34398.
146. Jensen, P. H., Nielsen, M. S., Jakes, R., Dotti, C. G., & Goedert, M. (1998). Binding of α-synuclein to brain vesicles is abolished by familial Parkinson's disease mutation. *Journal of Biological Chemistry*, *273*(41), 26292-26294.
147. Ulmer, T. S., & Bax, A. (2005). Comparison of structure and dynamics of micelle-bound human α-synuclein and Parkinson disease variants. *Journal of Biological Chemistry*, *280*(52), 43179-43187.
148. Perlmutter, J. D., Braun, A. R., & Sachs, J. N. (2009). Curvature Dynamics of α-Synuclein Familial Parkinson's Disease Mutants: Molecular Dynamics Simulations of the Micelle- and Membrane-Bound Forms. *Biophysical Journal*, *96*(3), 340a.
149. Robotta, M., Cattani, J., Martins, J. C., Subramaniam, V., & Drescher, M. (2017). Alpha-synuclein disease mutations are structurally defective and locally affect membrane binding. *Journal of the American Chemical Society*, *139*(12), 4254-4257.

150. Narayanan, V., & Scarlata, S. (2001). Membrane binding and self-association of α-synucleins. *Biochemistry*, *40*(33), 9927-9934.
151. Coskuner, O., & Wise-Scira, O. (2013). Structures and free energy landscapes of the A53T mutant-type α-synuclein protein and impact of A53T mutation on the structures of the wild-type α-synuclein protein with dynamics. *ACS chemical neuroscience*, *4*(7), 1101-1113.
152. Sahay, S., Ghosh, D., Dwivedi, S., Anoop, A., Mohite, G. M., Kombrabail, M., ... & Maji, S. K. (2015). Familial Parkinson disease-a
153. Thorne, N. J., & Tumbarello, D. A. (2022). The relationship of alpha-synuclein to mitochondrial dynamics and quality control. *Frontiers in molecular neuroscience*, *15*, 947191.
154. McCoy, M. K., & Cookson, M. R. (2011). DJ-1 regulation of mitochondrial function and autophagy through oxidative stress. *Autophagy*, *7*(5), 531-532.
155. Parihar, M. S., Parihar, A., Fujita, M., Hashimoto, M., & Ghafourifar, P. (2008). Mitochondrial association of alpha-synuclein causes oxidative stress. *Cellular and molecular life sciences*, *65*, 1272-1284.
156. Ludtmann, M. H., Angelova, P. R., Horrocks, M. H., Choi, M. L., Rodrigues, M., Baev, A. Y., ... & Gandhi, S. (2018). α-synuclein oligomers interact with ATP synthase and open the permeability transition pore in Parkinson's disease. *Nature communications*, *9*(1), 2293.
157. Calì, T., Ottolini, D., Negro, A., & Brini, M. (2012). α-Synuclein controls mitochondrial calcium homeostasis by enhancing endoplasmic reticulum-mitochondria interactions. *Journal of Biological Chemistry*, *287*(22), 17914-17929.
158. Guardia-Laguarta, C., Area-Gomez, E., Rüb, C., Liu, Y., Magrané, J., Becker, D., ... & Przedborski, S. (2014). α-Synuclein is localized to mitochondria-associated ER membranes. *Journal of Neuroscience*, *34*(1), 249-259
159. Kamp, F., Exner, N., Lutz, A. K., Wender, N., Hegermann, J., Brunner, B., ... & Haass, C. (2010). Inhibition of mitochondrial fusion by α-synuclein is rescued by PINK1, Parkin and DJ-1. *The EMBO journal*, *29*(20), 3571-3589.
160. Xie, W., & Chung, K. K. (2012). Alpha-synuclein impairs normal dynamics of mitochondria in cell and animal models of Parkinson's disease. *Journal of neurochemistry*, *122*(2), 404-414.

161. Davis, G. C., Williams, A. C., Markey, S. P., Ebert, M. H., Caine, E. D., Reichert, C. M., & Kopin, I. J. (1979). Chronic Parkinsonism secondary to intravenous injection of meperidine analogues. *Psychiatry research*, *1*(3), 249-254.
162. Liao, P. C., Bergamini, C., Fato, R., Pon, L. A., & Pallotti, F. (2020). Isolation of mitochondria from cells and tissues. In *Methods in cell biology* (Vol. 155, pp. 3-31). Academic Press.
163. Kamat, S. S., Camara, K., Parsons, W. H., Chen, D. H., Dix, M. M., Bird, T. D., ... & Cravatt, B. F. (2015). Immunomodulatory lysophosphatidylserines are regulated by ABHD16A and ABHD12 interplay. *Nature chemical biology*, *11*(2), 164-171.
164. Reeve, A. K., Ludtmann, M. H., Angelova, P. R., Simcox, E. M., Horrocks, M. H., Klenerman, D., ... & Abramov, A. Y. (2015). Aggregated α-synuclein and complex I deficiency: exploration of their relationship in differentiated neurons. *Cell death & disease*, *6*(7), e1820-e1820.
165. Quirós, P. M., Langer, T., & López-Otín, C. (2015). New roles for mitochondrial proteases in health, ageing and disease. *Nature reviews Molecular cell biology*, *16*(6), 345-359.
166. Mirzaei, H., & Regnier, F. (2008). Protein: protein aggregation induced by protein oxidation. *Journal of Chromatography B*, *873*(1), 8-14.
167. Mori, T., TAKAI, Y., YU, B., TAKAHASHI, J., NISHIZUKA, Y., & FUJIKURA, T. (1982). Specificity of the fatty acyl moieties of diacylglycerol for the activation of calcium-activated, phospholipid-dependent protein kinase. *The Journal of Biochemistry*, *91*(2), 427-431.